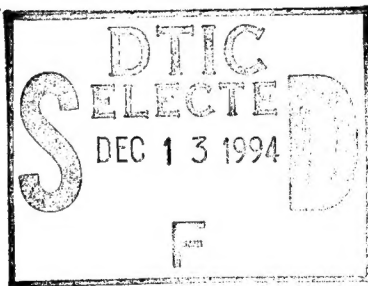


REPORT DOCUMENTATION PAGE

Form Approved
OMB No. 0704-0188

Public reporting burden for this collection of information is estimated to average 1 hour per response, including the time for reviewing instructions, searching existing data sources, gathering and maintaining the data needed, and completing and reviewing the collection of information. Send comments regarding this burden estimate or any other aspect of this collection of information, including suggestions for reducing this burden, to Washington Headquarters Services, Directorate for Information Operations and Reports, 1215 Jefferson Davis Highway, Suite 1204, Arlington, VA 22202-4302, and to the Office of Management and Budget, Paperwork Reduction Project (0704-0188), Washington, DC 20503.

1. AGENCY USE ONLY (Leave blank)		2. REPORT DATE Mar 94	3. REPORT TYPE AND DATES COVERED	
4. TITLE AND SUBTITLE The sufficiency of sinusoidal motions in seismic ground motion studies			5. FUNDING NUMBERS	
6. AUTHOR(S) Bryon W. Boyce			8. PERFORMING ORGANIZATION REPORT NUMBER AFIT/CI/CIA 94-129	
7. PERFORMING ORGANIZATION NAME(S) AND ADDRESS(ES) AFIT Students Attending: Colorado State University			10. SPONSORING/MONITORING AGENCY REPORT NUMBER	
9. SPONSORING/MONITORING AGENCY NAME(S) AND ADDRESS(ES) DEPTMENT OF THE AIR FORCE AFIT/CI 2950 P STREET WRIGHT-PATTERSON AFB OH 45433-7765			11. SUPPLEMENTARY NOTES	
12a. DISTRIBUTION/AVAILABILITY STATEMENT Approved for Public Release IAW 190-1 Distribution Unlimited MICHAEL M. BRICKER, SMSgt, USAF Chief Administration			12b. DISTRIBUTION CODE	
13. ABSTRACT (Maximum 200 words)				
				
<p>19941207 082</p> <p>DTIC QUALITY INSPECTED 1</p>				
14. SUBJECT TERMS			15. NUMBER OF PAGES 135	
			16. PRICE CODE	
17. SECURITY CLASSIFICATION OF REPORT	18. SECURITY CLASSIFICATION OF THIS PAGE	19. SECURITY CLASSIFICATION OF ABSTRACT	20. LIMITATION OF ABSTRACT	

COLORADO STATE UNIVERSITY

March 30, 1994

WE HEREBY RECOMMEND THAT THE THESIS PREPARED UNDER OUR SUPERVISION BY BRYON W. BOYCE ENTITLED THE SUFFICIENCY OF SINUSOIDAL MOTIONS IN SEISMIC GROUND MOTION STUDIES BE ACCEPTED AS FULFILLING IN PART REQUIREMENTS FOR THE DEGREE OF MASTER OF SCIENCE.

Committee on Graduate Work

Wayne A. Dordick

Donald O. Dordick

Thomas J. Allen

Adviser

N. J. Dordick

Department Head

[illegible]

ABSTRACT OF THESIS

THE SUFFICIENCY OF SINUSOIDAL MOTIONS IN SEISMIC GROUND MOTION STUDIES

This study evaluates the effectiveness of using sinusoidal input motions in seismic ground motion studies. The computer program SHAKE-88 is used to compute the peak surface accelerations in three different soil profiles subjected to sinusoidal and earthquake input motions. The input motions are scaled to cover a range of maximum accelerations and frequencies. A comparative analysis is made of the sinusoidal and earthquake "normalized" peak surface accelerations (amplification factors) resulting in the three soil profiles.

Results from 690 SHAKE-88 computer runs indicate that the peak surface accelerations induced by the sinusoidal motions generally come very close to matching those induced by the earthquake motions.

Bryon W. Boyce
Civil Engineering Department
Colorado State University
Fort Collins, CO 80523
Spring 1994

ACKNOWLEDGEMENTS

I am grateful to the United States Air Force for providing me with the opportunity and financial support to attend graduate school.

To my advisor, Dr. Thomas J. Siller, I wish to express my deep gratitude for all your direction, help, and patience in conducting this research. I also thank my committee members, Dr. Wayne A. Charlie and Dr. Donald O. Doehring, for your comments and insight on this thesis.

I am very grateful to my family for helping me through this challenge. Thank you Mom and Dad, Kymberly, and Stephanie for all your love, prayors, patience, and encouragement.

Finally and most importantly, I thank God who made this all possible. Thank you Lord for Your many blessings.

CONTENTS

1	Introduction	1
1.1	Problem Statement	1
1.2	Motivation for Research	2
1.3	Specific Objectives	4
1.4	Thesis Organization	5
2	Background	6
2.1	General	6
2.2	Influence of Soil Conditions on Ground Motions . .	9
2.2.1	General	9
2.2.2	Propagation of Earthquake Waves	9
2.2.3	Site Soil Conditions	10
2.2.4	Characteristics of Ground Motion	13
2.2.5	Non-Linear Behavior of Soil	18
2.2.6	Amplification of Ground Motion by Soil Layers . .	21
2.2.7	Analytical Procedures for Determining Ground Motions in Horizontal Soil Deposits	26
2.3	Seismic Building Code Provisions	29
2.3.1	General	29
2.3.2	Problems with Current Code Provisions	29
2.3.3	Alternatives to Current Code Provisions	30
3	Thesis Scope	32
3.1	Scope of Research	32
3.1.1	Selected Input Motions	32
3.1.2	Selected Soil Profiles	37
4	Computer Program SHAKE	39
4.1	General Description of SHAKE	39
4.2	Organization of Input Data	41
4.2.1	Input Data File	41
4.2.2	Input Motion	42
4.2.3	Dynamic Soil Properties	42
4.2.4	Soil Profile Modeling	47
5	Analytical Procedure	60
5.1	Chapter Overview	60
5.2	Modeling of Sinusoidal Input Motions	60
5.2.1	Modeling Procedure	60
5.2.2	Modeling Results	68
5.3	Comparison of Sinusoidal Induced Amplifications . .	72
5.3.1	Material Response	72

5.3.2	Cycle Response	78
5.3.3	Frequency Response	82
5.4	Chapter Summary	83
6	Comparative Analysis	85
6.1	Chapter Overview	85
6.2	Earthquake versus Sinusoidal Induced Amplifications in the Sand and Clay Profiles	86
6.2.1	Earthquake Scaled to Sinusoidal Parameters . . .	86
6.2.2	Sinusoidal Scaled to Earthquake Parameters . . .	112
6.3	Earthquake versus Sinusoidal Induced Amplifications in the Treasure Island Profile	116
6.3.1	Earthquake Scaled to Sinusoidal Parameters . . .	116
6.3.2	Sinusoidal Scaled to Earthquake Parameters . . .	120
6.4	Chapter Summary	122
6.4.1	Ideal Sand and Clay Profile Results	123
6.4.2	Treasure Island UM10 Profile Results	125
7	Summary and Conclusions	126
7.1	Summary of Research	126
7.2	Summary of Results	127
7.3	Conclusions	128
7.4	Recommendations	129
	References	130

LIST OF FIGURES

2.1	Typical SSI Schematic (after Seed, et al. [40]) . . .	7
2.2	Hysteretic Stress-Strain Relationship for Soil (after Idriss and Seed [19])	19
2.3	Equivalent Bi-Linear Stress-Strain Relationship for Soil (after Idriss and Seed [19])	19
2.4	Equivalent Linear Parameters for Soil (after Silver and Seed [44])	19
2.5	Acceleration on Soil & Rock Sites (after Finn [14])	22
2.6	Semi-Infinite Soil Layers (after Schnabel, et al. [34])	27
3.1	Sinusoidal Input Motions	33
3.2	Accelerograms (after Lysmer and Seed [25])	35
4.1	Normalized Shear Modulus and Damping - Cohesive Soils (after Lysmer and Seed [24])	44
4.2	Normalized Shear Modulus and Damping - Cohesionless Soils (after Lysmer, et al. [24]) . . .	45
4.3	Normalized Shear Modulus and Damping - Treasure Island Soils (after Ferritto [13])	46
4.4	Ideal Clay Profile	48
4.5	Ideal Sand Profile	49
4.6	Treasure Island Profile (after De Alba, et al. [12], Ferritto [13], Hanks and Brady [15], Rogers and Figuers [32], Seed, et al. [41], SRTSH [11])	52

4.7	Peak Acceleration vs Depth at UM10 Site (after Hryciw, et al. [16])	55
4.8	Response Spectrum for UM10 using SHAKE-88 and E-W YBI Accelerogram	57
4.9	Recorded and Computed Response Spectrum for UM10 and YBI (E-W Components) (after Seed, et al. [41]) .	57
4.10	Response Spectrum for UM10 using SHAKE-88 and N-S YBI Accelerogram	58
4.11	Recorded Response Spectrum for UM10 and YBI (N-S Components) (after Seed, et al. [41])	58
5.1	Single, 2.5 Hz Sine Wave	62
5.2	Sinusoidal Input Motion Records	63
5.3	Scaled Pulse Input Motion Records	66
5.4	Non-Scaled Pulse Input Motion Records	67
5.5	Amplification Factor vs. Input Motion Frequency for both Scaled and Non-Scaled Sinusoidal Motions .	71
5.6	Amplification Factor vs. Input Motion Frequency for Steady State Motions	74
5.7	Amplification Factor vs. Input Motion Frequency for 5 Cycle Motions	74
5.8	Amplification Factor vs. Input Motion Frequency for 2 Cycle Motions	74
5.9	Amplification Factor vs. Input Motion Frequency for 1 Cycle Motions	75
5.10	Amplification Factor vs. Input Motion Frequency for Pulse Motions	75
5.11	Amplification Factor vs. Input Motion Frequency for 0.2g and 0.4g Sinusoidal Motions in Sand . . .	79
5.12	Amplification Factor vs. Input Motion Frequency for 0.2g Sinusoidal Motions in Clay	79
5.13	Amplification Factor vs. Input Motion Frequency for 0.01g Sinusoidal Motions in Sand.	84

5.14	Amplification Factor vs. Input Motion Frequency for 0.01g Sinusoidal Motions in Clay	84
6.1	Amplification Factor vs. Input Motion Frequency, YBI90 and Sinusoidal Motions in Sand	89
6.2	Amplification Factor vs. Input Motion Frequency, YBI90 and Sinusoidal Motions in Clay	90
6.3	Amplification Factor vs. Input Motion Frequency, YBI0 and Sinusoidal Motions in Sand	92
6.4	Amplification Factor vs. Input Motion Frequency, YBI0 and Sinusoidal Motions in Clay	93
6.5	Amplification Factor vs. Input Motion Frequency, Presidio90 and Sinusoidal Motions in Sand	94
6.6	Amplification Factor vs. Input Motion Frequency, Presidio90 and Sinusoidal Motions in Clay	95
6.7	Amplification Factor vs. Input Motion Frequency, Presidio0 and Sinusoidal Motions in Sand	96
6.8	Amplification Factor vs. Input Motion Frequency, Presidio0 and Sinusoidal Motions in Clay	97
6.9	Amplification Factor vs. Input Motion Frequency, Piedmont45 and Sinusoidal Motions in Sand	99
6.10	Amplification Factor vs. Input Motion Frequency, Piedmont45 and Sinusoidal Motions in Clay	100
6.11	Amplification Factor vs. Input Motion Frequency, Pulgas90 and Sinusoidal Motions in Sand	101
6.12	Amplification Factor vs. Input Motion Frequency, Pulgas90 and Sinusoidal Motions in Clay	102
6.13	Amplification Factor vs. Input Motion Frequency, Pulgas0 and Sinusoidal Motions in Sand	103
6.14	Amplification Factor vs. Input Motion Frequency, Pulgas0 and Sinusoidal Motions in Clay	104
6.15	Amplification Factor vs. Input Motion Frequency, UCSC90 and Sinusoidal Motions in Sand	105
6.16	Amplification Factor vs. Input Motion Frequency, UCSC90 and Sinusoidal Motions in Clay	106

6.17	Amplification Factor vs. Input Motion Frequency, UCSC0 and Sinusoidal Motions in Sand	108
6.18	Amplification Factor vs. Input Motion Frequency, UCSC0 and Sinusoidal Motions in Clay	109
6.19	Amplification Factor vs. Input Motion Frequency, Pasadena 1952 and Sinusoidal Motions in Sand . . .	110
6.20	Amplification Factor vs. Input Motion Frequency, Pasadena 1952 and Sinusoidal Motions in Clay . . .	111
6.21	Amplification Factor vs. Predominant Frequency, Sand	113
6.22	Amplification Factor vs. Predominant Frequency, Clay	115
6.23	Amplification Factor vs. Input Motion Frequency, YBI90 and Sinusoidal Motions in UM10	117
6.24	Amplification Factor vs. Input Motion Frequency, YBI90 and Sinusoidal Motions in UM10	119
6.25	Amplification Factor vs. Predominant Frequency, UM10	121

LIST OF TABLES

3.1	Accelerogram Parameters (after Lysmer, et al.[25])	37
4.1	Soil Property Units for SHAKE (after Schnabel, et al. [34])	47
4.2	Peak Surface Accelerations at UM10 Site	54
5.1	Time Intervals for New Input Motion Frequencies . .	65
5.2	Amplification Factors for Scaled and Non-Scaled Sinusoidal Motions	69
5.3	Amplification Factors for Pulse Motions in Clay and Sand Profiles	73
6.1	Amplifications in Sand	113
6.2	Amplifications in Clay	115
6.3	Amplifications in UM10	121

LIST OF SYMBOLS

<u>Symbol</u>	<u>Description</u>	<u>Units</u>
f	Natural Frequency of Soil Layer	T^{-1}
G	Shear Modulus	F/L^2
g	Acceleration of Gravity	L/T^2
γ	Unit Weight of Soil	F/L^3
H	Thickness of Soil Layer	L
λ	Damping Ratio	decimal
ρ	Soil Density	M/L^3
T	Natural Period of Soil Layer	T
V_s	Shear Wave Velocity	L/T

1. INTRODUCTION

1.1 Problem Statement

The purpose of this study is to determine the effectiveness of using sinusoidal input motions in seismic ground motion studies. Sinusoidal motions have been used by researchers for soil-structure interaction (SSI) problems (e.g., Siller [43]) because it is more economical than using full earthquake records. In SSI problems, one has a choice of subjecting the system to either a representative earthquake record, or to a series of motions (e.g., earthquake or other), to determine behavior over a wide range of inputs. The problem with using earthquake records is, there never is a "correct" earthquake record to use, and it is computationally costly to use numerous records. Therefore, if the confidence level can be determined for the use of sinusoidal motions, this could provide a basis for subjecting systems to wider ranges of simplified input motions. The concern with using sinusoidal input motions is: How well do sinusoidal motions generate the values of the various significant ground motion characteristics (e.g., peak ground acceleration, peak spectral acceleration) that earthquakes generate? This thesis starts to address that issue by comparing the peak surface

accelerations induced by sinusoidal motions and earthquake records in two ideal soil profiles and one field site profile.

1.2 Motivation for Research

The structural designs of most large and/or critical structures are required by code to account for the potential damaging effects of earthquake generated ground motions. The interaction between such structures and the ground motions in the surrounding soils are typically analyzed using so-called "soil-structure interaction" (SSI) methods. Earthquake records are typically used as input motions for SSI analyses, but they are not very cost effective. Therefore, development of simpler, more economical types of input motions that could be used to augment or replace the earthquake records in SSI analyses is desirable. Sinusoidal motions are one possibility, but the confidence level for their effectiveness has not been determined.

Evaluation of the effectiveness of sinusoidal motions for ground motion studies is complicated by the influence that site soil conditions have on ground motions. For any particular site, the local geologic conditions are known to strongly influence the character of earthquake generated ground motions (Seed and Iriss [38]). This has been demonstrated by ground motion instrumentation and the structural damage patterns resulting from several past earthquake events, especially the recent 1985 Mexico City and

the 1989 Loma Prieta earthquakes. In the 1985 Mexico City earthquake, peak accelerations recorded in the soft Lake Bed region were up to 5 times greater than the incoming motions in rock (Finn [14]). The result: structures built on the city's rocky hillside received very little damage, while several structures located on the clay soils of the old lakebed received extensive damage. Later, in the 1989 Loma Prieta earthquake, accelerations recorded in the San Francisco Bay Area were up to 3 times larger at soft soil sites than at rock sites having similar epicentral distance (De Alba et al. [12]). Major structural damage in the San Francisco and Oakland areas occurred at sites underlain by soft marine deposits and man-made fills (Astaneh et al. [3]). This damage included the catastrophic collapse of a 1 mile elevated segment of the I-880 Cypress Street viaduct, in which 42 people were crushed to death in their cars. Evidence from these and other past earthquakes have shown that earthquake induced ground motions occurring in rock below the earth's surface are likely to be amplified within the soil layers above the rock. The degree of amplification, or in some cases the degree of attenuation, depends upon the characteristics of the soil deposit overlying the rock (Benuska [4]).

One current approach to predicting ground motions comprises the use of computer programs that implement one of several available ground motion equations (e.g., SHAKE) (Schnabel et al. [34]). This thesis uses SHAKE to compute the

peak surface accelerations developed in three soil profiles using both earthquake motions and sinusoidal motions as the input data to the program. If the sinusoidally induced peak surface accelerations are found to be sufficiently close in value to the earthquake generated peak surface accelerations, then the level of confidence can be significantly increased for using sinusoidal motions in SSI analyses.

1.3 Specific Objectives

The purpose of this thesis is to evaluate the effectiveness of using sinusoidal input motions in seismic ground motion studies. Pulse, 1 cycle, 2 cycle, 5 cycle, and steady state sinusoidal wave forms were selected for the sinusoidal input motions. The specific objectives of the study are as follows:

1. Compare the peak surface accelerations induced in two ideal soil profiles by pulse, 1 cycle, 2 cycle, 5 cycle and steady state sinusoidal motions having the same maximum amplitude and frequency. Determine if any of the lesser cycle sinusoidal motions induce the same peak surface accelerations as one having a greater number of cycles.

2. Compare the peak surface accelerations induced in two ideal soil profiles and one field site profile by both earthquake records, and sinusoidal motions determined from the

outcome of Objective No. 1. Determine any similarities between the sinusoidal and earthquake induced accelerations.

Objective No. 1 serves to limit the number of different cycle sinusoidal motions used in the earthquake-sinusoidal comparisons of Objective No. 2. For example, if the results of Objective No. 1 find that the 5 cycle sinusoidal motion induces the same peak accelerations as the steady state sinusoidal motion, then only the pulse, 1 cycle, 2 cycle and 5 cycle sinusoidal motions would be compared with the earthquake records in Objective No. 2.

1.4 Thesis Organization

Chapter 2 provides a background for the study which includes a discussion of the various soil conditions, ground motion parameters, and other factors that influence the amplification of ground accelerations. Chapter 3 outlines the scope of the study. The computer program SHAKE-88 (Lysmer and Seed [24]), which is used to compute the peak surface accelerations in the study, is covered in Chapter 4. Chapter 5 is a discussion of results from SHAKE-88 using sinusoidal input motions, and Chapter 6 gives a comparative analysis using earthquake motions versus sinusoidal. A summary of the study with conclusions and recommendations is provided in Chapter 7.

2. BACKGROUND

2.1 General

Earthquakes induce vibratory motions in the ground and thus at the base or sides of structures that are supported by the ground. Seismic design involves determining the forces that will act on the structures due to the ground motion and designing structures to resist those forces. Two general approaches are used to determine seismic forces: an equivalent static force procedure and a dynamic analysis procedure (ASCE [2]).

The equivalent static force procedure incorporates seismic design codes to specify a static force that represents the earthquake load (Okamoto [29]). An estimate of anticipated peak ground motion values (e.g., acceleration) is usually all that is necessary for the procedure. However, this procedure does not account for all aspects of a structure's response to complex ground motion. In contrast, the dynamic analysis procedure analyzes the dynamic interaction between the structure and the surrounding soil. While it is a more complex and expensive design, a dynamic analysis can incorporate the earthquake's ground motion time-history to calculate structural vibration (ASCE [2]).

Two different dynamic analysis procedures are typically used for soil-structure interaction (SSI) analysis. One procedure models the soil-structure system as a series of springs and dashpots, the other procedure models the system using a finite element method (Seed, et al. [40]). The input motions for SSI analyses are typically applied in the surrounding soil, as shown in Figure 2.1.

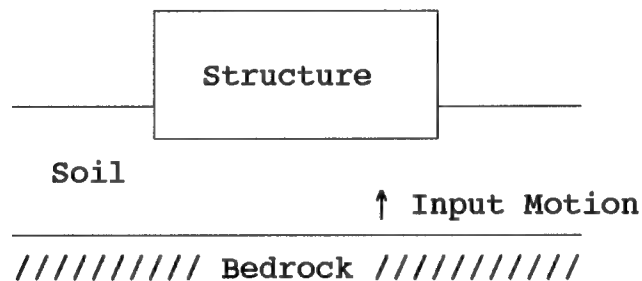


Figure 2.1: Typical SSI Schematic (after Seed, et al. [40])

Because structural response is dependent on ground motion characteristics, it is desirable in SSI analyses to have a time-history record of the ground motion likely to be experienced at the site during a major earthquake. In rare instances, an earthquake accelerogram already exists that is a suitable example of the worst shaking anticipated (i.e., an accelerogram recorded at the proper distance from an earthquake of the desired size and mechanism in a similar geologic setting). However in most cases, a suitable ground motion recording cannot be found, so artificially generated earthquake records, or modifications of either actual or

artificial earthquake records, are developed to use in SSI analyses. However, in using such records, there is almost always some uncertainty concerning the form of the ground motions likely to develop at the site (Seed and Idriss [37]). Thus, to obtain reliable results, the analysis is often made for not just one, but several earthquake records, representing a range of possible but realistic ground motions. This process brackets the range of expected design accelerations (Roesset [31]). Using lengthy earthquake records in this manner is often tedious and cost ineffective. These limitations warrant the development of simplified input motions to supplement or replace earthquake records for SSI analyses.

Sinusoidal motions, such as a single half-sine pulse, are a form of simplified motion that have been tried by researchers as input motions to SSI analyses (e.g., Siller [43]). While using sinusoidal motions are simpler and more economical than using full earthquake records, it is not known how well sinusoidal input motions imitate ground motions induced by actual earthquakes.

Site conditions are an important factor in ground motion studies and complicate efforts to analyze the effectiveness of sinusoidal motions. The soil filters ground motions by increasing their amplitude in some cases and decreasing it in others. The remainder of Chapter 2 discusses the various factors that influence accelerations in the ground.

2.2 Influence of Soil Conditions on Ground Motions

2.2.1 General

It has been recognized for many years that the surface geology of a site has a strong influence on the intensity of ground motions induced, and thus the intensity of the shaking that structures receive during an earthquake. Perhaps, the earliest recognition of this phenomenon was the observation that ground motions developed on soil deposits are usually greater than those occurring on adjacent rock outcrops (Seed and Idriss [37]). For instance, structural damage observed after an earthquake in India in 1819 was described as notably less for buildings situated on rock versus those situated on soil (Seed and Idriss [38]). It was not until the late 1960's when instrumental data became available for the study of several catastrophically damaging earthquakes of the 1950's and 1960's, that a basis was provided for an improved understanding of the influence of soils on earthquake induced ground motions (Seed [36]).

2.2.2 Propagation of Earthquake Waves

In an earthquake event, the sudden slip along all or part of a fault surface within the earth's crust or upper mantle releases elastic strain energy that has accumulated within the nearby rock (Ziony [48]). This released energy is radiated in the form of wave motions called earthquake waves. The vibrational earthquake waves are propagated through large distances in all directions away from the fault. As these

waves pass through an area they produce the shaking effects (ground motions) that are the predominant cause of earthquake damage.

Earthquake waves may be made up of two wave types: (1) Body Waves consisting of longitudinal waves (known as P-waves or compressional waves) and transverse waves (known as S-waves or shear waves), and (2) Surface Waves consisting of Rayleigh Waves and Love Waves (Okamoto [29]). The chief wave motions transmitted near the earth's surface are Surface Waves and transverse waves. Of the two types, transverse (shear) waves have the most influence on damage to structures. A shear wave displaces soil particles in a direction perpendicular to the direction of the wave (Richart, et al. [30]).

2.2.3 Site Soil Conditions

2.2.3.1 General

The soil deposit at a particular site has a variety of physical properties, commonly referred to as site soil conditions, which influence the ground motions that develop in the deposit during an earthquake. Among the site soil conditions considered to be the most influential on seismic response are the shear wave velocity, V_s , shear modulus, G , natural period, T , void ratio, e , layer thickness, depth to bedrock, and depth to water table. One, a few, or all of these soil conditions significantly influence ground motion behavior. Studies have not fully determined which ones have the predominant influence.

2.2.3.2 Shear Wave Velocity

The shear wave velocity, V_s , is the speed at which a shear wave travels through the ground. Shear wave velocity is dependent on the rigidity of the structure of a soil or rock mass and is controlled by the porosity of the structure and the forces holding the structure together, including cohesion, friction, cementation, and effective stress (Ziony [48]). Denser materials such as rock and well compacted soils have higher shear wave velocities than softer materials such as loose sands and soft clays. The shear wave velocity is thus a good indicator of the relative hardness or softness of a soil layer.

2.2.3.3 Shear Modulus

Soil strength is based on the shear modulus that controls the instantaneous response of a soil deposit (Finn [14]). The shear modulus, G , is proportional to the shear wave velocity and is calculated as follows (BOR [8]):

$$G = \rho V_s^2 = \frac{\gamma}{g} V_s^2 \quad (\text{EQ 2.1})$$

where: ρ = Soil Density
 V_s = Shear Wave Velocity
 γ = Unit Weight of Soil
 g = Acceleration of Gravity

A soil layer composed mainly of stiff cohesive soils might be considered to have a uniform shear modulus, but for a layer

composed mainly of cohesionless soils, the shear modulus will vary with depth (Idriss and Seed [19]).

2.2.3.4 Natural Period

Okamoto [29] states that the effect of transverse waves propagating through the soil is that the ground will vibrate with an appearance of dominant vibrations of certain specific periods. These periods are called the natural period of the ground and are determined by the composition of the surface layer. (Note: It is assumed for this study that Okamoto's reference to the "surface layer" refers to the soil layer(s) extending from the surface down to the base rock). The natural period, T (in seconds), for a surface layer comprised of a single soil layer of uniform character is calculated by the following equation (Kanai [22], Okamoto [29]):

$$T = 4H/V_s \quad (\text{EQ 2.2})$$

where: H = Thickness of Soil Layer

Equation 2.2 shows that for sites with the same layer thickness, longer natural periods are associated with softer soil sites due to their lower shear wave velocities. Also, for sites having the same shear wave velocity, thicker sites are associated with longer natural periods.

For a surface layer that consists of a number of different layers with little difference between the properties of the

various layers, Okamoto [29] indicates that the longest natural period of the surface layer may be determined from the following equation:

$$T = \sum (H_i / V_{si}) \quad (\text{EQ 2.3})$$

where: H_i = Thickness of each layer
 V_{si} = Shear wave velocity of each layer

The natural period can be used interchangeably with the natural frequency, f (Hz), which is the inverse of the natural period (i.e., $f = 1/T$).

2.2.4 Characteristics of Ground Motion

2.2.4.1 General

Ground motion is characterized by displacements, velocities, and accelerations which are erratic in direction, magnitude, duration, and sequence (BOR [8]). The severity of earthquake induced ground motion at a site depends mainly upon: (1) the magnitude of the earthquake (energy released), (2) the source mechanism (fault type), (3) the distance of the site from the fault, (4) the geology of the wave path, and (5) the local geologic conditions (e.g., soil conditions and topographic features) that either amplify or attenuate the earthquake waves (Okamoto [29]).

The severity of ground motion from an earthquake is characterized either qualitatively (e.g., the observed or expected effects of strong motion on man and structures) or

quantitatively (e.g., parameters that can be instrumentally recorded). The quantitative parameters next described (i.e., maximum amplitude, predominant frequency, duration of motion, and the response spectrum) are typically referred to as ground motion parameters (Idriss [17]). Schnabel, et al. [34] indicate that the maximum acceleration, predominant period (or predominant frequency), and effective duration are the most important parameters of an earthquake motion.

2.2.4.2 Maximum Amplitude

Maximum, or peak amplitude values of acceleration, velocity, and displacement are important parameters of earthquake motion and are commonly used in engineering design. The premise has been that the horizontal shaking force that is transmitted to a structure by the ground is a direct function of the ground surface acceleration (Okamoto [29], Mitchell, et al. [26]). Therefore, it is common practice to characterize the intensity of an earthquake by its maximum acceleration. Acceleration is typically expressed in percent of gravity (i.e., 20% of g , or $0.2g$) where g is the acceleration due to gravity, 32 ft/sec^2 (9.81 m/sec^2).

The essential instrument for observation of earthquake motion is the seismograph which records ground motion as a function of time in a format proportional to either acceleration, velocity, or displacement. A seismograph that records ground motion proportional to acceleration is termed

an accelerograph, and the record from an accelerograph showing acceleration as a function of time is termed an accelerogram.

2.2.4.3 Predominant Frequency and Duration of Motion

While the maximum ground acceleration is an important and popular parameter used in engineering, it alone does not determine the intensity of the shaking effects of ground motion. The frequency characteristics and duration of the ground motion are also important parameters (Seed [36]). Finding an accelerogram with a suitable frequency content is part of what makes selecting a representative input motion for SSI analyses a difficult task (Finn [14]).

Earthquake waves are nonperiodic and can have several different frequency components (Ohsaki [28]). By means of a Fast Fourier Transform (FFT), the nonperiodic earthquake motion can be represented as the sum of a series of sinusoidal wave components (Schanabel, et al. [34]). The wave component frequency that occurs most often is the predominant frequency of the earthquake motion. The predominant frequency is used interchangeably with the predominant period, which is the inverse of the predominant frequency.

The duration of motion is the length of time during which the earthquake induced ground shaking occurs. The duration of strong shaking, or significant duration, is the length of time that accelerations greater than about 0.05g occur (Benuska [4], Benuska [5]).

Seed and Idriss [37] relate two examples of how the ground motion's frequency content and duration can influence the intensity of shaking. During a 1966 earthquake near Parkfield, California, a (high) maximum ground acceleration of 0.5g was reached, but due to the earthquake's short duration and possible high frequency of motion, no significant structural damage occurred. In contrast, during a 1957 Mexico City earthquake, relatively small accelerations (0.05g to 0.1g) developed in the ground but continued for several seconds with a uniform frequency. This motion was able to build up large accelerations in multi-story structures and cause their complete collapse.

Studies have shown that the frequency characteristics of seismically induced motions change with increasing distance from an earthquake. As motions travel through the ground over long distances, the short period (high frequency) components tend to be filtered out, allowing the longer period (lower frequency) components of the motion to have the greater influence at a site (Kanai [22], Rosenblueth and Ovando [33], Solnes [45]).

2.2.4.4 Response Spectrum

The response spectrum reflects the combined influence of the ground motion's maximum amplitude, frequency components and, to some extent, duration, on different structures (Seed [36]). A response spectrum is defined as a plot of the maximum response induced by the ground motion on a series of

simple, single-degree-of-freedom (SDOF) oscillators (spring-mass systems) having different fundamental periods but the same degree of internal damping (Seed and Idriss [37]). In a typical plot, the response spectrum shows the variation of either peak spectral acceleration, velocity, or displacement of the oscillators as a function of oscillator fundamental period or frequency (Ziony [48]). If a structure behaves as a SDOF system and its fundamental period is known, the response spectrum provides a means of evaluating the maximum acceleration developed in the structure when subjected to a base motion (Seed [36]). The maximum acceleration is then used to determine the maximum lateral force on the structure. Response spectrums are used to determine the maximum lateral forces on multi-degree-of-freedom (MDOF) systems as well (Seed and Idriss [37]).

2.2.4.5 Number of Significant Cycles

In most seismic events, the number of significant cycles is likely to be less than 20 (Silver and Seed [44]).

Okamoto [29] studied the response of elasto-plastic systems due to external forces consisting of 3 sinusoidal waves. He indicates that there was not much difference between the response due to 3 sinusoidal waves, and that due to actual seismic waves. The explanation he gave was that, when damping becomes large in a system, only the waveform occurring in a short period of time at the initiation of the vibration has significant influence on the vibration.

2.2.5 Non-Linear Behavior of Soil

Most soils exhibit non-linear stress-strain properties when subjected to strong ground shaking or cyclic loading conditions such as those induced by an earthquake (Idriss, et al. [18]). The non-linear behavior of soils is strain dependent and determined primarily by the shear modulus and damping characteristics of the soil (Seed and Idriss [37]).

The soil's non-linear stress-strain characteristics are typically displayed in the form of a hysteresis loop as shown in Figure 2.2 (Idriss and Seed [19]). In order to obtain shear modulus and damping characteristics, the hysteresis loop can be represented by an equivalent bi-linear relationship as shown in Figure 2.3 (Idriss and Seed [19]). A similar method to obtain the same characteristics involves an equivalent linear analysis (shown in Figure 2.4), in which the equivalent shear modulus, G_{eq} , is identified by the slope of the line joining the peaks of the hysteresis loop, and the equivalent damping ratio, λ_{eq} , is determined by the following equation (Silver and Seed [44]):

$$\lambda = \frac{1}{2\pi} \frac{\text{Area of Hysteresis Loop}}{\text{Area of Triangles OAB + OCD}}$$

(EQ 2.4)

Because the shear modulus and damping ratio are strain-dependent properties, their values for high intensity (large strain) motions are significantly different than those for low

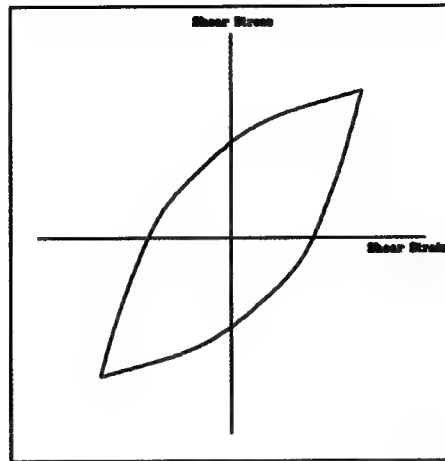


Figure 2.2: Hysteretic Stress-Strain Relationship for Soil (after Idriss and Seed [19])

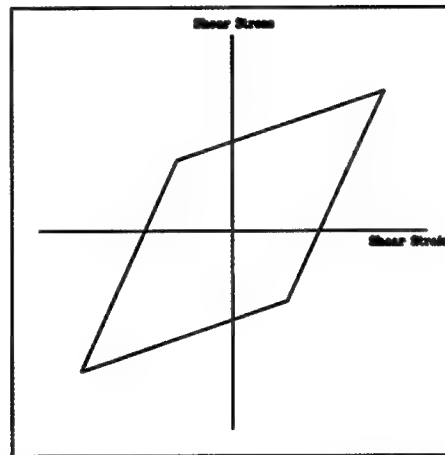


Figure 2.3: Equivalent Bi-Linear Stress-Strain Relationship for Soil (after Idriss and Seed [19])

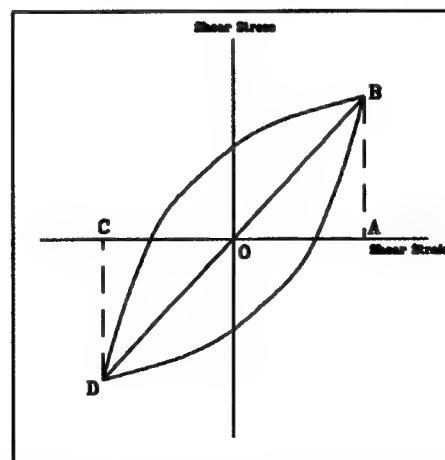


Figure 2.4: Equivalent Linear Parameters for Soil (after Silver and Seed [44])

intensity (small strain) motions. Silver and Seed [44] documented numerous shear modulus/shear strain relationships after conducting several dynamic simple shear tests on cohesive soils at varying numbers of cycles. Typically, their tests showed that for a constant confining pressure, a significant decrease in the shear modulus and a significant increase in damping occurred with increasing shear strain. Figures 4.1, 4.2 and 4.3 in Chapter 4 are examples of such relationships.

Some laboratory-based studies indicate that soils don't behave in a non-linear fashion until strain levels exceed about 10^{-5} (0.001 %) (Ziony [48]). Other studies indicate that the non-linear behavior does not occur until strain levels exceed 10^{-4} (0.01 %) or even 10^{-3} (0.1 %) (Finn [14]). With respect to acceleration levels, Finn [14] also indicates that in the 1989 Loma Prieta earthquake, nonlinear effects became significant in the acceleration range 0.1g to 0.3g. Regardless of which strain level is more accurate, soils apparently behave linearly (and nondestructively) at lower strain levels where there is small relative movement between soil particles and soil strength is maintained (NRC [27]). At the higher strain levels where the nonlinear stress-strain behavior becomes pronounced, the larger relative movement between soil particles results in a decrease in soil strength (as reflected by the decrease in shear modulus) and an increase in damping (as reflected by the increase in the

damping factor). The soil is then said to behave inelastically.

2.2.6 Amplification of Ground Motion by Soil Layers

2.2.6.1 General

In relation to ground motion studies, amplification is an increase in seismic wave signal amplitude within some range of frequency (or period) as waves propagate through different Earth materials (Ziony [48]). Deamplification (or attenuation) refers to a decrease in the signal. An "amplification factor" is often referred to as the ratio of the peak acceleration occurring at the ground surface to that of the incident motion (e.g., base rock motion). The amplification factor usually ranges from 1 to 4, although its value may be less than 1 since it is also possible for soil deposits to attenuate underlying rock motions.

Researchers have found that at approximately 0.4g, a boundary exists between amplification and attenuation of rock motions by soils, as shown in Figure 2.5 (Finn [14]).

Amplification of the base rock motion may or may not be induced in a soil deposit based on the dynamic characteristics and thickness of the soil, and also on the amplitude and frequency characteristics of the base motions (Seed [36]). The remainder of this section addresses how some of the different soil conditions and ground motion parameters introduced in Sections 2.2.3 and 2.2.4 respectively, influence amplification.

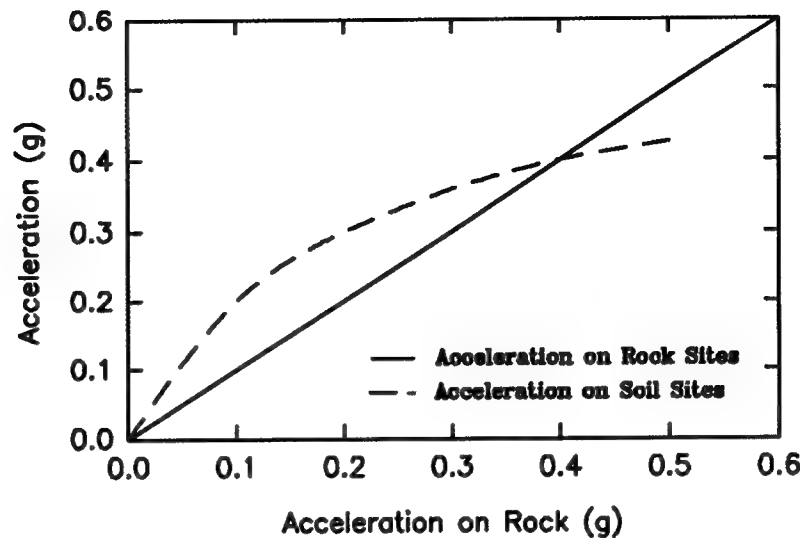


Figure 2.5: Acceleration on Soil & Rock Sites (after Finn [14])

2.2.6.2 Natural Period or Frequency Influences

In general, the amplifying effects of a soil deposit on base accelerations are greatest when the predominant period of the base motion coincides with the natural period of the deposit (Kanai [22], Rosenblueth and Ovando [33]). This is a phenomenon known as resonance. The peak response will not always be generated at the natural period of the site however (Finn [14]). In some cases the peak may develop at or close to the predominant period of the base rock motion (Seed and Idriss [37]).

An example of period dependent spectral response of six different sites is documented by Seed and Idriss [37]. The six sites had varying degrees of stiffness and were located at similar distances from earthquakes of like magnitude. The response spectrum ordinates were normalized (i.e., each

spectral acceleration was divided by the maximum ground acceleration) to eliminate the influence of the different spectral acceleration values occurring at the different sites. The normalized response spectra for the sites showed that as the ground conditions became progressively softer, the period at which the peak spectral response developed increased. This example showed that the softer sites, which exhibited longer natural periods, developed a greater amplification of base accelerations having predominantly longer period (lower frequency) characteristics. The stiffer sites, which exhibited shorter natural periods, developed a greater amplification of base accelerations having predominantly shorter period (higher frequency) characteristics. According to Seed and Idriss [37], the structural significance of such results is that stiff structures (those with short fundamental periods) that are constructed on stiff soil sites could be severely affected by an earthquake. In contrast, adjacent structures with longer fundamental periods (such as tall buildings) that are constructed on the same stiff soil deposit may be only slightly affected. Likewise, long period structures on soft soil deposits may be severely damaged by an earthquake, while short period structures on the same soft deposit may be only slightly influenced.

Amplification is generally greater at soil sites than at rock sites by a factor of 2 to 3 for base motions with periods

longer than 0.2 seconds (Aki [1], Su, et al. [46]). The relation is reversed for periods shorter than 0.2 seconds.

2.2.6.3 Shear Wave Velocity Influences

Generally, the amplification at the surface of a soil deposit tends to increase with a decrease in the deposit's shear wave velocity (Kanai [22], Borchardt and Glassmoyer [6]). As a result, damage at sites underlain by unconsolidated soils is often greater than that of sites underlain by consolidated soils. Amplification also typically decreases with increasing geological age since older deposits are usually more compact and competent, and thus have higher shear wave velocities (Ziony [48], Su, et al. [46]). It was stated in Section 2.2.4.3 that as distance from the epicenter increases, the earthquake's longer period components have the greater influence. Therefore, the above relationships are partly explained by EQ 2.2, which indicates that longer period sites are associated with lower shear wave velocities, and vice versa.

2.2.6.4 Influence of Deposit Thickness

Kanai [22] indicates that when the rigidity of the surface layer is constant, the amplification at the ground surface increases as the layer becomes thicker. Once again, at distances where the earthquake's longer period components have the greater influence, the above relationships can be partly explained by EQ 2.2, which indicates that longer period sites are associated with thicker deposits, and vice versa.

Earthquake induced ground motions tend to vary considerably with depth. Data collected in the basements of buildings in downtown Tokyo during a 1968 earthquake showed that maximum accelerations for structures founded near the ground surface were approximately 4 times larger than those recorded for buildings founded at depths of about 80 ft (24 m) (Seed, et al. [40]). Seed [36] indicates that soil properties at a depth of about 200 to 300 ft (61 to 91 m) have little influence on the characteristics of surface motions, while soil properties in the upper 200 ft are of most significance. Finn [14] reports that surface motions for the Treasure Island site in the 1989 Loma Prieta earthquake were modified significantly by the near surface sediments located at depths of less than 66 to 98 ft (20 to 30 m).

2.2.6.5 Base Acceleration Influence

Studies indicate that there is a marked reduction in amplification factor at the soil surface with increasing levels of base rock acceleration (Seed and Idriss [37], Ferritto [13]). Ziony [48] indicates that amplification factors usually range from 1 to 2 for strong motions to 10 or greater for microtremors. In the central Bay Area during the 1989 Loma Prieta earthquake, relatively modest peak acceleration levels (0.06g to 0.12g) on rock produced peak ground surface accelerations on soft bayshore sites that were amplified approximately 2 to 3 times (Seed, et al. [41]). After the main shock, amplifications of peak surface

accelerations were even more pronounced (4 to 8 times higher) for low level aftershock recordings.

The phenomena described above are caused by non-linear soil response, which is one reason why amplification factors measured during small earthquakes (microtremors) cannot be applied directly to predict performance during large earthquakes (Finn [14]).

2.2.6.6 Non-Linearity Influences

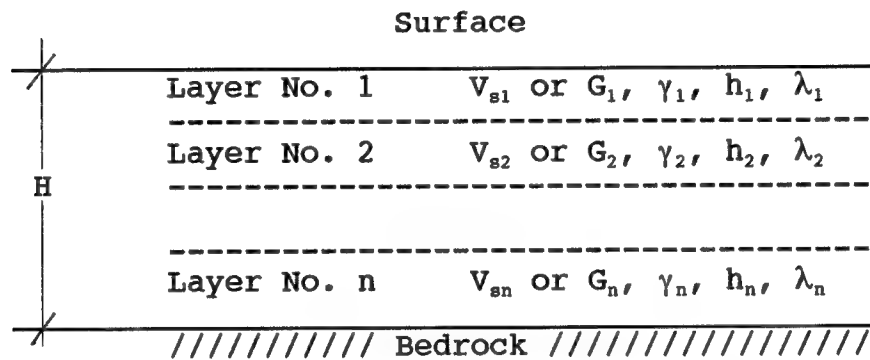
The non-linear stress-strain behavior of most soils causes amplification factors to decrease with increasing strain levels (Seed and Idriss [37]). Basically, the decrease in shear modulus with increasing strain tends to cause increased wave amplitudes, although the increase in damping (which tends to cause decreased wave amplitudes) has the dominant effect (Ziony [48]).

2.2.7 Analytical Procedures for Determining Ground Motions in Horizontal Soil Deposits

2.2.7.1 General

In many cases the ground motions developed near the surface of a soil deposit during an earthquake may be attributed primarily to the upward propagation of shear waves from an underlying rock formation (Idriss and Seed [19]). Analytical procedures have been developed for determining ground response under these conditions. The method of analysis depends on whether the soil deposit has horizontal or sloping boundary conditions.

For cases where all boundaries (e.g., ground surface, interface between any two sublayers, and base rock surface) of a soil deposit are essentially horizontal, the soil may be treated as a series of semi-infinite layers as shown in Figure 2.6 (Schnabel, et al. [34], Kausel and Roesset [23]).



V_s = Shear Wave Velocity
 G = Shear Modulus
 γ = Unit Weight of Soil
 h = Soil Layer Thickness
 λ = Damping Ratio
 H = Deposit Thickness = $\sum h$

Figure 2.6: Semi-Infinite Soil Layers (after Schnabel, et al. [34])

Semi-infinite means that each layer is assumed to extend infinitely in the horizontal direction so that the lateral extent of the deposit has no influence on the response. Other assumptions included in this approach are that the induced ground motions are the result of shear deformations only, all displacements are horizontal, and each layer is homogeneous and isotropic (Schnabel, et al. [35]). The computer program

SHAKE (Schnabel, et al. [34]) incorporates an analytical procedure for horizontal soil layers.

If a deposit has irregular or sloping boundaries, it can no longer be treated as a series of semi-infinite layers, and more complex analytical procedures (e.g., a finite element method which accounts for the two-dimensional aspects of the problem) are required (Idriss, et al. [18]).

Two methods are typically used to analyze ground response under horizontal soil conditions: (1) an analysis based on the use of the wave equation, and (2) an analysis in which the soil deposit is represented by a lumped mass system (Schnabel, et al. [35]). Analysis of simple soil profiles using similar soil characteristics and base rock motions indicate that wave propagation and lumped mass analyses give essentially the same values of ground surface motions.

2.2.7.2 Wave Equation Analysis

The computer program SHAKE (Schnabel, et al. [34]) uses the wave equation method of analysis. In this method, the soil comprising each layer is considered to have uniform properties and the motion in the underlying bedrock consists of a series of sinusoidal motions of different frequencies. The surface response is then computed by (Roesset [31]):

- a) obtaining the Fourier transform of the input motion.
- b) multiplying it by the Transfer function of the soil.
- c) obtaining the inverse Fourier transform of the resulting function.

2.3 Seismic Building Code Provisions

2.3.1 General

The seismic provisions of most building codes (e.g., UBC (ICBO [21]), BOCA (BOCA [7]), ASCE 7-88 (ASCE [2])) specify seismic loads and forces to be used in an equivalent static force procedure, with some guidance given for a dynamic analysis. This simplification is used primarily because the traditional equivalent static force procedure is less complex and is still valid for a majority of building designs. However, complaints from the engineering community regarding the current code provisions indicate that a shift in emphasis from an equivalent static force procedure to a dynamic analysis procedure may be necessary (Whitman [47]). This trend supports the development of simplified input motions (e.g., sinusoidal motions) for SSI analyses.

2.3.2 Problems with Current Code Provisions

The seismic provisions of most building codes account for the influence of site soil conditions through a single site factor, S . The site factor is used in a formula specified by the code to compute the shear at the base of a structure. The ASCE 7-88 code uses the following formula (ASCE [2]):

$$V = ZIKCSW \quad (\text{EQ 2.5})$$

where: V = the total lateral force or shear at the base
 Z = seismic zone coefficient
 I = occupancy importance factor
 K = horizontal force factor
 C = indefinite
 S = soil factor
 W = the total dead load

Depending upon the code, there are 3 to 5 values of S ranging from 1.0 to 2.0 that are based on broad categories of soil conditions. Regarding efforts to improve estimates of seismic demand on structures, nothing better than site factors has been developed over the last 40 years (Finn [14]).

According to several workshops and committees supported by the National Center for Earthquake Engineering Research, there have been a large number of complaints from the engineering community regarding the present seismic provisions (Whitman [47]). The complaints indicate that the current specifications are incapable of properly dealing with site effects and present difficulties when attempts are made to classify sites according to the present site factor categories.

2.3.3 Alternatives to Current Code Provisions

According to a 1991 Site Effects Workshop, the present arrangement of 3 to 5 site categories is overly simplistic and should be overhauled (Whitman [47]). The workshop participants concluded that the actual non-linear behavior of soils can be captured only through dynamic analyses using a time-history of ground motion (e.g., an accelerogram) as input, and agreed that several motion time-histories (at least 3 or 4) should be used for each building. The attendees also indicated that the use of dynamic analysis employing time-history of motion for input is increasing. They predicted that by the year 2000, the use of such analyses will be much

more widespread. Additionally, they recommended that guidelines and standards be developed for future building codes that define a satisfactory dynamic analysis.

One possible alternative to the current code provisions could be the use of a series of simple input motions that a structure would have to withstand. Several problems arise, however, with this alternative: What is a representative series of simple motions, and what is the cost of a fully dynamic analysis of structural response to these motions? If the use of simple motions can be justified, then the dynamic analysis may become more realistic for a wider range of structures.

3. THESIS SCOPE

3.1 Scope of Research

The computer program SHAKE-88 (Lysmer and Seed [24]) is used in this study to compute the peak surface accelerations developed in three different soil-rock system profiles when subjected to sinusoidal and earthquake input motions. The peak surface accelerations are normalized by dividing each one by the peak acceleration of the input motion. The normalized peak surface accelerations, or "amplification factors," are then plotted against the predominant frequency of the input motion. A comparative analysis of the sinusoidal and earthquake induced peak surface accelerations is made by comparing the shapes of the amplification factor versus predominant frequency plots.

3.1.1 Selected Input Motions

The input motions selected for use in this study consist of sinusoidal motions and earthquake accelerograms as identified in the next two sections.

3.1.1.1 Sinusoidal Input

The sinusoidal motions selected for this study consist of half sine wave pulses and 1 cycle, 2 cycle, 5 cycle and multi cycle (steady state) sine waves as shown in Figure 3.1.

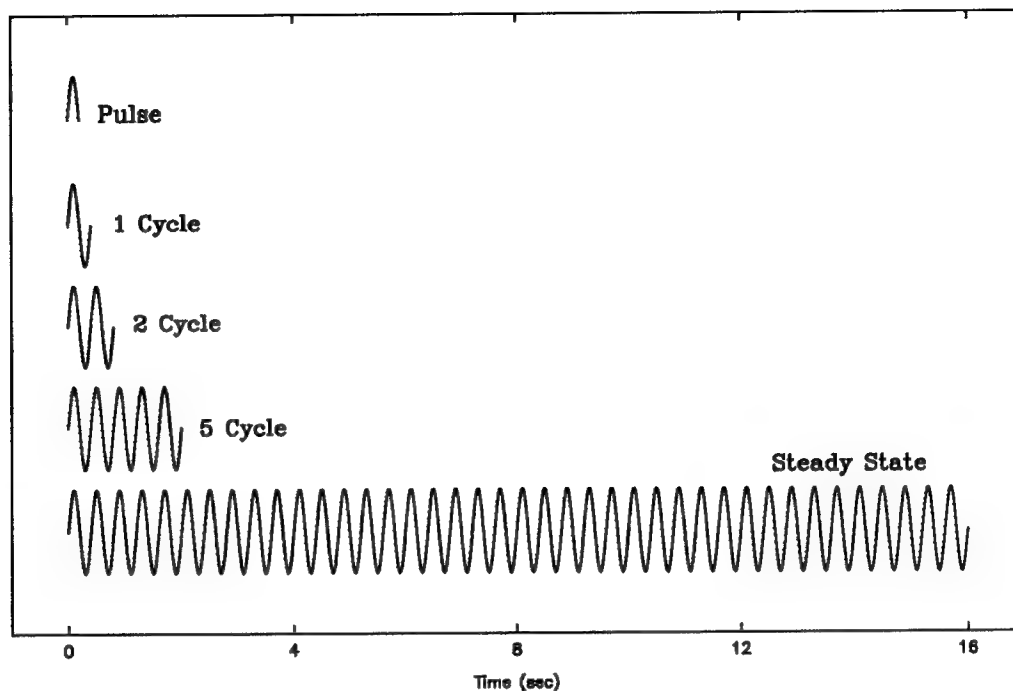


Figure 3.1: Sinusoidal Input Motions

The sinusoidal motions shown in Figure 3.1 are used in this study at the following frequencies:

0.5 Hz	2.0 Hz	4.0 Hz
0.75 Hz	2.5 Hz	5.0 Hz
1.0 Hz	3.0 Hz	6.5 Hz
1.5 Hz	3.7 Hz	

and at the following maximum amplitudes:

0.2g
0.4g
0.6g

In addition to the above frequencies and maximum amplitudes, the sinusoidal motions are also used at frequencies and maximum amplitudes that match the predominate frequencies and maximum accelerations of the earthquake

records described in the next section. The sinusoidal motions are defined by digitized acceleration values at equal spacing. Modeling of the sinusoidal motions is addressed in Chapter 5.

3.1.1.2 Earthquake Input

Ten different earthquake accelerograms obtained from Lysmer and Seed [25] are used in this study and are shown in Figure 3.2. All but the Pasadena 1952 accelerogram were recorded during the 1989 Loma Prieta Earthquake. Table 3.1 summarizes for each accelerogram the maximum acceleration, predominant frequency, and estimated duration of strong shaking for accelerations greater than 0.05g and 0.02g. The maximum accelerations and predominant frequencies were computed by SHAKE-88. CSMIP [9] and Shakal, et al. [42] contain a few of the accelerograms shown in Figure 3.2, so they were used to check some of the parameters in Table 3.1.

The Pasadena 1952 accelerogram in Figure 3.2 is defined by 800 digitized acceleration values at 0.02 second spacing. The 9 Loma Prieta accelerograms in Figure 3.2 are each defined by 2000 digitized acceleration values at 0.02 second spacing.

In addition to the as-recorded accelerograms of Figure 3.2, altered accelerograms are also used which have predominant frequencies and maximum accelerations that match the frequencies and maximum amplitudes of the sinusoidal motions listed in the previous section.

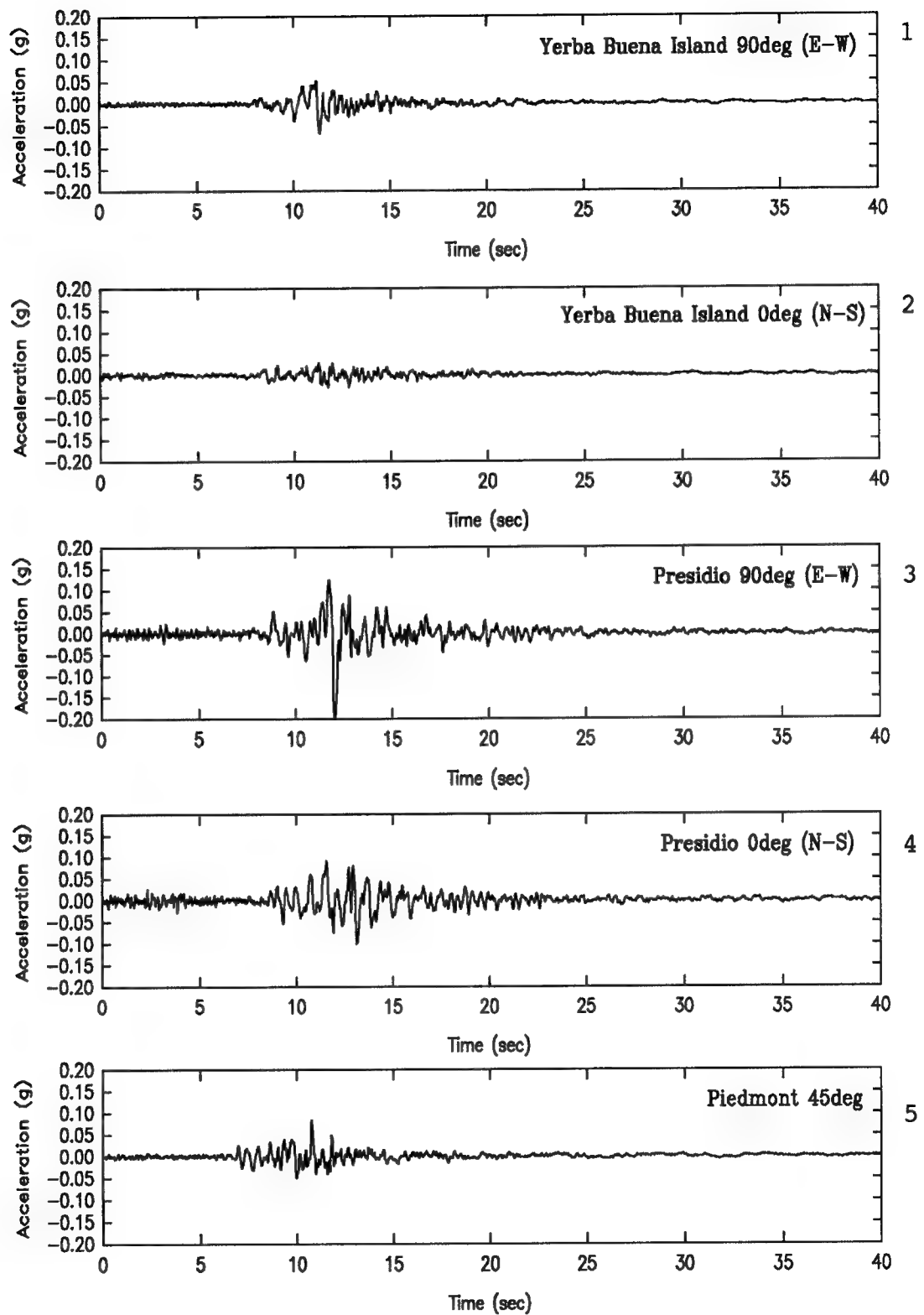


Figure 3.2: Accelerograms (after Lysmer and Seed [25])

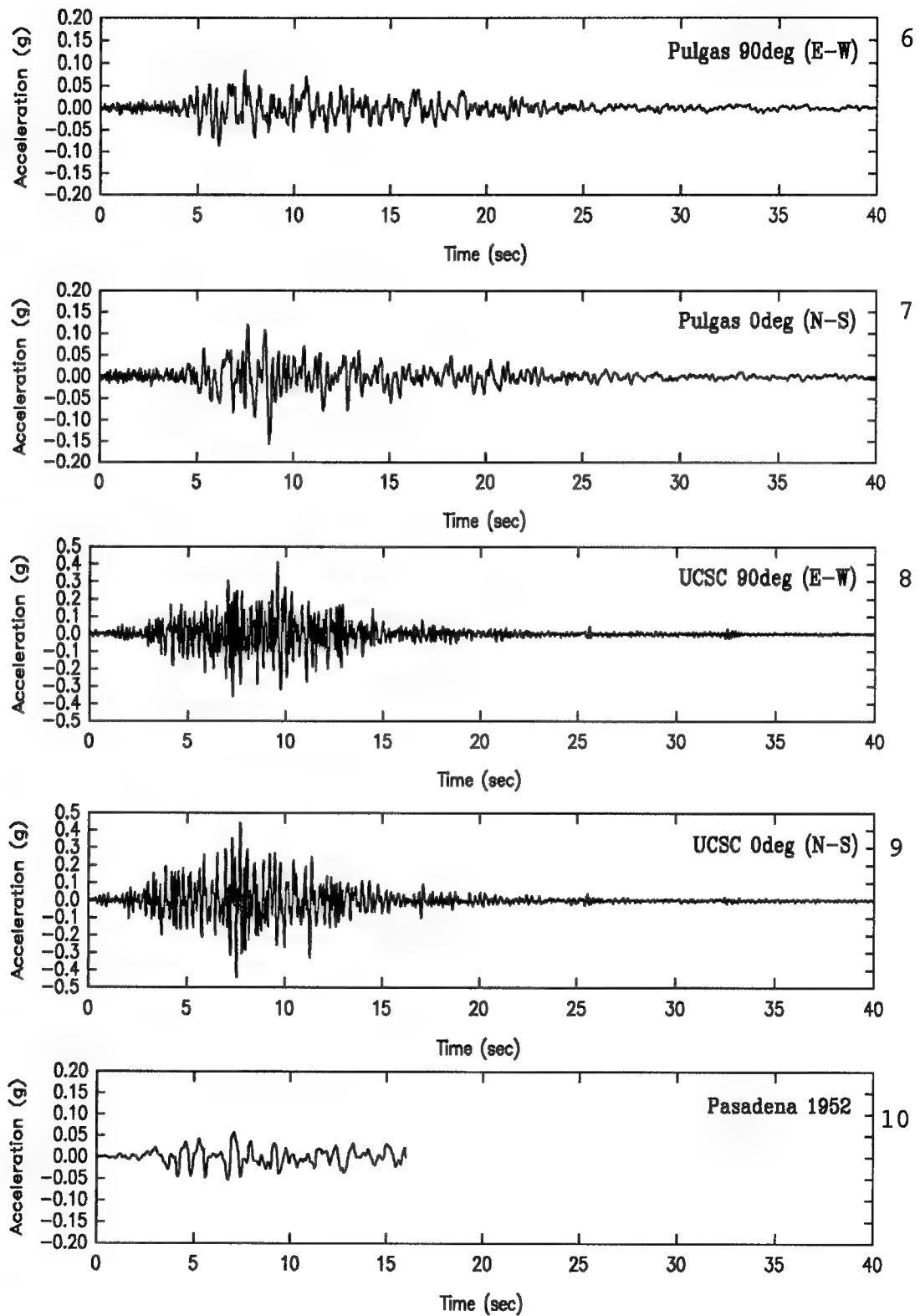


Figure 3.2 (Cont'd): Accelerograms (after Lysmer, et al. [25])

Table 3.1: Accelerogram Parameters (after Lysmer, et al. [25])

	Earthquake	Max Accel (g)	Predom Freq (Hz)	Duration of Strong Shaking (sec)	
				$\geq 0.05g$	$\geq 0.02g$
1	Yerba Buena Is. (E-W)	0.07	2.15	0.5	6
2	Yerba Buena Is. (N-S)	0.03	2.87	0	4
3	Presidio (E-W)	0.20	1.88	6	19
4	Presidio (N-S)	0.10	2.16	5	19
5	Piedmont, 45 deg	0.08	2.61	2	7
6	Pulgas (E-W)	0.09	2.42	8	18.5
7	Pulgas (N-S)	0.16	2.48	10	20
8	UCSC (E-W)	0.41	5.95	16	32.5
9	UCSC (N-S)	0.44	4.74	16.5	32
10	Pasadena 1952	0.06	1.59	0.5	13

3.1.2 Selected Soil Profiles

The soil profiles selected for use in this study consist of two hypothetical "ideal" profiles and one field site profile as identified in the next two sections.

3.1.2.1 Ideal Soil Profiles

One of the two ideal soil profiles models a 50 ft (15 m) clay layer underlain by base rock, while the other models a 50 ft sand layer underlain by base rock. Modeling of the ideal soil profiles is addressed in Chapter 4.

3.1.2.2 Field Site Profile

The field site profile selected for this study models a site located at Treasure Island in San Francisco Bay. The

Treasure Island site is referred to as "University of Michigan No. 10" or "UM10" (Seed, et al. [41]). Modeling of the UM10 field site profile is addressed in Chapter 4.

4. COMPUTER PROGRAM SHAKE

4.1 General Description of SHAKE

The computer program SHAKE (Schnabel, et al. [34]) computes the response in a horizontally layered (one-dimensional) soil-rock system subjected to transient, vertical travelling shear waves. The program is based on the continuous solution to the wave equation and is adapted for transient motions through the Fast Fourier Transform (FFT) algorithm.

SHAKE-88 (Lysmer and Seed [24]) is an updated version of SHAKE, and is the version used in this study. The main difference between SHAKE-88 and SHAKE is that SHAKE-88 can accommodate up to 13 different soil shear modulus and damping versus shear strain relationships, where as SHAKE can only accommodate 3 different relationships.

In computing the response of a soil deposit to base-rock motions, SHAKE uses the equivalent linear method (a linear analysis) to account for the non-linearity of the soil's shear modulus and damping with shear strain (Schnabel, et al. [34]). Under this method, SHAKE adjusts the modulus and damping, iteratively, until there is consistency between these values and the computed shear strains (NRC [27], Kausel and Roesset [23]).

The basic operations that SHAKE performs to calculate the response of a soil deposit to the base motions in the underlying rock are as follows (Schnabel, et al. [34], Idriss and Seed [20]):

- 1) Read the input motion (acceleration-time history).
- 2) Read the soil deposit properties for each layer, including the shear modulus and damping curves, and the small-strain shear modulus and damping values.
- 3) Compute the maximum shear stresses and strains in the middle of each layer.
- 4) Reduce the maximum strains to average effective strains. In general, the ratio of average effective strain to maximum strain is approximately $2/3$ (67 %) (Idriss, et al. [18], Seed, et al. [39]).
- 5) Compute new values for the shear modulus and damping based on the average effective strain. The operation of steps 3, 4 and 5 is repeated (an iterative procedure) until strain-compatible soil properties (i.e., shear modulus and damping) are obtained within the specified error limit or until a specified maximum number of iterations is reached.
- 6) Compute the new motions at the top of any specified layer in the soil profile.

4.2 Organization of Input Data

4.2.1 Input Data File

To run the SHAKE program, an input data file must be created which comprises the instruction set to activate various 'options' available (16 total) in the program. The instructions written in the input data file are organized by option number, such that Option 1 instructions activate program Option 1, Option 2 instructions activate program Option 2, etc.

The program options (and their functions) selected for this study are indicated below in the sequence they appear in the input data file:

- Option 1 - Read input motion.
Find maximum acceleration of input motion.
Scale values of input motion if desired.
Compute predominant period of input motion.
- Option 8 - Read relations between dynamic soil properties and strain (shear modulus and damping curves).
- Option 2 - Read soil profile data (i.e., V_s or G , γ , h , λ , etc. for each layer).
Compute natural period of deposit.
- Option 3 - Assign the input motion to top of a specified layer.
- Option 4 - Iterate to obtain strain compatible soil properties.
- Option 5 - Compute new motions at the top of specified layers (e.g. peak acceleration).
- Option 9 - Compute response spectra for any specified motion.
- Option 0 - Stop, no more data.

4.2.2 Input Motion

The input motion is defined in Option 1 of the input data file as digitized acceleration values (in g's) of equal time intervals. The program's use of the FFT requires that the number of terms in the Fourier series be specified in the input data file as some power of 2 (e.g., 1024, 2048, etc.) and that the number of terms be greater than the number of acceleration values contained in the input motion record (Schnabel, et al. [34]). The input motion can be assigned to any layer of the soil-rock system via Option 3. For this study, the input motion is always assigned to the base of the soil deposit (i.e., at the soil-rock interface).

4.2.3 Dynamic Soil Properties

The normalized shear modulus and damping as a function of shear strain relationships are the dynamic soil properties defined in Option 8 of the input data file. Such relationships have been established for several soil types as illustrated in Figures 4.1 and 4.2 (Lysmer and Seed [24]), and Figure 4.3 (Ferritto [13]).

Figure 4.1 shows the normalized shear modulus, G/G_{\max} , (top graph) and damping (bottom graph) versus shear strain relationships for four cohesive soils (C1 to C4) with different Plasticity Index (PI) values. The PI is based on the amount of water required to transform a remolded soil from a semisolid to a liquid state (Ferritto [13]).

Figure 4.2 shows the normalized shear modulus (top graph) and damping (bottom graph) versus shear strain relationships for three cohesionless soils (S1 to S3) with different mean effective stresses (σ'_m) acting on the soils. The damping versus shear strain relationships are the same for all three cohesionless soils.

Figure 4.3 shows the normalized shear modulus (top graph) and damping (bottom graph) versus shear strain relationships for Bay Mud, Old Bay Sediments, and sand at Treasure Island in San Francisco Bay. The three normalized shear modulus curves, and the damping curves for the Bay Mud and sand, were given in Ferritto [13]. However, a damping curve for the Old Bay Sediments was not provided in Ferritto [13]. Referring to Figure 4.3, since the normalized shear modulus curve for the Old Bay Sediments lies in between the sand and Bay Mud curves, and since it is reasonably similar in shape to the sand curve, it was assumed for this study that the damping curve for the Old Bay Sediments would also lie in between the sand and Bay Mud curves, and it would be similar in shape to the sand curve. This assumption for the Old Bay Sediments damping curve resembles the damping curve for the sands in Figure 4.2. Therefore, the damping curve in Figure 4.2 was used in Figure 4.3 to represent the damping with shear strain relationship for the Old Bay Sediments.

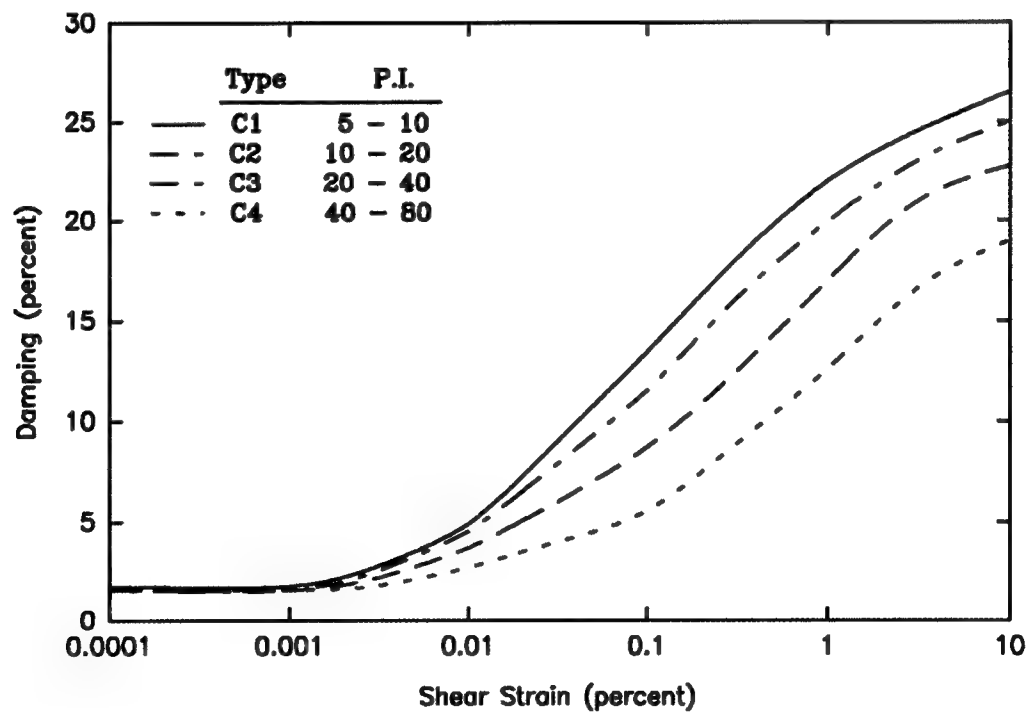
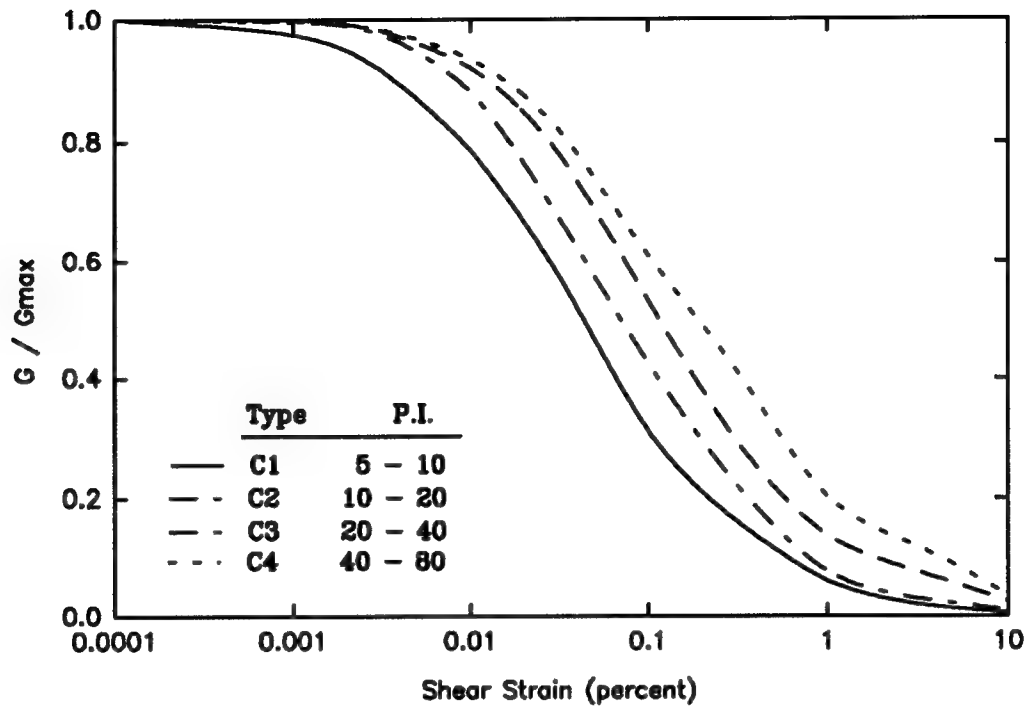


Figure 4.1: Normalized Shear Modulus and Damping - Cohesive Soils (after Lysmer and Seed [24])

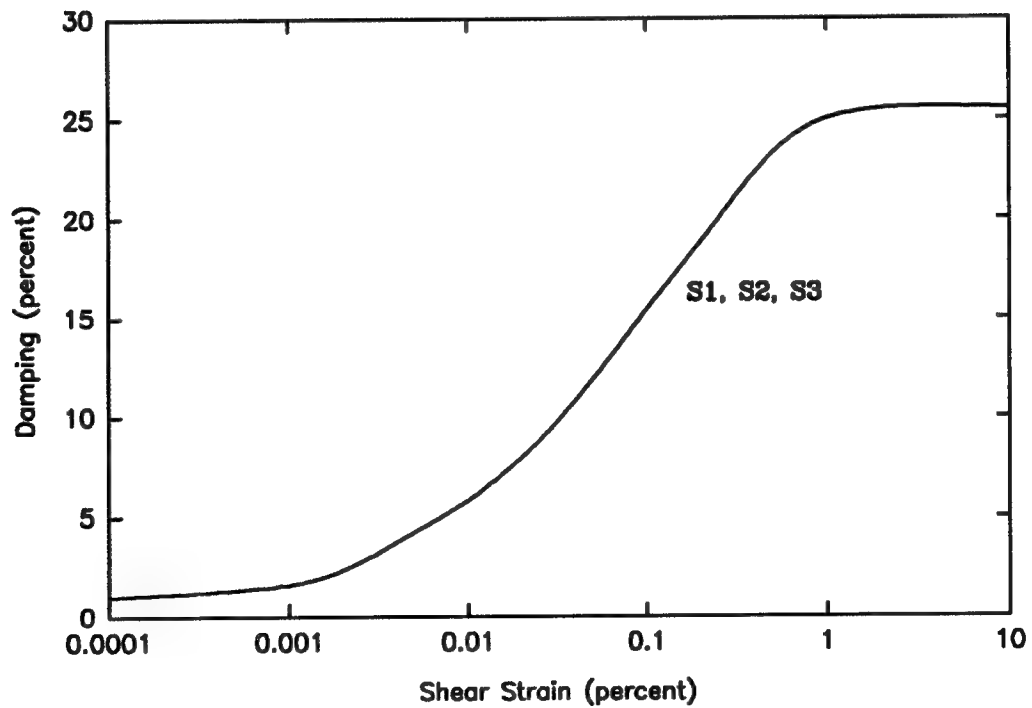
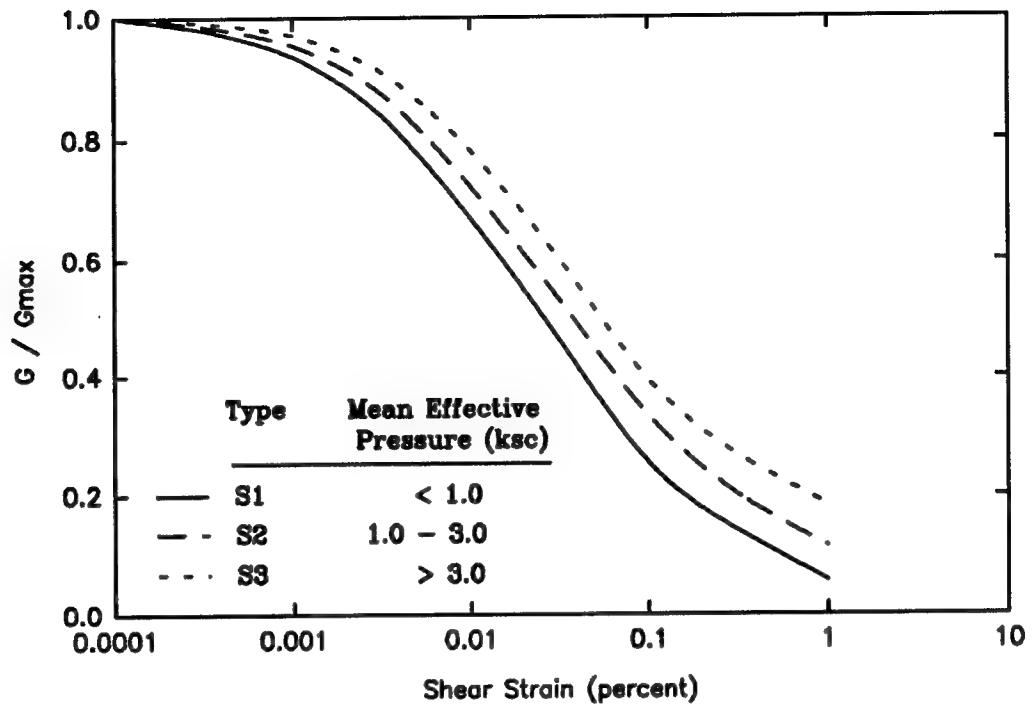


Figure 4.2: Normalized Shear Modulus and Damping - Cohesionless Soils (after Lysmer, et al. [24])

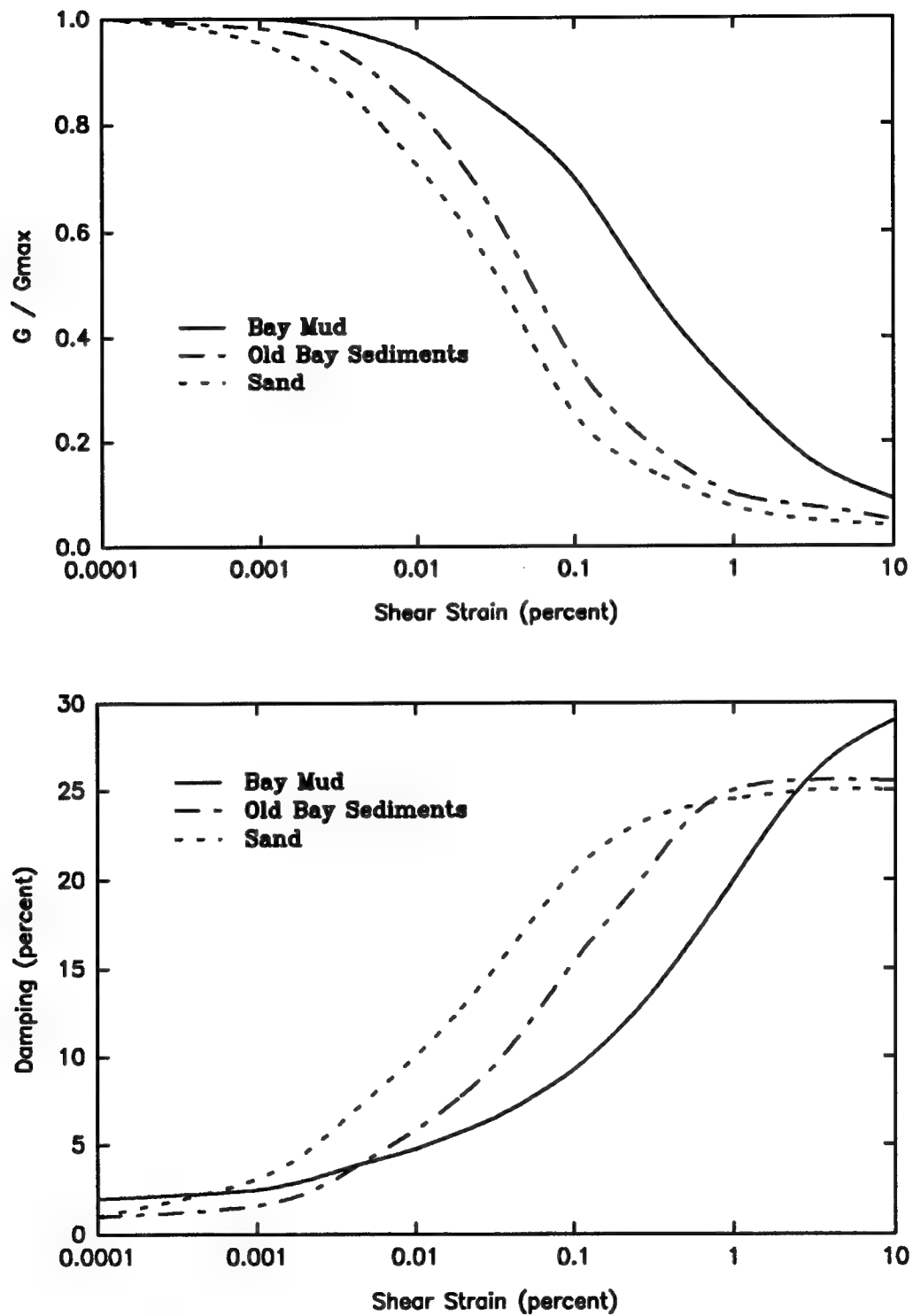


Figure 4.3: Normalized Shear Modulus and Damping - Treasure Island Soils (after Ferritto [13])

4.2.4 Soil Profile Modeling

4.2.4.1 General

This section addresses modeling of the ideal clay and sand profiles and the Treasure Island site profile introduced in Chapter 3.

Profile soil properties, other than the dynamic soil properties specified in Option 8, are defined in the input data file under Option 2. Each soil profile is treated as a series of horizontal, semi-infinite layers as shown in Chapter 2, Figure 2.6. Soil properties required for each layer are the shear wave velocity or shear modulus, unit weight, layer thickness, and damping ratio. SHAKE-88 automatically calculates the shear modulus (assumingly using Equation 2.1) if the shear wave velocity is given. SHAKE-88 requires that the soil properties for each layer be for small strains, and that they be defined in the units indicated in Table 4.1 (Schnabel, et al. [34]):

Table 4.1: Soil Property Units for SHAKE (after Schnabel, et al. [34])

Soil Property	Units
Shear Wave Velocity, V_s	ft/sec (fps)
Shear Modulus, G	kips/sq ft (ksf)
Unit Weight, γ	kips/cu ft (kcf)
Layer Thickness, h	ft
Damping Ratio, λ	decimal

4.2.4.2 Ideal Clay Profile

The hypothetical clay profile selected for this study is modeled as a 50 ft (15 m) clay deposit over bedrock, as shown in Figure 4.4. The shear wave velocity, unit weight, and damping ratio selected for the clay and rock are indicated in the figure. The natural period of the clay deposit is 0.27 seconds calculated from Equation 2.2. The corresponding natural frequency of the clay deposit is 3.7 Hz. The clay deposit's corresponding small strain shear modulus, calculated from Equation 2.1, is 1,986 ksf (951×10^5 kN/m²). The corresponding shear modulus of the bedrock is 32,828 ksf ($15,718 \times 10^5$ kN/m²).

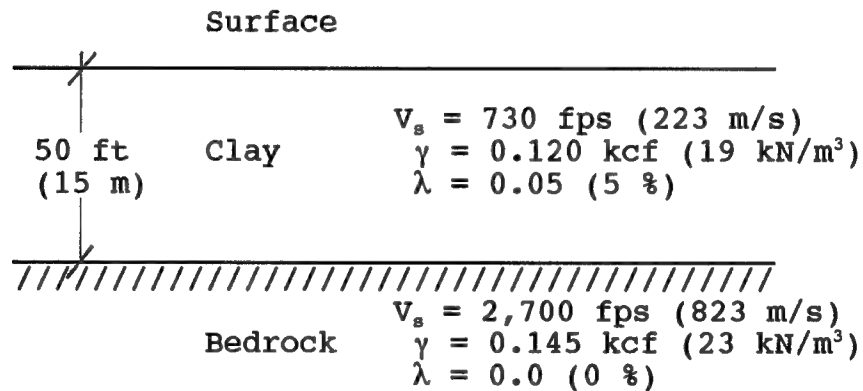


Figure 4.4: Ideal Clay Profile

The shear modulus and damping versus shear strain relationships selected for the clay are those indicated by curve C1 in Figure 4.1.

4.2.4.3 Ideal Sand Profile

The hypothetical sand profile selected for this study is modeled as a 50 ft (15 m) sand deposit over bedrock, as shown in Figure 4.5. The shear wave velocity, unit weight, and damping ratio selected for the sand and rock are indicated in the figure. The corresponding small strain shear modulus, natural period, and natural frequency of the sand deposit are 2,485 ksf ($1,190 \times 10^5$ kN/m²), 0.25 seconds, and 4.0 Hz respectively. The corresponding shear modulus of the bedrock is identical to that of the bedrock in the clay profile.

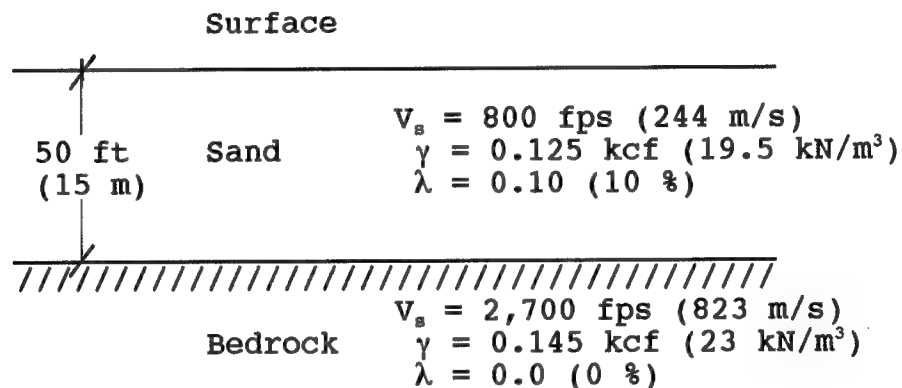


Figure 4.5: Ideal Sand Profile

For sand, SHAKE requires that the sand's relative density and the coefficient of lateral earth pressure, K , be identified. Respective values of 75 % and 0.45 were selected.

The shear modulus and damping versus shear strain relationships selected for the sand are those indicated by curve S2 in Figure 4.2.

4.2.4.4 Treasure Island UM10 Field Site Profile

The field site profile used for this study models a site at Treasure Island in San Francisco Bay, identified as University of Michigan No. 10 (UM10) (Seed, et al. [41]). The UM10 site is also a strong motion recording station and recorded the surface accelerations in the 0 degree (N-S) and 90 degree (E-W) directions during the 1989 Loma Prieta Earthquake.

In developing the UM10 profile for this study, soil properties of the site were first obtained from De Alba, et al. [12], Ferritto [13], Hanks and Brady [15], Rogers and Figuers [32], Seed, et al. [41], and SRTSH [11], to prepare a preliminary profile of UM10. Using SHAKE-88 (Lysmer and Seed [24]), the preliminary UM10 profile was then subjected to input motions at the base of the soil column using the E-W and N-S Yerba Buena Island (YBI) accelerograms (Lysmer and Seed [25]) from the 1989 Loma Prieta Earthquake. The two YBI accelerograms are shown in Chapter 3, Figure 3.2. Because Yerba Buena Island is a rock outcrop of the base rock underlying man-made Treasure Island, the rock motion recorded at Yerba Buena Island is believed to be very close to the base rock motion that actually developed beneath Treasure Island during the 1989 earthquake (Seed, et al. [41]). The soil properties of the preliminary UM10 profile were adjusted slightly between SHAKE runs with the YBI accelerograms until the computed accelerations resembled the recorded

accelerations for the site, and the computed accelerations and spectral accelerations obtained by others.

Figure 4.6 shows the finalized, Treasure Island UM10 profile used in this study. The UM10 profile is modeled as 39 feet (12 m) of loose sand fill, underlain by 56 feet (17 m) of soft-to-medium stiff clay (Young Bay Mud), underlain by 39.5 feet (12 m) of dense sand, further underlain by 144.6 feet (44 m) of stiff-to-hard clay (Old Bay Sediments). Bedrock is at a depth of approximately 279 feet (85 m). The water table is approximately 5 feet (2 m) below the surface. For modeling purposes, the thicker soil layers were further divided into more than one layer. The shear wave velocity, unit weight, and damping ratio for each of the layers are indicated in Figure 4.6.

SHAKE-88 computed the average shear wave velocity of the deposit (1047 fps), assumingly in the following manner:

$$V_{s \text{ ave}} = \frac{\sum (v_{si})(h_i)}{H} = 1047 \text{ fps (319 m/s)}$$

SHAKE-88 then incorporated the above average shear wave velocity to compute the natural period of the deposit, equal to 1.07 seconds. The same value for the natural period is obtained when using the above average shear wave velocity in Equation 2.2. Equation 2.3 should not be used to calculate the natural period of the UM10 profile because there is too

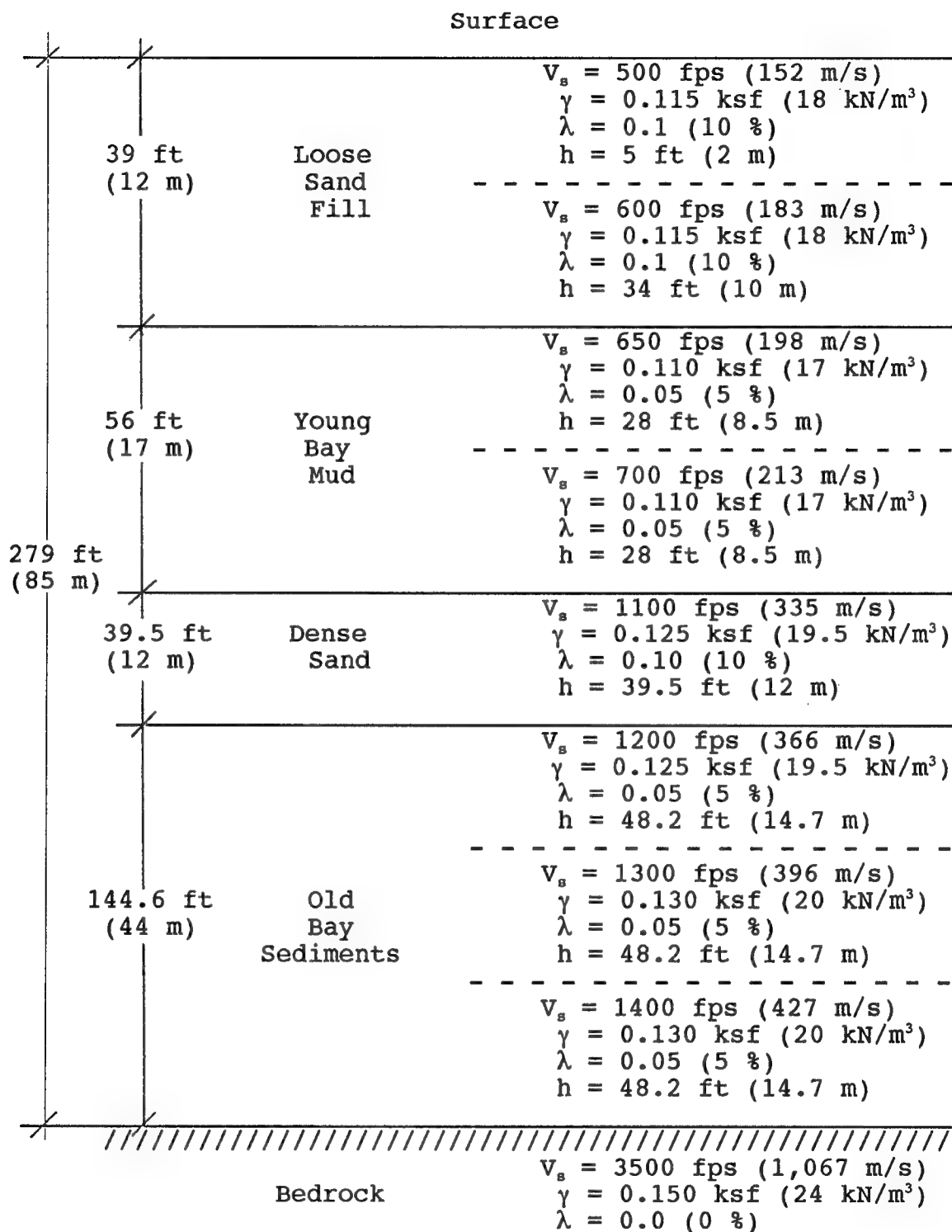


Figure 4.6: Treasure Island UM10 Profile (after De Alba, et al. [12], Ferritto [13], Hanks and Brady [15], Rogers and Figuers [32], Seed, et al. [41], SRTSH [11])

much difference between the soil properties of the layers. The corresponding natural frequency of the deposit is 0.94 Hz.

The shear modulus and damping with shear strain relationships for both the loose sand fill and the dense sand layers in the UM10 profile are modeled by the sand curves in Figure 4.3. The Young Bay Mud and Old Bay Sediments are modeled respectively, by the Bay Mud and Old Bay Sediments curves in Figure 4.3.

As previously mentioned, several comparisons were made to develop the UM10 site profile shown in Figure 4.6. These comparisons are described in the next three paragraphs. The purpose of presenting the comparisons is to show that the UM10 profile used in this study is a reasonably accurate model of the actual UM10 field site. It should be noted for the following comparisons that, since the YBI accelerograms are rock outcrop motions, some of the researchers slightly decreased the accelerations and slightly increased the predominant period of their YBI accelerograms to obtain a more representative "bedrock" motion for the Treasure Island site (Seed, et al. [41]). That was not done with the YBI accelerograms in this study.

One comparison made in developing the UM10 profile was between the recorded and computed peak surface accelerations generated by the 1989 Loma Prieta Earthquake at the UM10 site. A summary of the peak surface accelerations are shown in Table 4.2.

Table 4.2: Peak Surface Accelerations at UM10 Site

Component	Recorded ¹	Computed by Others ²	SHAKE-88
N-S	0.10 g	0.06 g	0.08 g
E-W	0.16 g	0.18 g	0.18 g

1. After Seed, et al. [41]

2. After Hryciw, et al. [16]

The first column of the table indicates the peak surface accelerations recorded in the N-S and E-W directions at the UM10 site during the earthquake (Seed, et al. [41]). The second column gives the computed peak surface accelerations obtained by other researchers for their UM10 models using YBI accelerograms (Hryciw, et al. [16]). The third column shows the SHAKE-88 computed peak surface accelerations induced in this study's UM10 profile by the YBI accelerograms. The results of the third column agree closely with both the recorded accelerations, and the computed accelerations obtained by others.

A second comparison made in developing the UM10 profile was between the peak accelerations computed at various depths in this study's UM10 profile and those obtained from a UM10 site amplification study by Hryciw, et al. [16]. Hryciw, et al. modeled the UM10 site and computed peak acceleration versus depth using an E-W YBI accelerogram and SHAKE-90. SHAKE-90 is a more current version of the SHAKE program, but still computes peak accelerations in the same manner as SHAKE-88. Using the E-W YBI accelerogram and SHAKE-88, an attempt was made to replicate in this study's UM10 profile,

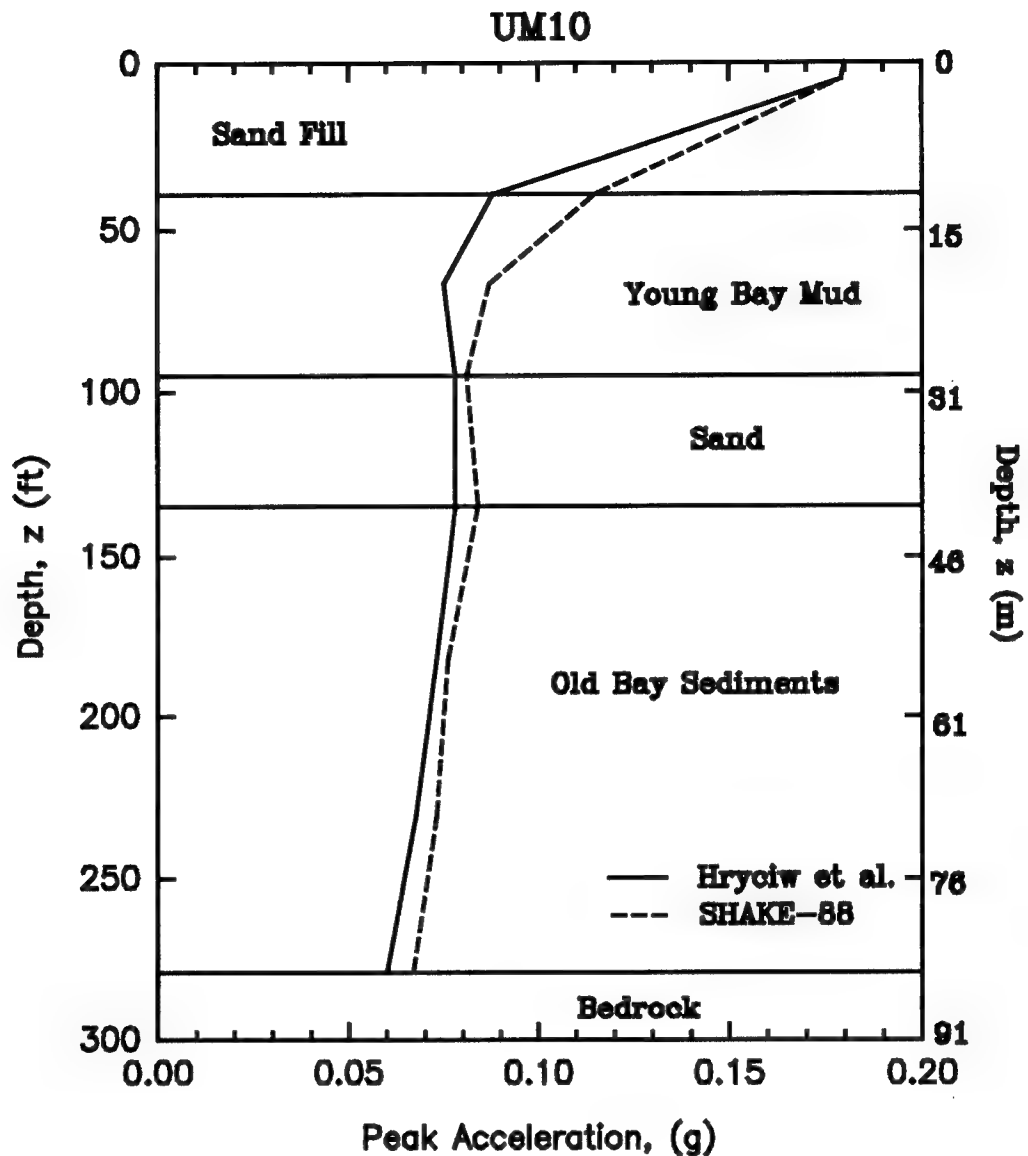


Figure 4.7: Peak Acceleration vs Depth at UM10 Site (after Hryciw, et al. [16])

accelerations that matched those computed by Hryciw, et al. Figure 4.7 shows the computed peak accelerations versus depth obtained by Hryciw, et al., and by SHAKE-88 with this study's UM10 profile. The largest acceleration difference occurs at the top of the Young Bay Mud where the 0.115g induced in this

study's UM10 profile exceeds the Hryciw, et al. computed acceleration by 31 percent. The accelerations at the other depths are reasonably close, especially at the surface and at a depth of 5 ft (2 m) where the accelerations match identically at 0.18g and 0.179g respectively.

A final comparison made in developing the UM10 profile was between the recorded and computed peak surface spectral accelerations induced by the Loma Prieta earthquake at the UM10 site. Figure 4.8 shows the SHAKE-88 computed response spectrum for this study's UM10 profile using the E-W YBI accelerogram. Figure 4.9 shows the recorded and computed response spectrums at UM10 and YBI for the E-W component of the Loma Prieta earthquake (Seed, et al. [41]). Figure 4.8 portrays a primary peak spectral response of 0.53g at $T = 0.65$ seconds, which agrees well with the computed primary peak spectral response in Figure 4.9 of 0.57g at $T = 0.6$ seconds. Figure 4.8 also portrays a secondary peak spectral response of 0.36g at $T = 1.3$ seconds. This agrees well with the recorded and computed peak spectral responses in Figure 4.9 of 0.34g at $T = 1.4$ seconds and 0.31g at $T = 1.3$ seconds respectively.

Figure 4.10 shows the SHAKE-88 computed response spectrum for this study's UM10 profile using the N-S YBI accelerogram. Figure 4.11 shows the recorded response spectrum for UM10 and YBI for the N-S Loma Prieta earthquake component (Seed, et al. [41]). Figure 4.10 portrays a primary, secondary, and third peak spectral response of 0.36g at $T = 1.0$ seconds, 0.28g at

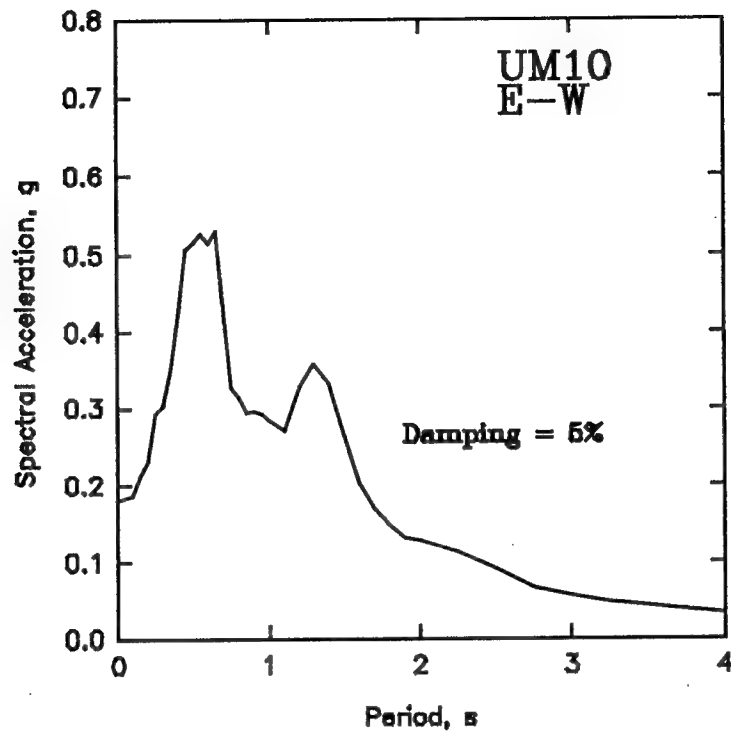


Figure 4.8: Response Spectrum for UM10 using SHAKE-88 and E-W YBI Accelerogram

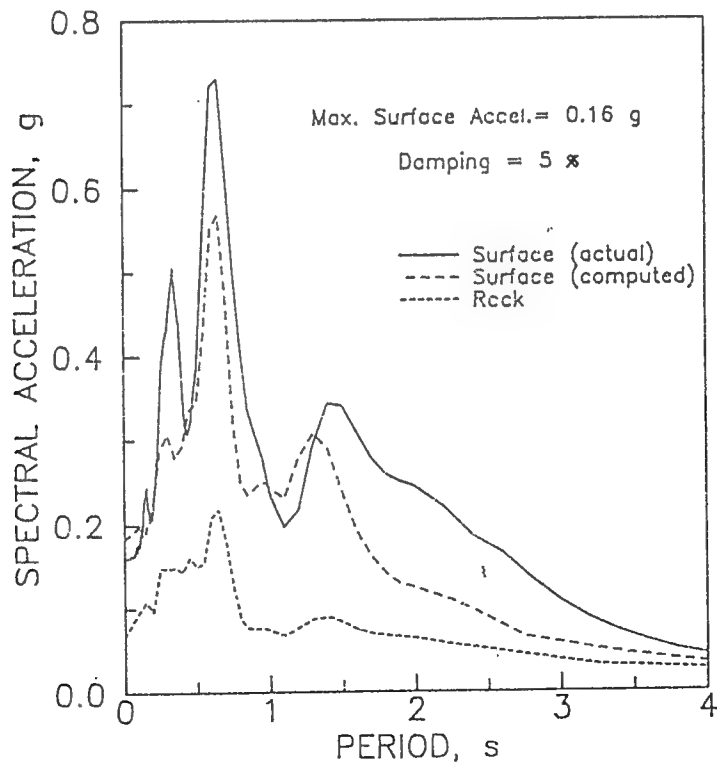


Figure 4.9: Recorded and Computed Response Spectrum for UM10 and YBI (E-W Components) (after Seed, et al. [41])

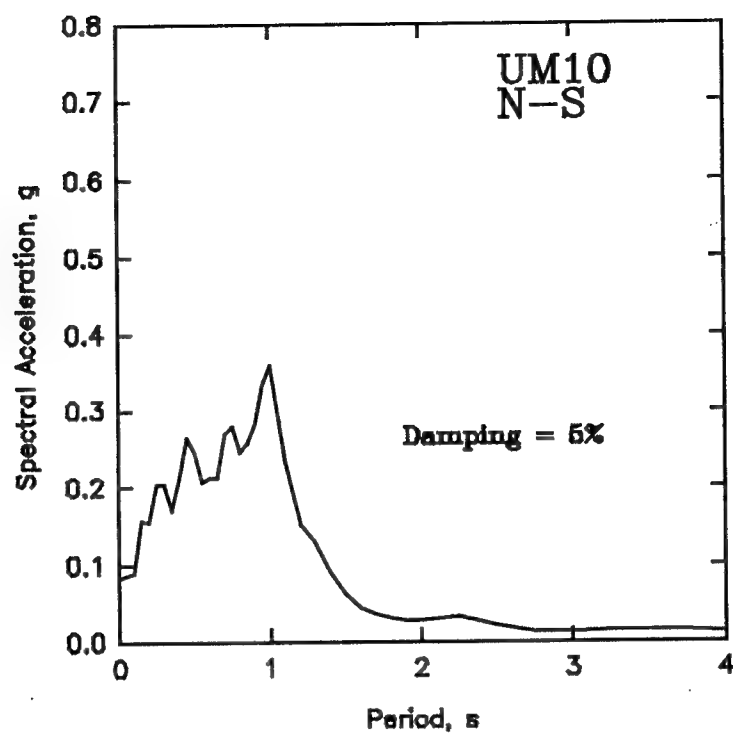


Figure 4.10: Response Spectrum for UM10 using SHAKE-88 and N-S YBI Accelerogram

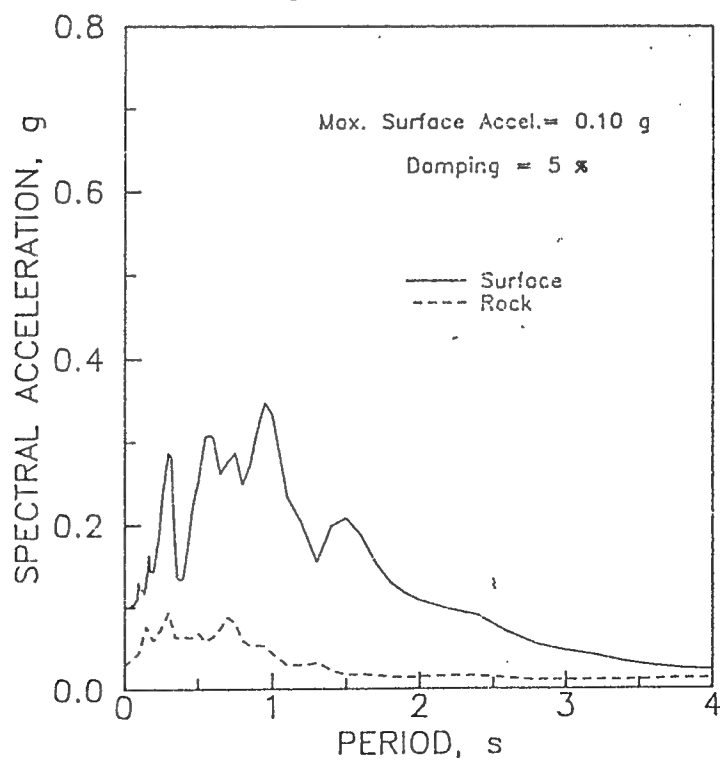


Figure 4.11: Recorded Response Spectrum for UM10 and YBI (N-S Components) (after Seed, et al. [41])

$T = 0.75$ seconds, and $0.27g$ at $T = 0.45$ seconds respectively. These three responses agree well with the primary, secondary, and third recorded peak spectral responses in Figure 4.11 of $0.35g$ at $T = 0.9$ seconds, $0.31g$ at $T = 0.6$ seconds, and $0.28g$ at $T = 0.3$ seconds respectively.

5. ANALYTICAL PROCEDURE

5.1 Chapter Overview

This chapter first addresses modeling of the selected sinusoidal input motions (i.e. pulse, 1 cycle, 2 cycle, 5 cycle and steady state motions shown in Figure 3.1) having the maximum amplitudes and frequencies given in Chapter 3. The remainder of the chapter compares the peak surface accelerations induced by the sinusoidal input motions in the ideal clay and sand profiles described in chapter 4, using the program SHAKE-88 (Lysmer and Seed [24]). The purpose of the comparisons is to determine, for the same maximum amplitude and frequency content, which sinusoidal motions (if any) would induce the same peak surface accelerations as a sinusoidal motion having a greater number of cycles.

5.2 Modeling of Sinusoidal Input Motions

5.2.1 Modeling Procedure

As described in Chapter 4, program SHAKE (Schnabel, et al. [34]) requires that the input motion be given as digitized acceleration values (in g's) at equal time intervals. The input data file containing the input motion must specify the time interval of the accelerations, the maximum acceleration, the number of acceleration values in the record, and the

number of terms for the Fast Fourier Transformation (FFT). Incorporation of the FFT algorithm adapts the program for transient input motions. As described earlier, the number of terms in the FFT should be greater than the number of acceleration values, and must be a power of 2 (Schnabel, et al. [34]).

Modeling of the sinusoidal input motions was accomplished by first generating a 2.5 Hz, 0.2g maximum amplitude, sine wave acceleration record consisting of 800 acceleration values at 0.02 second intervals. This number of acceleration values and time interval were selected because they were the values that defined the Pasadena 1952 accelerogram (Figure 3.2). (Note: During the sinusoidal motion modeling, only the Pasadena 1952 accelerogram was available as an example input motion record. It was the input motion given in an example input data file provided in the SHAKE User's Manual (Schnabel, et al. [34])). A FORTRAN program was written to generate the sine wave record and present it in the format required by SHAKE. The sine wave record was of 16 seconds duration ($800 \text{ acceleration values} \times 0.02 \text{ sec} = 16 \text{ sec duration}$) and consisted of 40 cycles ($16 \text{ sec duration} \times 2.5 \text{ Hz} = 40 \text{ cycles}$). Each cycle of the sine wave record was represented by 20 acceleration values ($800 \text{ acceleration values} \div 40 \text{ cycles} = 20 \text{ acceleration values/cycle}$), as shown in Figure 5.1. An FFT term of 1024 was selected for the record's input data file

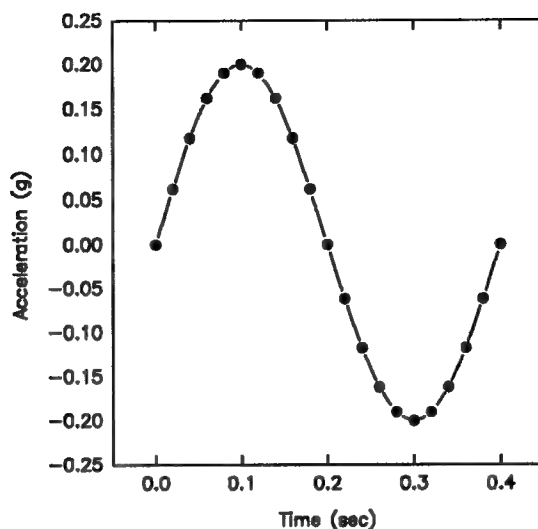


Figure 5.1: Single, 2.5 Hz Sine Wave

because it was the value given in the SHAKE User's Manual for the Pasadena 1952 accelerogram.

One numerical modeling guideline suggested that sine waves be represented by at least 4 points per half-cycle (Siller [43]). Another suggested that the time interval between points be less than one tenth of the waves' natural period (Charlie [10]). A 2.5 Hz sine wave has a natural period of 0.4 seconds, one tenth of which is 0.04 seconds. Therefore, the 2.5 Hz sine wave with 10 acceleration values per half-cycle and 0.02 second spacing satisfied both numerical modeling guidelines.

Next, the 2.5 Hz, 0.2g, 40 cycle sine wave record was modified by removing the number of cycles needed to establish a pulse, 1 cycle, 2 cycle, 5 cycle and steady state sinusoidal input motion record, each of which is shown in Figure 5.2.

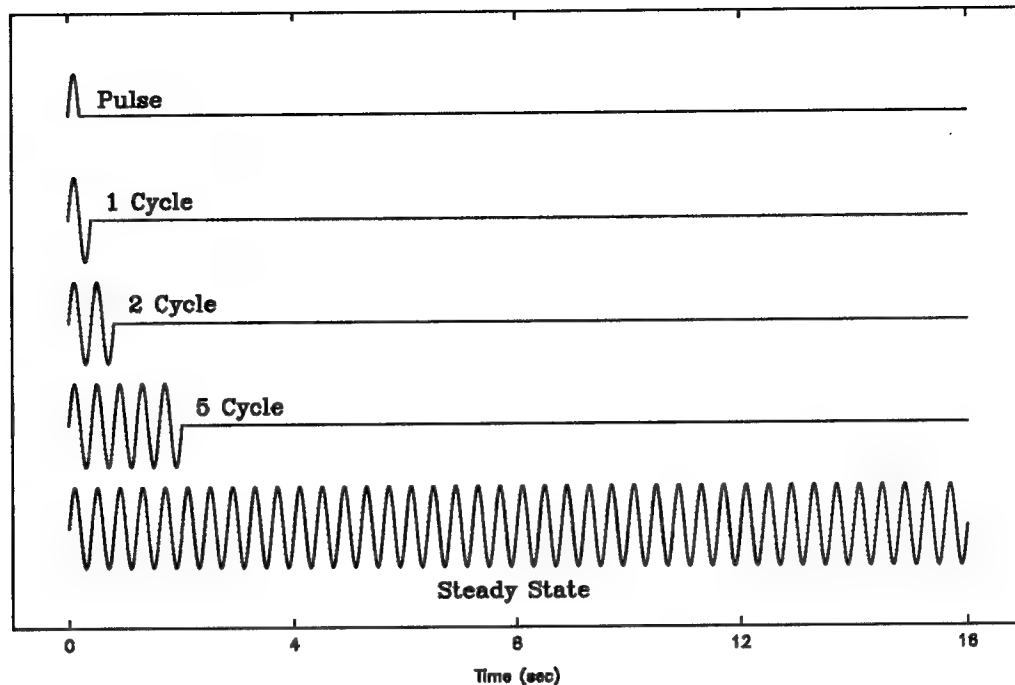


Figure 5.2: Sinusoidal Input Motion Records

A brief description of each sinusoidal input motion record shown in Figure 5.2 follows:

Steady State: A multi cycle, 2.5 Hz sine wave record.

5 Cycles: A five cycle, 2.5 Hz sine wave record with the remainder of the 800 acceleration values set to zero.

2 Cycles: A two cycle, 2.5 Hz sine wave record with the remainder of the 800 acceleration values set <x zero.

1 Cycle: A one cycle, 2.5 Hz sine wave record with the remainder of the 800 acceleration values set to zero.

Pulse: A half cycle, 2.5 Hz sine wave record with the remainder of the 800 acceleration values set to zero.

Each sinusoidal input motion record shown in Figure 5.2 has a tail of zeros, making it 800 acceleration values long. Trial SHAKE-88 runs made in a test profile with shorter length records produced slightly different acceleration values than those produced with 800 value records. Changing the record length also involved changing the FFT value, which also appeared to influence the SHAKE output. Therefore, in order to eliminate the influence of variable record lengths, each of the sinusoidal input motion records was held at 800 acceleration values. An FFT term of 1024 was selected for the input data file of each sinusoidal input motion record.

The SHAKE program enabled an input motion record to be "scaled" to a new maximum acceleration and/or predominate frequency by simply changing the maximum acceleration and time interval parameters (Schnabel, et al. [34]). The new time interval is obtained from the following equation found in the SHAKE User's Manual:

$$\Delta t_2 = (T_2/T_1)\Delta t_1 \quad (\text{EQ 5.1})$$

where T_1 and Δt_1 are the predominant period and time interval of the original acceleration record, and T_2 and Δt_2 are the same values of the new "scaled" acceleration record.

Each of the 2.5 Hz, 0.2g, sinusoidal input motion records (Figure 5.2) were scaled to obtain new records having maximum amplitudes of 0.2g, 0.4g, and 0.6g, and the frequencies indicated in Table 5.1. The right column of Table 5.1 shows the time interval, Δt_2 , obtained using Equation 5.1, that was

used to scale the 2.5 Hz input motion record to the new frequency shown in the left column.

Table 5.1: Time Intervals for New Input Motion Frequencies

<u>Frequency (Hz)</u>	<u>Δt, (sec)</u>
0.5	0.10
0.75	0.0667
1.0	0.05
1.5	0.033
2.0	0.025
3.0	0.0167
3.7	0.0135
4.0	0.0125
5.0	0.01
6.5	0.0077

After scaling the 2.5 Hz, 800 acceleration value, sinusoidal input motion records to the frequencies in Table 5.1, each cycle of the new input motion records is still represented by 20 acceleration values per cycle. However, since the time interval of each record has changed, the total duration of each record also changes. Figure 5.3 illustrates the 16 second duration of the original 2.5 Hz pulse record, and the change in duration for the 1 Hz and 5 Hz pulse records when scaled from the 2.5 Hz pulse record.

Because of the different durations, a concern with using the scaled records was their potential for influencing SHAKE predictions. An alternate method to model the sinusoidal input motions having the frequencies indicated in Table 5.1 was to create them in the same manner as the original 2.5 Hz, 0.2g records. This alternative method was used to create 'non-scaled' 0.2g pulse, 5 cycle and steady state sinusoidal

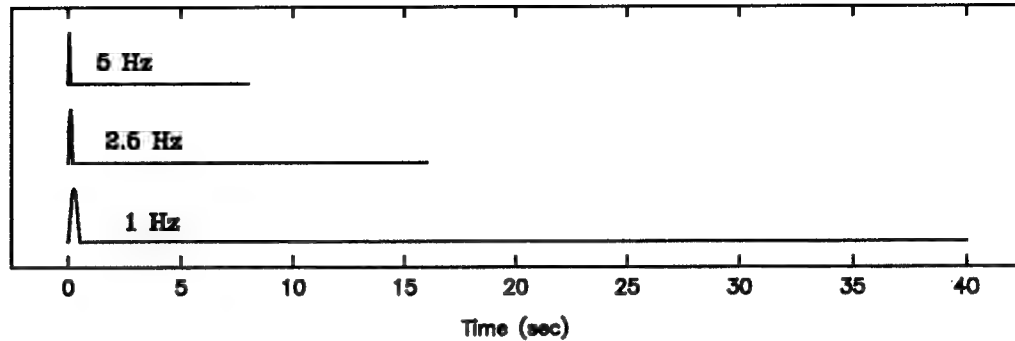


Figure 5.3: Scaled Pulse Input Motion Records

input motion records having frequencies of 0.5, 0.75, 1.0, 1.5, 3.7, 5.0 and 6.5 Hz and 0.02 second time intervals.

Each non-scaled sinusoidal input motion record consisted of 800 acceleration values at 0.02 second time intervals. Thus, all the non-scaled records have a duration of 16 seconds. However, because each different frequency sine wave was generated at the same time interval of 0.02 seconds, the number of acceleration values per cycle is different for each different frequency non-scaled record. In comparison to the 20 acceleration values per cycle of the 2.5 Hz records, the slower frequency records are represented by a greater number of acceleration values per cycle, and the higher frequency records are represented by a lower number of acceleration values per cycle. This is illustrated in Figure 5.4, which shows the non-scaled pulse input motion records having frequencies of 1.0, 2.5, and 6.5 Hz. While the 2.5 Hz pulse is represented by 10 acceleration values (20 acceleration values/cycle), the 1.0 Hz pulse is represented by 25

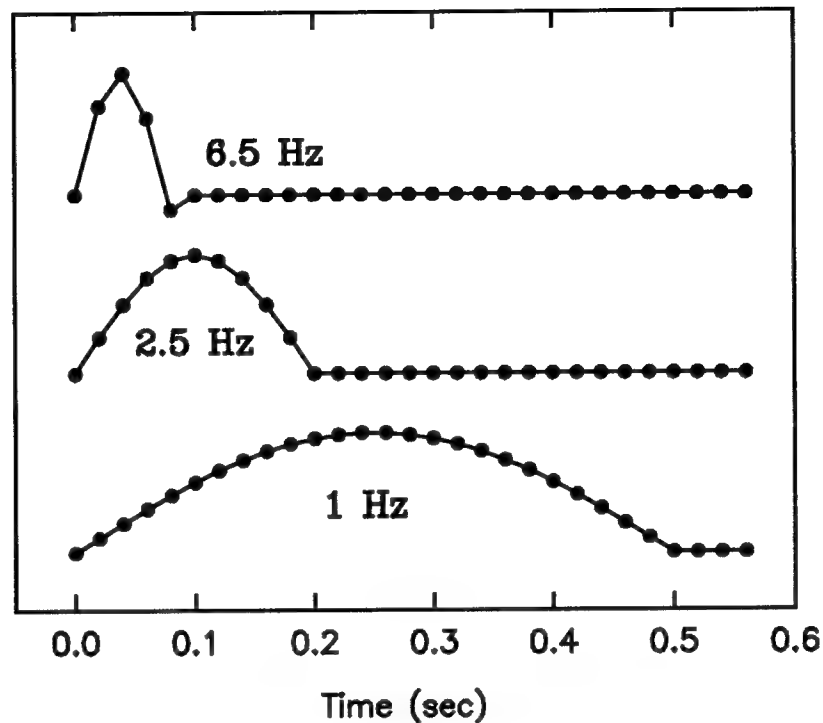


Figure 5.4: Non-Scaled Pulse Input Motion Records

acceleration values (50 acceleration values/cycle), and the 6.5 Hz pulse is only represented by 4 acceleration values (8 acceleration values/cycle).

Each of the non-scaled sinusoidal input motion records are acceptable under the numerical modeling guidelines. Also, since only 0.2g non-scaled records were created, each non-scaled record will be scaled to obtain corresponding 0.4g and 0.6g records.

Another implication of the different frequency non-scaled records having a different number of acceleration values per cycle is that the total number of cycles contained in the non-scaled steady state motion records is also different. For

instance, the number of cycles contained in the 1.0, 2.5, and 6.5 Hz non-scaled steady state motion records are 16, 40, and 104 cycles respectively.

To determine if using a scaled or non-scaled input motion record makes a difference in the SHAKE-88 output (i.e. peak surface acceleration), a comparison was made of the SHAKE-88 computed peak surface accelerations induced in the ideal clay deposit (Figure 4.4) by several scaled and corresponding non-scaled sinusoidal input motion records. The results of these comparisons are covered in the next section.

5.2.2 Modeling Results

Program SHAKE-88 was used to compute the peak surface accelerations induced in an ideal clay deposit by both scaled and non-scaled pulse, 5 cycle, and steady state sinusoidal input motion records having maximum amplitudes of 0.2g, 0.4g, and 0.6g, and frequencies of 0.5, 0.75, 1.0, 1.5, 2.5, 3.7, 5.0, and 6.5 Hz. The peak surface accelerations were then normalized by dividing each by the maximum amplitude of the input motion. The normalized peak surface accelerations (amplification factors) for the scaled and non-scaled pulse, 5 cycle, and steady state input motions having the above mentioned frequencies and maximum amplitudes are shown in Table 5.2.

Examination of Table 5.2 reveals that the largest difference between the scaled and non-scaled amplification factors are 0.13 (i.e., 1.36 - 1.23) for the 0.4g pulse at

Table 5.2: Amplification Factors for Scaled and Non-Scaled Sinusoidal Motions

Input Motion	Input Motion Freq. (Hz)	Amplification Factor due to input motion					
		0.2g		0.4g		0.6g	
		S	NS	S	NS	S	NS
Pulse	0.5	1.09	1.08	1.36	1.23	*	*
	0.75	1.42	1.43	1.26	1.27	0.94	0.95
	1.0	1.56	1.55	1.20	1.21	0.88	0.89
	1.5	1.53	1.53	1.20	1.21	0.95	0.95
	2.5	1.38	1.38	1.13	1.13	0.98	0.98
	3.7	1.39	1.40	1.16	1.15	0.99	0.99
	5.0	1.43	1.48	1.16	1.20	1.03	1.07
	6.5	1.46	1.44	1.16	1.16	1.02	1.03
5 Cycle	0.5	1.15	1.13	1.32	1.32	*	*
	0.75	1.38	1.44	1.28	1.31	0.89	0.91
	1.0	1.70	1.71	1.40	1.40	0.81	0.82
	1.5	2.37	2.37	1.26	1.26	0.89	0.89
	2.5	1.89	1.89	1.27	1.27	0.91	0.91
	3.7	1.49	1.48	1.12	1.11	0.96	0.96
	5.0	1.40	1.46	1.13	1.17	1.13	1.22
	6.5	1.43	1.43	1.63	1.60	1.31	1.34
Steady State	0.5	1.15	1.13	1.30	1.30	*	*
	0.75	1.43	1.44	1.31	1.31	0.93	0.96
	1.0	1.69	1.70	1.39	1.39	0.82	0.82
	1.5	2.38	2.38	1.25	1.26	0.90	0.90
	2.5	1.89	1.89	1.27	1.27	0.92	0.92
	3.7	1.48	1.47	1.12	1.11	0.97	0.97
	5.0	1.41	1.46	1.13	1.17	1.13	1.22
	6.5	1.44	1.43	1.60	1.60	1.28	1.27

S = Scaled, NS = Non-Scaled, * = SHAKE-88 could not compute

0.5 Hz, and 0.09 (i.e., 1.22 - 1.13) for the 0.6g steady state motion at 5.0 Hz. Otherwise, for a particular frequency and maximum amplitude, the scaled and associated non-scaled amplification factors for the pulse, 5 cycle, and steady state input motions are very similar. To illustrate some of these similarities, the amplification factors for the scaled and non-scaled, 0.2g pulse, 5 cycle, and steady state input motions are plotted against the input motion frequency in the top, middle, and bottom graphs of Figure 5.5 respectively.

As a result of the small amplification factor differences in Table 5.2, it was concluded for purposes of this study that using SHAKE-88 to subject a soil profile to a scaled input motion would result in essentially the same peak acceleration as subjecting the soil profile to a corresponding non-scaled input motion. This conclusion is beneficial to this study because creating scaled input motion records, which involves changing one or two parameters within the input data file of an original input motion record, is much simpler and requires far less time than developing the corresponding non-scaled motion records. As such, most of the input motion records used in succeeding portions of this study are scaled from an original motion record whenever a record is needed with a maximum amplitude and/or frequency different from that of the original motion record. The original sinusoidal motion records are the steady state, 5 cycle, 2 cycle, 1 cycle and pulse records generated at 2.5 Hz, 0.2g, and 0.02 second time

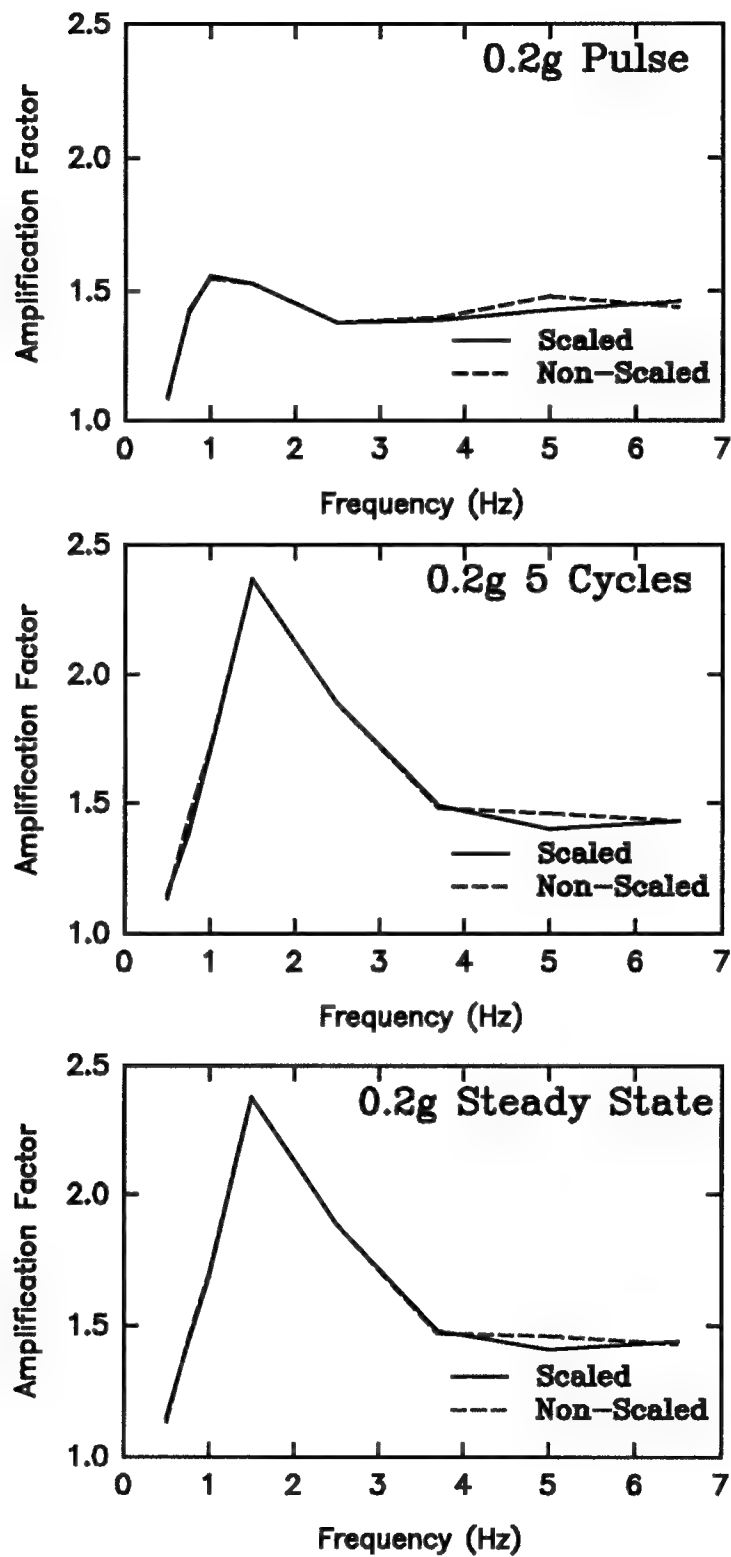


Figure 5.5: Amplification Factor vs. Input Motion Frequency for both Scaled and Non-Scaled Sinusoidal Motions

interval. The original earthquake motion records are the 'as-recorded' accelerograms given in Chapter 3, Figure 3.2.

5.3 Comparison of Sinusoidal Induced Amplifications

In the following sections, a comparison is between the 'normalized' peak surface accelerations (amplification factors) induced in both the ideal sand and clay soil profiles when subjected to the sinusoidal input motions (i.e. pulse, 1 cycle, 2 cycle, 5 cycle and steady state) using SHAKE-88.

Amplification factor comparisons are made based on the soil profile material, number of cycles in the sinusoidal motion, and frequency of the sinusoidal motion, in turn. The purpose of these comparisons are to determine, for the same maximum amplitude and frequency content, which of the sinusoidal motions (if any) will induce the same peak surface accelerations as a sinusoidal motion having a greater number of cycles.

5.3.1 Material Response

For the material response comparisons, the ideal sand and clay profiles were each subjected to the pulse, 1 cycle, 2 cycle, 5 cycle and steady state sinusoidal input motions having frequencies of 0.5, 0.75, 1.0, 1.5, 2.0, 2.5, 3.0, 5.0 and 6.5 Hz with maximum amplitudes of 0.2g, 0.4g and 0.6g. Additionally, the clay and sand profiles were subjected to the sinusoidal motions having a frequency equal to the natural frequency of the profile; 3.7 Hz and 4.0 Hz for the clay and

sand respectively. The resulting peak surface accelerations were then normalized to obtain amplification factors. To help visualize this procedure, Table 5.3 shows the amplification factors that resulted in the clay and sand profiles due to the pulse input motions.

Table 5.3: Amplification Factors for Pulse Motions in Clay and Sand Profiles

Input Motion	Input Motion Freq. (Hz)	Amplification Factor due to input motion					
		Clay			Sand		
		0.2g	0.4g	0.6g	0.2g	0.4g	0.6g
Pulse	0.5	1.09	1.36	*	1.04	1.12	1.20
	0.75	1.42	1.26	0.94	1.29	1.36	1.39
	1.0	1.56	1.20	0.88	1.50	1.46	1.40
	1.5	1.53	1.20	0.95	1.58	1.42	1.34
	2.0	1.45	1.17	0.88	1.54	1.35	1.27
	2.5	1.38	1.13	0.98	1.48	1.30	1.21
	3.0	1.35	1.14	1.00	1.44	1.28	1.18
	3.7	1.39	1.16	0.99	-	-	-
	4.0	-	-	-	1.46	1.27	1.16
	5.0	1.43	1.16	1.03	1.45	1.24	1.13
	6.5	1.46	1.16	1.02	1.47	1.24	1.10

* = SHAKE-88 could not compute

All of the amplification factors that resulted in the clay and sand profiles from the sinusoidal input motions are plotted against the frequency of the input motion in Figures 5.6 through 5.10. Each figure contains two graphs, both showing the amplification factor versus input motion frequency

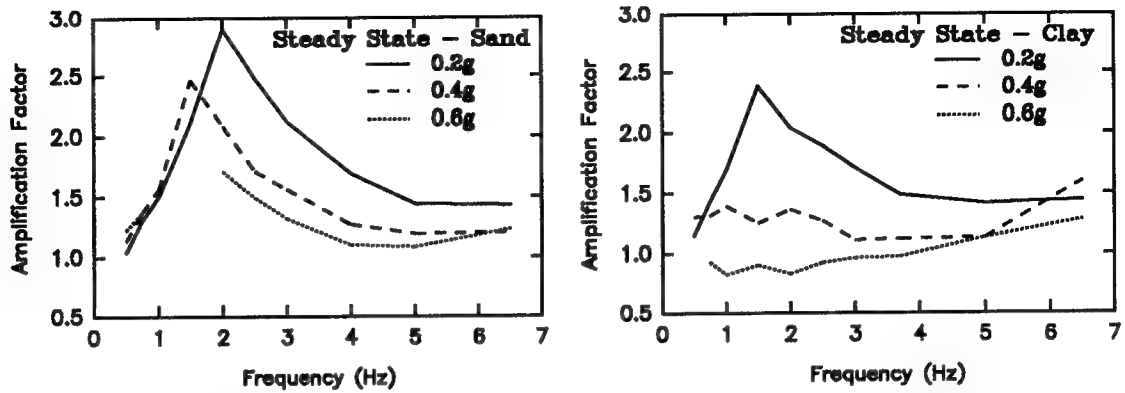


Figure 5.6: Amplification Factor vs. Input Motion Frequency for Steady State Motions

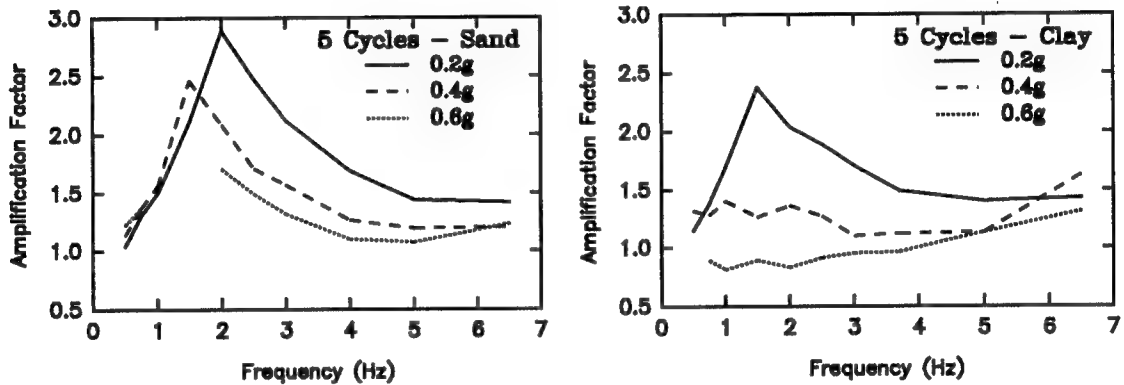


Figure 5.7: Amplification Factor vs. Input Motion Frequency for 5 Cycle Motions

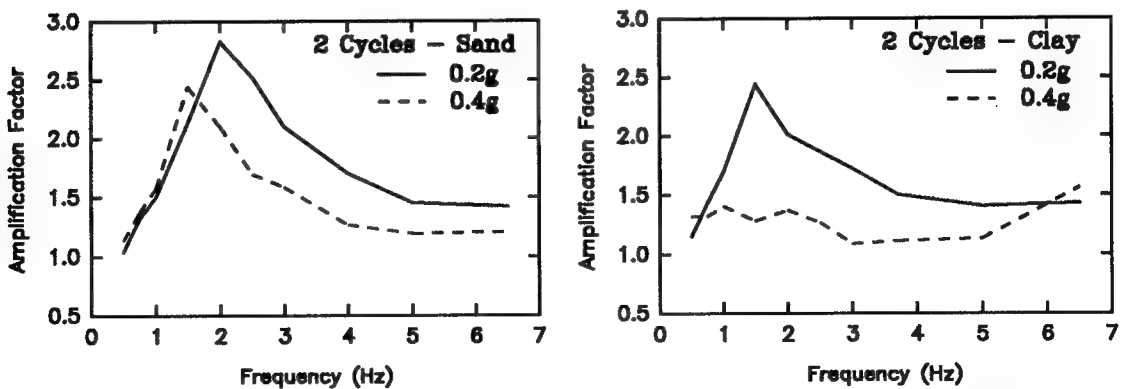


Figure 5.8: Amplification Factor vs. Input Motion Frequency for 2 Cycle Motions

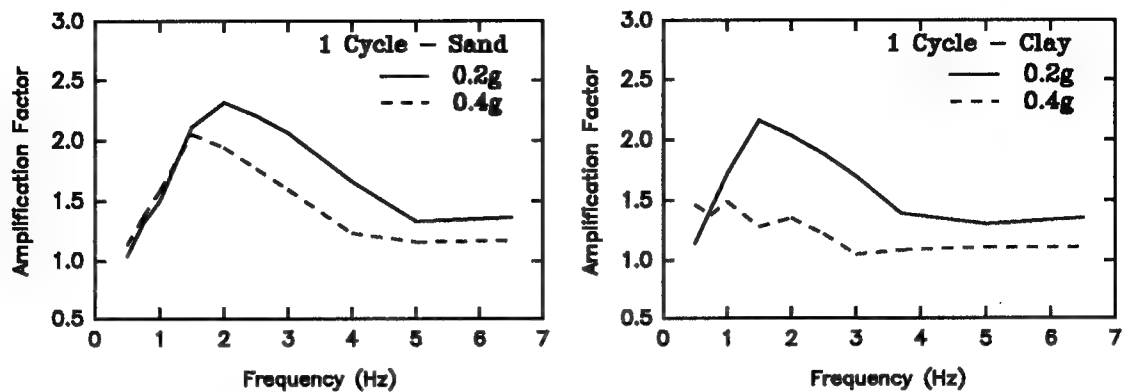


Figure 5.9: Amplification Factor vs. Input Motion Frequency for 1 Cycle Motions

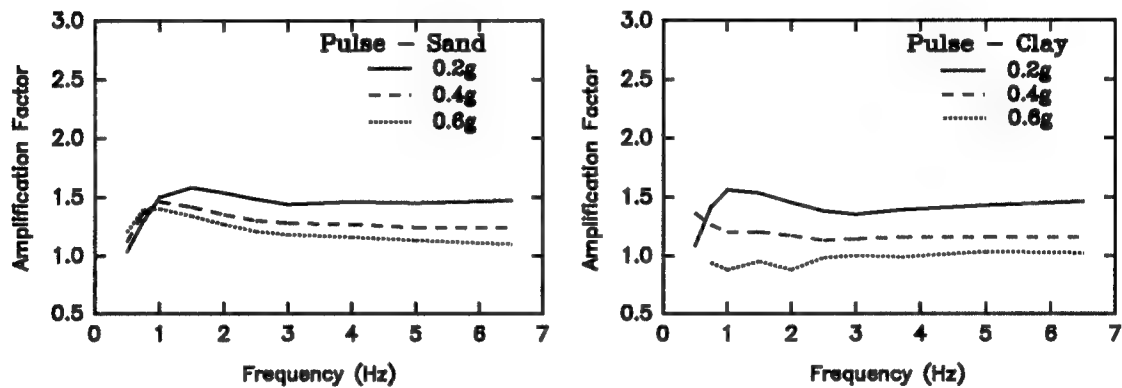


Figure 5.10: Amplification Factor vs. Input Motion Frequency for Pulse Motions

for the indicated sinusoidal motion in the sand profile (left graph) and clay profile (right graph). Figure 5.6 shows the response to the steady state sinusoidal motions, while Figures 5.7, 5.8, 5.9, and 5.10 show the response to the 5 cycle, 2 cycle, 1 cycle and pulse sinusoidal motions respectively. The amplification factor vs. frequency patterns for the 0.2g, 0.4g, and 0.6g sinusoidal motions are plotted separately in each graph.

Figures 5.6 through 5.10 show similar amplification factor vs. frequency patterns for all the 0.2g and 0.4g sinusoidal motions in the sand profile and 0.2g sinusoidal motions in the clay profile. The similarity is that of a steady increase and then decrease in the amplification at the lower frequencies, forming a prominent peak in the graph. This is followed by a leveling of the amplifications at the higher frequencies. This amplification vs. frequency pattern was expected, with the exception that the prominent peak was expected to occur at the natural frequency of the soil deposit (i.e., 3.7 Hz for the clay profile, 4.0 Hz for the sand profile). Instead, the prominent peaks in Figures 5.6 through 5.10 occurred at lower frequencies than the natural frequency of the soil deposit. One possible reason for this occurrence is discussed ahead in Section 5.3.3.

The amplification factors produced by the 0.6g sinusoidal motions in the sand profile and the 0.4g and 0.6g sinusoidal motions in the clay profile, demonstrated amplification factor vs frequency patterns that deviated from the expected "prominent peak" pattern. One possible explanation for the deviations might be that at the higher g levels (i.e., 0.6g in the sand profile, and 0.4g and 0.6g in the clay profile), the input motion is severe enough that the soil deposit becomes unstable and does not respond consistently across the frequency range of the input motion. (Note: According to Su, et al. [46], 0.04g to 0.2g is a strong motion range). The

fact that the amplification factors in Figures 5.6 through 5.10 decreased with increasing input motion g level (i.e., 0.2 g motions induced higher amplifications than 0.4 g motions, which in turn induced higher amplifications than 0.6 g motions) agrees with the information given in Chapter 2, Section 2.2.6.5.

Figures 5.6 and 5.7 show that SHAKE-88 was not able to compute peak surface accelerations for the 0.6 g steady state and 5 cycle motions in the sand profile at frequencies of 1.0 Hz and 1.5 Hz. (Note: SHAKE-88 computations were not attempted for the 0.6 g 2 cycle and 1 cycle motions in the sand and clay profiles because the responses were suspected to be similar to the 0.6 g steady state and 5 cycle responses shown in Figures 5.6 and 5.7).

The conclusion drawn from the material response comparisons made in Figures 5.6 through 5.10 is that the best conditions for a comparative analysis using the sand and clay profile models involve input motion records (e.g. sinusoidal or earthquake) having maximum amplitudes of approximately 0.2 g to 0.4 g for the sand profile, and of approximately 0.2 g for the clay profile. Therefore in Chapter 6, the sand and clay profile models are generally not subjected to input motion records having maximum accelerations greater than approximately 0.4 g and 0.2 g , respectively. Also, the comparisons made in the remaining sections of this chapter do not include the amplification factors resulting from the 0.6 g

motion in the sand profile, and the 0.4g and 0.6g motions in the clay profile.

5.3.2 Cycle Response

Several of the amplification factor vs. frequency patterns obtained from Figures 5.6 to 5.10 in the last section were used to make the cycle response comparison. Figure 5.11 shows the amplification factor vs. input motion frequency responses for the 0.2g (top graph) and 0.4g (bottom graph) pulse, 1 cycle, 2 cycle, 5 cycle and steady state sinusoidal motions in the sand profile. The amplification factor vs. input motion frequency responses for the 0.2g sinusoidal motions in the clay profile are shown in Figure 5.12. Figures 5.11 and 5.12 are the product of 150 SHAKE-88 computer runs (50 runs per graph).

Figures 5.11 and 5.12 both show that, for a particular maximum amplitude of input motion, the amplification factor vs. frequency responses for the 2 cycle, 5 cycle and steady state sinusoidal motions are practically identical. This suggests that the 2 cycle sinusoidal motions induced essentially the same peak accelerations as the longer 5 cycle and steady state sinusoidal motions.

Figures 5.11 and 5.12 also show that the amplification factor vs. frequency response for the 1 cycle sinusoidal motions are also very close to the responses for the 2 cycle, 5 cycle and steady state sinusoidal motions at the lower and higher frequencies (i.e., at the lower frequencies of 0.5 to

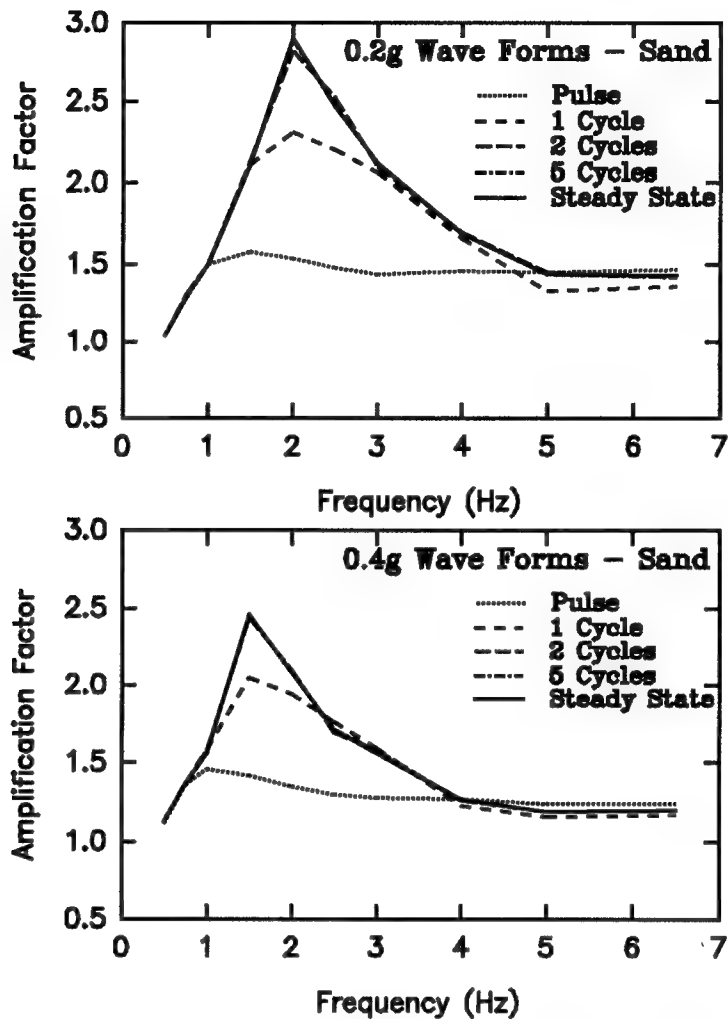


Figure 5.11: Amplification Factor vs. Input Motion Frequency for 0.2g and 0.4g Sinusoidal Motions in Sand

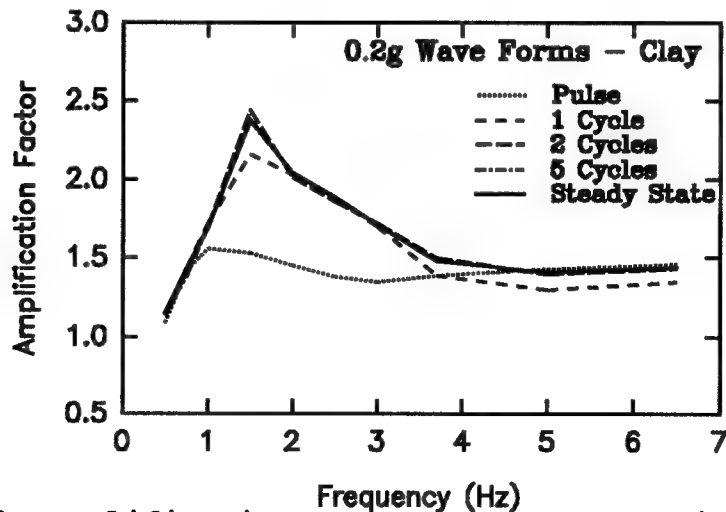


Figure 5.12: Amplification Factor vs. Input Motion Frequency for 0.2g Sinusoidal Motions in Clay

1.5 Hz and higher frequencies of 3.0 to 6.5 Hz for 0.2g sinusoidal motions in sand; at the lower frequencies of 0.5 to 1.0 Hz and higher frequencies of 2.5 to 6.5 Hz for 0.4g sinusoidal motions in sand; and at the lower frequencies of 0.5 to 1.0 Hz and higher frequencies 2.0 to 6.5 Hz for 0.2g sinusoidal motions in clay). The 1 cycle sinusoidal motions induce a peak amplification factor at the same frequency as the longer cycle sinusoidal motions, however the peak amplification factors for the 1 cycle motions are roughly 20 percent lower, 16 percent lower, and 10 percent lower than the amplification factors for the longer cycle 0.2g motions in sand, 0.4g motions in sand, and 0.2 motions in clay, respectively.

Finally, Figures 5.11 and 5.12 show that the amplification factor vs. frequency response for the pulse sinusoidal motions are almost identical to those for the longer cycle sinusoidal motions at the lower frequencies of 0.5 to 1.0 Hz for 0.2g motions in sand, 0.5 to 0.75 Hz for 0.4g motions in sand, and 0.5 to 0.75 Hz for 0.2g motions in clay. The amplification factors then taper off and are much lower than the amplification factors for the longer cycle motions, until they again converge near 5.0 Hz for 0.2g motions in sand, at 4.0 Hz for 0.4g motions in sand, and at 3.7 Hz for 0.2g motions in clay. The 0.2g pulse response in sand reaches a peak near 1.5 Hz at an amplification that is roughly 45 percent lower and at a frequency that is 0.5 Hz lower than the longer cycle peak

responses. The 0.4g pulse response in sand reaches a peak near 1.0 Hz at an amplification that is roughly 40 percent lower and at a frequency that is 0.5 Hz lower than the longer cycle peak responses. The 0.2g pulse response in clay reaches a peak near 1.0 Hz at an amplification that is roughly 35 percent lower and at a frequency that is 0.5 Hz lower than the longer cycle peak responses.

In general, the comparisons made in Figures 5.11 and 5.12 indicate that, for the sand and clay profiles subjected to sinusoidal motions having the same maximum amplitudes and frequencies, all of the sinusoidal motions induce similar amplifications at the lower and higher frequency ranges. The pulse induced amplifications however, do not match very closely those induced by the longer cycle motions at the mid range frequencies. The 1 cycle induced amplifications more closely match those induced by longer cycle motions at the mid range frequencies, except at the frequency range near where the peak amplifications occur. The slightly longer 2 cycle sinusoidal motion essentially induces the same amplifications as the longer 5 cycle and steady state sinusoidal motions for all the frequencies analyzed. These results suggest that, for the frequency range of 0.5 to 6.5 Hz and for maximum amplitudes of approximately 0.2g to 0.4g in the sand profile and approximately 0.2g in the clay profile, a 2 cycle sinusoidal motion should induce the same peak accelerations as

any longer cycle sinusoidal motion having the same maximum amplitude and frequency.

5.3.3 Frequency Response

This section re-examines Figures 5.11 and 5.12 to compare the amplification factor vs. frequency response in the sand and clay profiles with the frequency of the sinusoidal input motion.

It was expected (as referenced in Chapter 2, Section 2.2.6.2) that the peak amplifications induced by the sinusoidal motions would develop when the frequency of the sinusoidal motion matched the natural frequency of the soil deposit (i.e., 4.0 Hz in the sand and 3.7 Hz in the clay). However, referring to Figures 5.11 and 5.12, the peak amplifications occurred at frequencies lower than the natural frequency of the soil profile.

One possible explanation for the above phenomenon may be that the 0.2g and 0.4g sinusoidal input motions induced high strain levels in the sand and clay deposits, resulting in non-linear soil behavior. The degrading shear modulus associated with the non-linear behavior decreased the strength of the each deposit below that for low strain levels. Thus, each deposit had a higher natural period (lower natural frequency) than that predicted by Equation 2.2.

To test this explanation, several SHAKE-88 runs were made to determine the response of the sand and clay deposits at a low g level. Both the sand and clay profiles were subjected

to 1 cycle and 2 cycle sinusoidal input motions having maximum amplitudes of 0.01g and frequencies equal to those used in Figures 5.11 and 5.12. The resulting amplification factor versus input motion frequency responses for the sand and clay profiles are shown in Figures 5.13 and 5.14 respectively. Figure 5.13 shows that the amplifications peaked at the expected natural frequency of the sand deposit (i.e., 4Hz), and Figure 5.14 shows that the amplifications peaked very close to the expected natural frequency of the clay deposit (i.e., 3.7 Hz). This suggests that the 0.01g sinusoidal input motions induced low strain levels in the deposits, resulting in linear soil behavior and natural period (and frequency) as predicted by Equation 2.2.

This explanation agrees with Finn [14] and Ziony [48], which indicate that for low levels of shaking, soil response will be primarily linear and amplification factors will peak at the natural period predicted by Equation 2.2. However, as the amplification of the input motion increases, the increasing strains in the soil result in nonlinear behavior and a shift in site period towards longer periods.

5.4 Chapter Summary

The purpose of this chapter was to determine which of the sinusoidal motions (if any) would induce the same peak surface acceleration as a sinusoidal motion having a greater number of cycles. The normalized peak surface acceleration

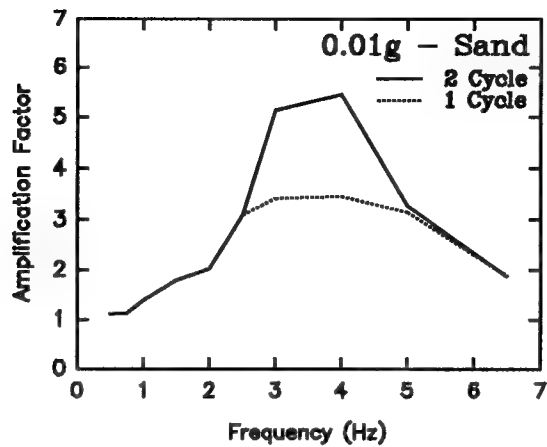


Figure 5.13: Amplification Factor vs. Input Motion Frequency for 0.01g Sinusoidal Motions in Sand

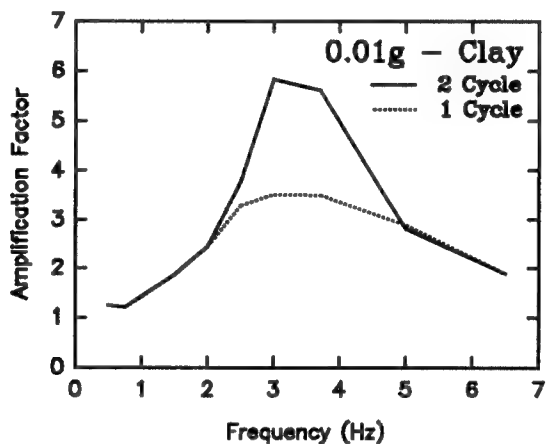


Figure 5.14: Amplification Factor vs. Input Motion Frequency for 0.01g Sinusoidal Motions in Clay

(amplification factor) versus input motion frequency comparisons made in this chapter indicate that the 2 cycle sinusoidal motion achieves this purpose. As a result, only the pulse, 1 cycle, and 2 cycle sinusoidal input motions developed in this chapter will be used in the earthquake-sinusoidal comparative analysis addressed in Chapter 6.

6. COMPARATIVE ANALYSIS

6.1 Chapter Overview

This chapter compares the "normalized" peak surface accelerations (amplification factors) resulting from both earthquake and sinusoidal input motions in two ideal soil profiles and one field site profile. The purpose of the comparisons is to determine if any of the sinusoidal motions induce peak surface accelerations similar to those induced by the earthquake records. The peak surface accelerations were obtained using SHAKE-88 (Lysmer, et al. [24]). Based on the findings of Chapter 5, only the pulse, 1 cycle and 2 cycle sinusoidal input motions are used for the earthquake-sinusoidal comparisons.

The comparative analysis is discussed in two main parts. The first part addresses earthquake versus sinusoidal induced amplifications in the ideal sand and clay profiles. The second part addresses the earthquake versus sinusoidal induced amplifications in the Treasure Island UM10 site profile. Both of the main parts are divided into two sections. For the comparisons made in the first section, the maximum acceleration and predominant frequency of the original earthquake accelerograms were scaled to match the maximum amplitudes and frequencies of the sinusoidal motions. For the

Seed [25], used a FFT term of 4096. This same FFT term was selected for the input data files of the 2000 acceleration value earthquake records used in this study.

Before comparing the scaled earthquake induced amplifications to the sinusoidally induced amplifications from Chapter 5, a question arose whether the amplifications from the 800 acceleration value sinusoidal records could be compared to the 2000 acceleration value earthquake induced amplifications. Ideally, the comparisons should be made with sinusoidal motion records consisting of 2000 acceleration values. To test if the 800 acceleration value sinusoidal induced amplifications developed in Chapter 5 could be utilized, an additional tail of zeros (0's) was added to a 800 acceleration value, 0.2g, 2.5 Hz, 2 cycle sinusoidal record, so that it consisted of 2000 acceleration values. An FFT term of 4096 was assigned to the input data file and the record was applied to the sand and clay profiles using SHAKE-88. The resulting amplification factors were the same as those generated by the 0.2g, 2.5 Hz, 2 cycle motion records consisting of 800 acceleration values with FFT term of 1024. With this comparison, it was assumed that all the 800 acceleration value records would induce the same amplifications as corresponding 2000 acceleration value records. With this information, it was determined that the sinusoidal induced amplifications from Chapter 5 could be

utilized for comparison with the earthquake induced amplifications developed in this chapter.

Comparisons of the "normalized" peak surface accelerations (amplification factors) induced in the ideal sand and clay profiles by the scaled earthquake accelerograms and sinusoidal motions, are addressed in the following ten sub-sections, each corresponding with the earthquake record used in the analysis. For each of the ten earthquakes, three graphs are used to illustrate the comparisons. These are the same three graphs used in Figures 5.11 and 5.12 in Chapter 5, except that the 5 cycle and steady state amplifications are not shown, and the earthquake amplifications are included. The graphs for all ten earthquakes represent a total of 390 SHAKE-88 computer runs (90 sinusoidal + 300 earthquake input motions).

6.2.1.1 Yerba Buena Island, 90 Degrees (E-W)

Figure 6.1 shows the amplification factor versus input motion frequency relationships produced in the sand profile by the scaled Yerba Buena Island, 90 degree (YBI90) earthquake accelerogram and the sinusoidal motions having maximum accelerations of 0.2g (top graph) and 0.4g (bottom graph). At both 0.2g and 0.4g maximum accelerations, all three sinusoidal motions induce close to the same amplifications as YBI90 at the lower and higher frequencies. From approximately 1.0 to 5.0 Hz at the 0.2g level, and from approximately 0.75 to 4.0 Hz at the 0.4g level, the pulse induced amplifications fall well below that of YBI90. At the same frequencies, the

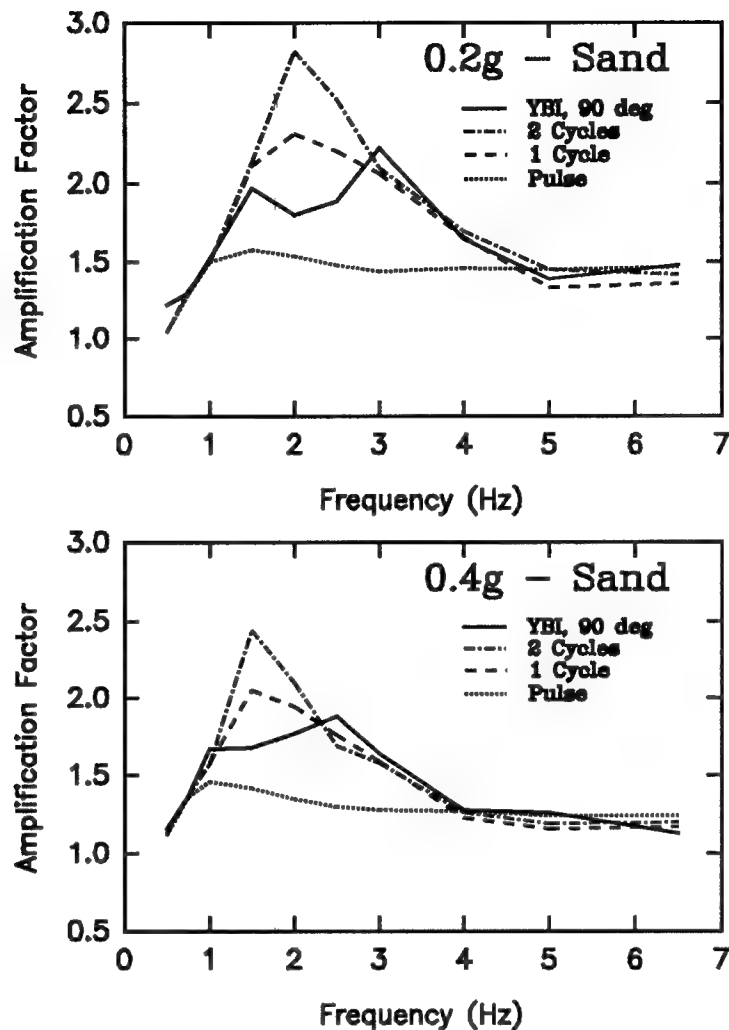


Figure 6.1: Amplification Factor vs. Input Motion Frequency, YBI90 and Sinusoidal Motions in Sand

1 cycle and 2 cycle induced amplifications continue to closely match that of the YBI90, except they are not able to replicate the valley that the YBI90 amplification pattern produces from approximately 1.5 to 3.0 Hz at the 0.2g level, and from 1.0 to 2.5 Hz at the 0.4g level. At the frequencies where the YBI90 induced amplification valley occurs, the 1 cycle motion

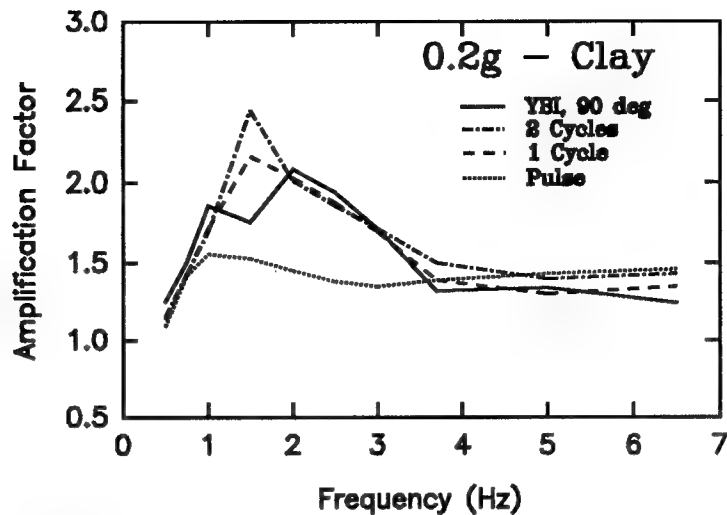


Figure 6.2: Amplification Factor vs. Input Motion Frequency, YBI90 and Sinusoidal Motions in Clay

generally provides the closest conservative amplification match.

Figure 6.2 shows the amplification factor versus input motion frequency relationships produced in the clay profile by the YBI90 accelerogram and the sinusoidal motions having a maximum acceleration of 0.2g. Again all three sinusoidal motions come close to matching the YBI90 amplifications at the lower and higher frequencies, with the pulse amplification falling below those of YBI90 from approximately 1.0 to 3.5 Hz. The 1 cycle and 2 cycle induced amplifications continue to closely match those of YBI90 from 1.0 to 3.5 Hz, except where the valley in the pattern occurs. Again, the 1 cycle induced amplifications provide the closest conservative amplifications where the valley occurs.

Inspection of the YBI90 accelerogram in Figure 3.2 shows that the strong shaking portion of the accelerogram, somewhat, resembles the shape of a 1 cycle sine wave (i.e. a prominent positive and negative peak acceleration in close proximity to each other). The similarity between the shape of the 1 cycle motion and the YBI90 accelerogram might help to explain the similarity between their induced amplifications.

6.2.1.2 Yerba Buena Island, 0 Degrees (N-S)

Figure 6.3 shows the amplification factor versus input motion frequency relationships produced in the sand profile by the scaled Yerba Buena Island, 0 degree (YBI0) earthquake accelerogram and the sinusoidal motions having maximum accelerations of 0.2g and 0.4g. Figure 6.3 shows that, compared to the YBI90 induced amplifications, the sinusoidal induced amplifications do not match as closely those induced by YBI0. From approximately 1.25 to 4.0 Hz at the 0.2g level, and from approximately 1.0 to 3.25 Hz at the 0.4g level, the 1 cycle induced amplifications provide the closest conservative match of YBI0. Above and below these frequency ranges, all the sinusoidal induced amplifications fall below those of YBI0.

Figure 6.4 shows the amplification factor versus input motion frequency relationships produced in the clay profile by the YBI0 and sinusoidal motions having a maximum acceleration of 0.2g. As with Figure 6.3, all the sinusoidally induced amplifications fall below those of YBI0 at the lower and

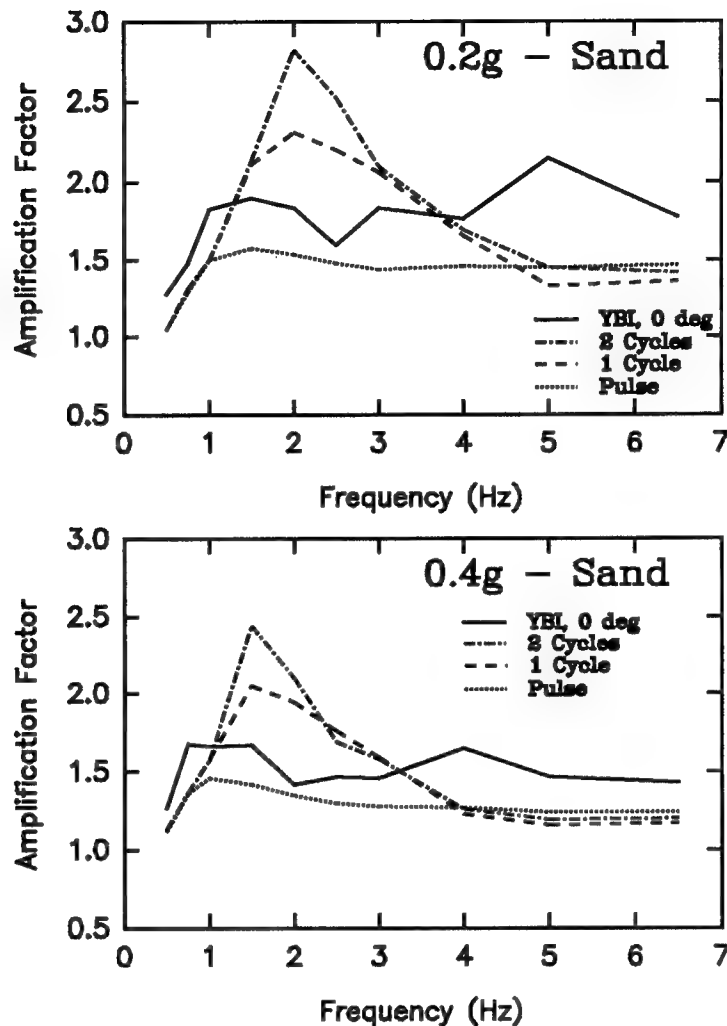


Figure 6.3: Amplification Factor vs. Input Motion Frequency, YBI0 and Sinusoidal Motions in Sand

higher frequencies. From approximately 1.0 to 3.0 Hz, the 1 cycle induced amplifications are the closest conservative match to YBI0.

Inspection of the YBI0 accelerogram in Figure 3.2 shows that the strong motion portion of the accelerogram consists of several, approximately equal positive and negative peak accelerations that are distributed over a wide time range.

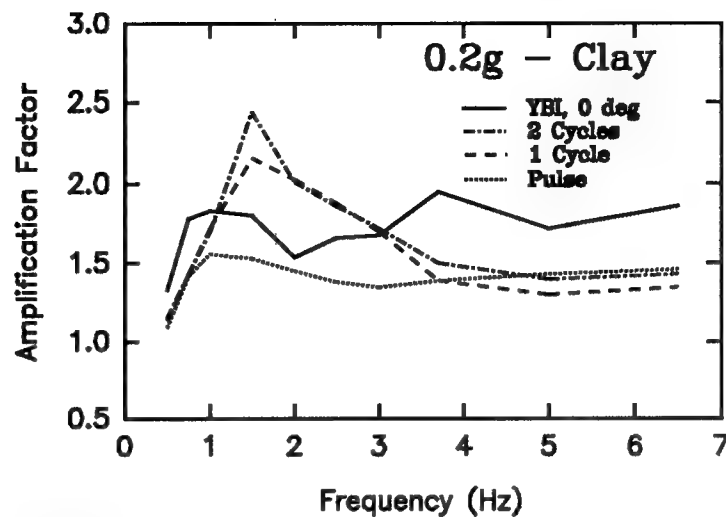


Figure 6.4: Amplification Factor vs. Input Motion Frequency, YBI0 and Sinusoidal Motions in Clay

Thus, the accelerogram does not appear to resemble the shape of any of the sinusoidal motions. This may help to account for the greater difference between their amplifications.

6.2.1.3 Presidio, 90 Degrees (E-W)

Figure 6.5 shows the amplification factor versus input motion frequency relationships produced in the sand profile by the scaled Presidio, 90 degree (Presidio90) earthquake accelerogram and the sinusoidal motions having maximum accelerations of 0.2g and 0.4g. At the lower and higher frequencies, all amplifications induced by the sinusoidal motions fall below, but are still fairly close to those of Presidio90, with the pulse input providing the closest match at the higher frequencies. From approximately 1.25 to 4.5 Hz at the 0.2 g level, and from approximately 1.0 to 4.0 Hz at the 0.4 g level, the 1 cycle induced amplifications are

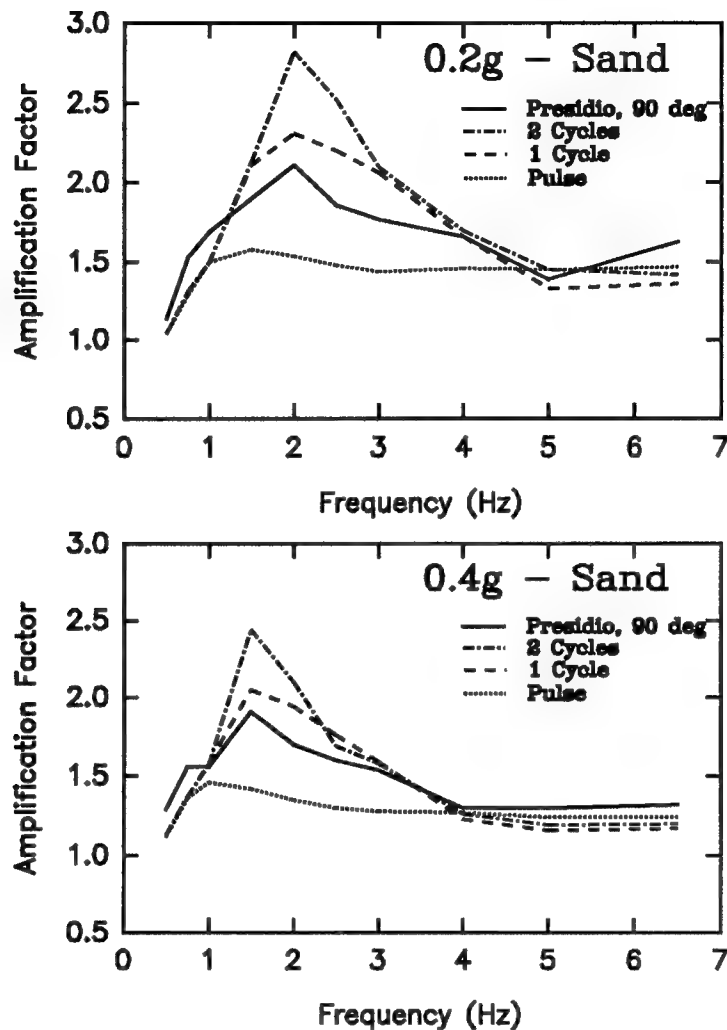


Figure 6.5: Amplification Factor vs. Input Motion Frequency, Presidio90 and Sinusoidal Motions in Sand

generally the closest conservative match to the Presidio90 induced amplifications.

Figure 6.6 shows the amplification factor versus input motion frequency relationships produced in the clay profile by the Presidio90 and sinusoidal motions having a maximum acceleration of 0.2g. When compared to Figure 6.5, the sinusoidal induced amplifications more closely resemble those

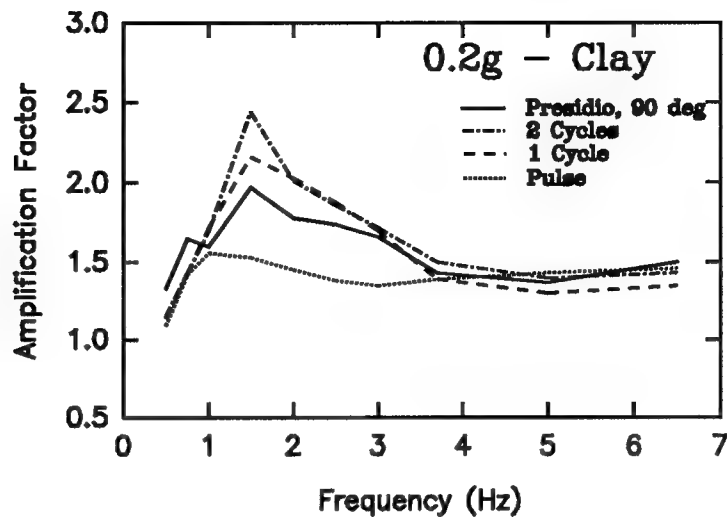


Figure 6.6: Amplification Factor vs. Input Motion Frequency, Presidio90 and Sinusoidal Motions in Clay

produced by Presidio90 at the higher frequencies, with the pulse and 2 cycle wave forms achieving the closest match. All sinusoidal induced amplifications fall below those of Presidio90 at the lower frequencies. From approximately 1.0 to 3.5 Hz, the 1 cycle induced amplifications provide the closest conservative fit to those of Presidio90.

Inspection of the Presidio90 accelerogram in Figure 3.2 shows that the strong motion portion of the accelerogram somewhat resembles the shape of a 1 cycle sine wave (i.e. a prominent positive and negative peak acceleration in close proximity to each other). This may serve to explain the similarities in the amplification factor for the 1 cycle and earthquake motion.

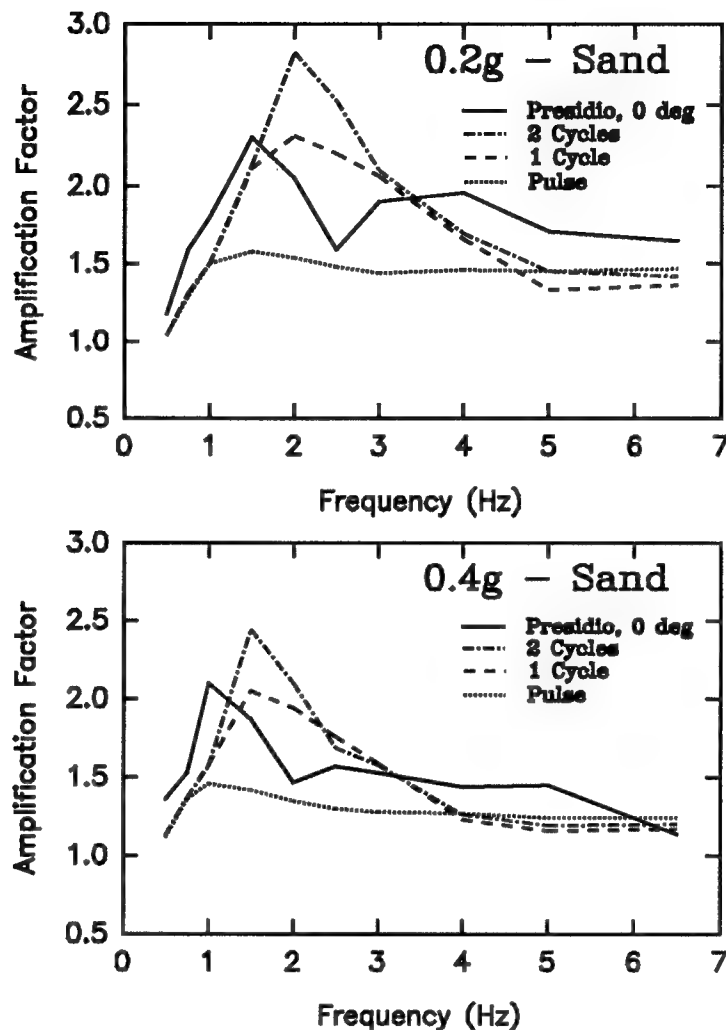


Figure 6.7: Amplification Factor vs. Input Motion Frequency, Presidio0 and Sinusoidal Motions in Sand

6.2.1.4 Presidio, 0 Degrees (N-S)

Figure 6.7 shows the amplification factor versus input motion frequency relationships produced in the sand profile by the scaled Presidio, 0 degree (Presidio0) earthquake accelerogram and the sinusoidal motions having maximum accelerations of 0.2g and 0.4g. The sinusoidally induced amplifications resemble the amplification pattern induced by

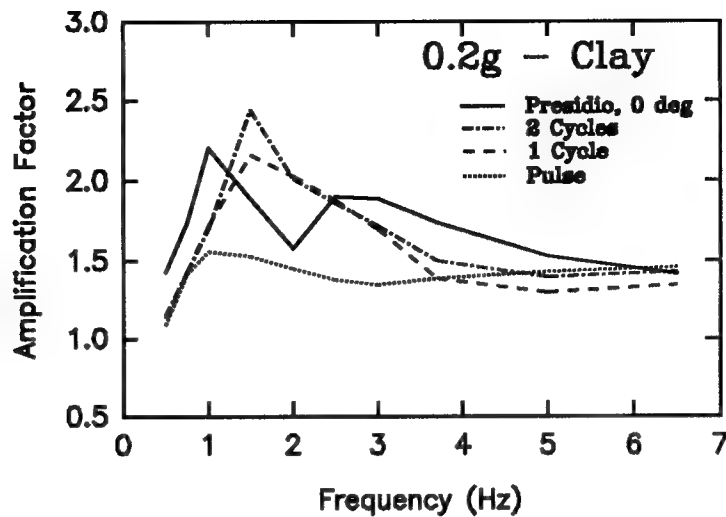


Figure 6.8: Amplification Factor vs. Input Motion Frequency, Presidio0 and Sinusoidal Motions in Clay

Presidio0 at the lower frequencies, but all fall below the Presidio0 amplifications. From approximately 1.75 to 3.5 Hz at the 0.2g level, and from approximately 1.5 to 3.25 Hz at the 0.4g level, the 1 cycle induced amplifications generally achieve the closest conservative match of Presidio0. Otherwise, with the exception of 6.0 to 6.5 Hz at the 0.4g level, the sinusoidal induced amplifications underestimate those of Presidio0.

Figure 6.8 shows the amplification factor versus input motion frequency relationships produced in the clay profile by the Presidio0 and sinusoidal motions having a maximum acceleration of 0.2g. Except from approximately 1.25 to 2.5 Hz, and from approximately 6.0 to 6.5 Hz, the sinusoidal induced amplifications underestimate those of Presidio0.

Between 1.25 and 2.5 hz, the 1 cycle induced amplifications generally provide the closest conservative match to Presidio0.

Inspection of the Presidio0 accelerogram in Figure 3.2 shows that the strong motion portion of the accelerogram consists of several, approximately equal positive and negative peak accelerations that are distributed over a wide range of time. Thus, the shape of the accelerogram does not appear to resemble the shape of any of the sinusoidal motions.

6.2.1.5 Piedmont, 45 Degrees

Figure 6.9 shows the amplification factor versus input motion frequency relationships produced in the sand profile by the scaled Piedmont, 45 degree (Piedmont45) earthquake accelerogram and the sinusoidal motions having maximum accelerations of 0.2g and 0.4g. In general the pulse induced amplifications provide the closest match to the Piedmont45 induced amplifications. From approximately 4.75 to 6.5 Hz at the 0.2g level, and from approximately 4.0 to 5.75 Hz at the 0.4g level, the 1 cycle induced amplifications provide the closest conservative match to Piedmont45.

Figure 6.10 shows the amplification factor versus input motion frequency relationships produced in the clay profile by the Piedmont45 and sinusoidal motions having a maximum acceleration of 0.2g. As in Figure 6.9, the pulse induced amplifications generally provide the closest match to those of Piedmont45. From approximately 3.75 to 5.5 Hz, the 1 cycle induced amplifications provide the closest conservative match.

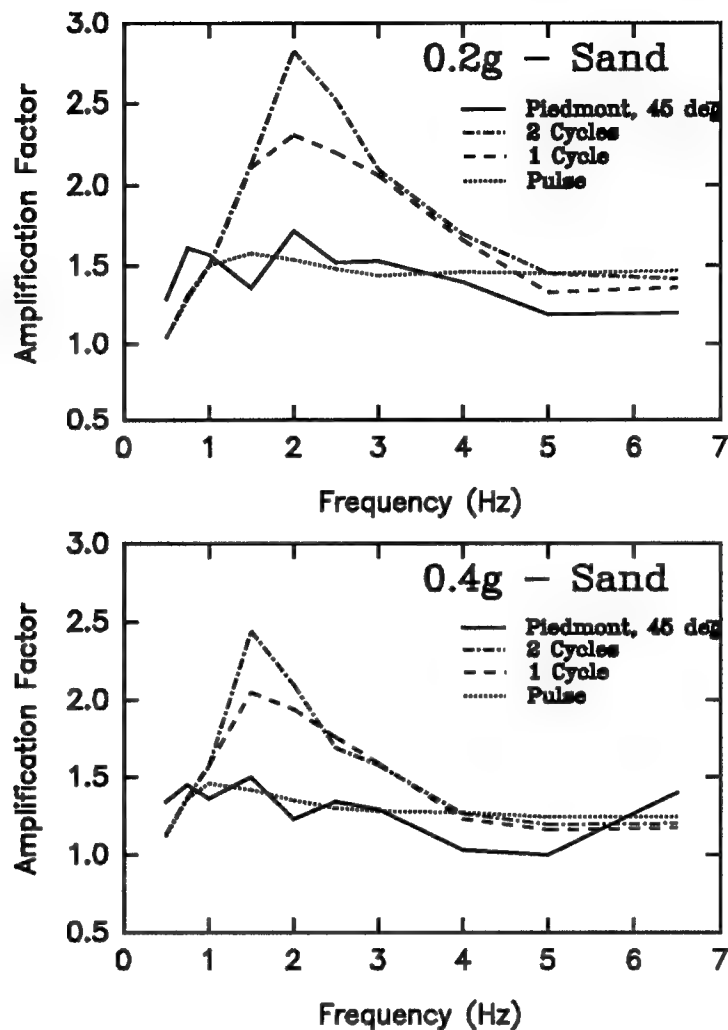


Figure 6.9: Amplification Factor vs. Input Motion Frequency, Piedmont45 and Sinusoidal Motions in Sand

Inspection of the Piedmont45 accelerogram in Figure 3.2 shows that the strong motion portion of the accelerogram somewhat resembles a pulse (i.e. one prominent positive peak acceleration). The similarity between the shape of the pulse motion and the Piedmont45 accelerogram may help explain the similarities between their induced amplifications.

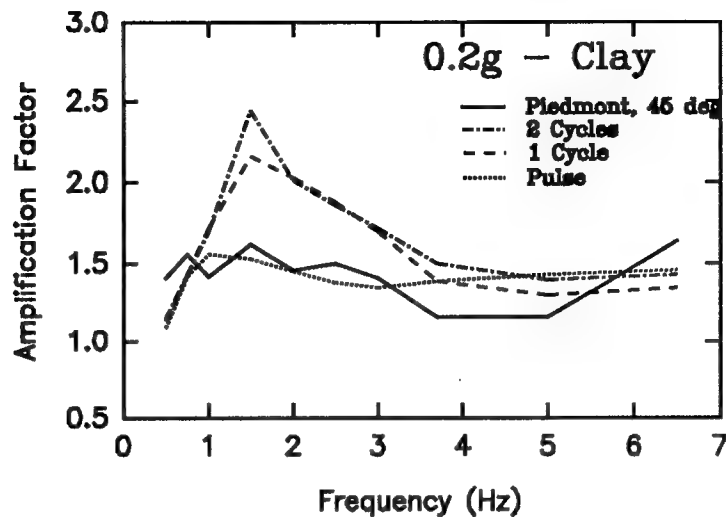


Figure 6.10: Amplification Factor vs. Input Motion Frequency, Piedmont45 and Sinusoidal Motions in Clay

6.2.1.6 Pulgas, 90 Degrees (E-W)

Figure 6.11 shows the amplification factor versus input motion frequency relationships produced in the sand profile by the scaled Pulgas, 90 degree (Pulgas90) earthquake accelerogram and the sinusoidal motions having maximum accelerations of 0.2g and 0.4g. The 1 cycle and 2 cycle induced amplifications are an approximate match to those of Pulgas90 from approximately 0.5 to 1.0 Hz at both the 0.2g and 0.4g level. From the high end of these frequency ranges, to approximately 3.75 Hz at the 0.2g level, and to approximately 3.0 Hz at the 0.4g level, the closest conservative amplification match to Pulgas90 is generally achieved by the 1 cycle motion. Otherwise, with the exception of the reasonably close match at the frequency range of 6.0 to 6.5 Hz

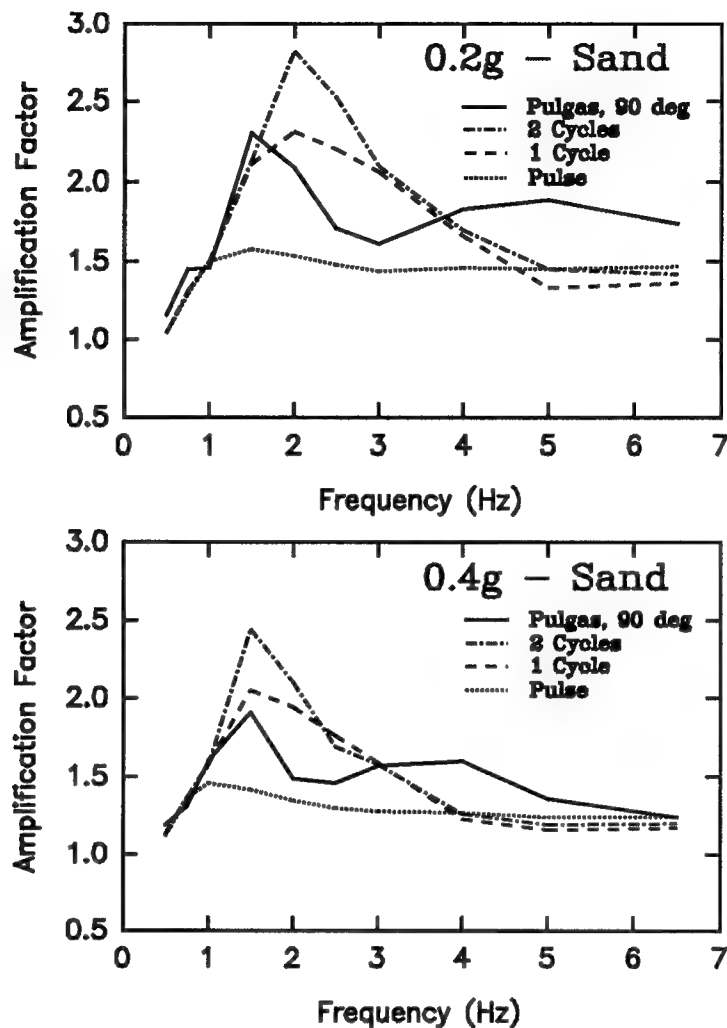


Figure 6.11: Amplification Factor vs. Input Motion Frequency, Pulgas90 and Sinusoidal Motions in Sand

at the 0.4g level, the sinusoidally induced amplifications fall below those of Pulgas90.

Figure 6.12 shows the amplification factor versus input motion frequency relationships produced in the clay profile by the Pulgas90 and sinusoidal motions having a maximum acceleration of 0.2g. Except for the frequency ranges of approximately 1.25 to 3.0 Hz and 5.75 to 6.5 Hz, the

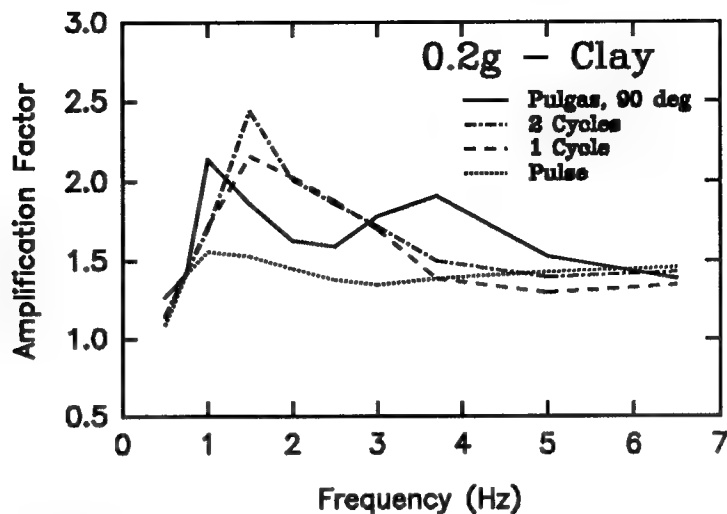


Figure 6.12: Amplification Factor vs. Input Motion Frequency, Pulgas90 and Sinusoidal Motions in Clay

sinusoidal induced amplifications fall below those of Pulgas90. From 1.25 to 3.0 Hz, the 1 cycle induced amplifications are generally the closest conservative match to Pulgas90.

Inspection of the Pulgas90 accelerogram in Figure 3.2 shows that the strong motion portion of the accelerogram consists of several, approximately equal, positive and negative peak accelerations that are distributed over a wide range of time. The shape of the accelerogram does not appear to have the form of any of the sinusoidal motions.

6.2.1.7 Pulgas, 0 Degrees (N-S)

Figure 6.13 shows the amplification factor versus input motion frequency relationships produced in the sand profile by the scaled Pulgas, 0 degree (Pulgas0) earthquake accelerogram and the sinusoidal motions having maximum accelerations of

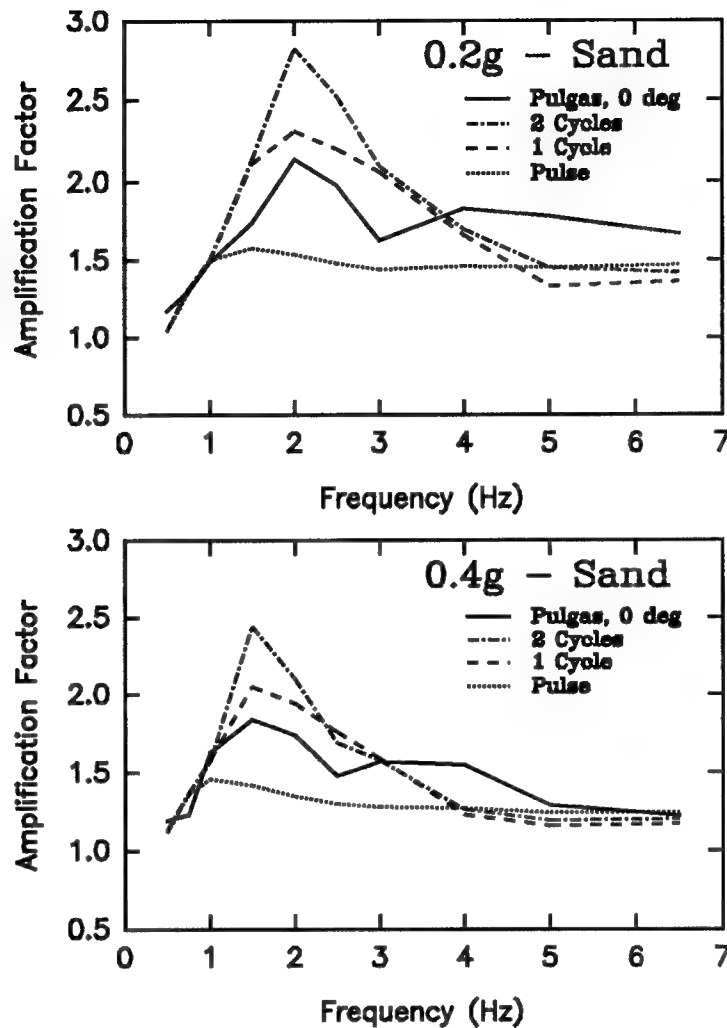


Figure 6.13: Amplification Factor vs. Input Motion Frequency, Pulgas0 and Sinusoidal Motions in Sand

0.2g and 0.4g. The amplifications induced by Pulgas0 generally fall in between the 1 cycle and pulse induced amplifications in the frequency ranges of 0.75 to 3.75 Hz at the 0.2g level, and of 0.5 to 3.0 Hz at the 0.4g level; the 1 cycle induced amplifications generally providing the closest conservative match. Otherwise, at the higher frequency ranges, the Pulgas0 induced amplifications are higher than the

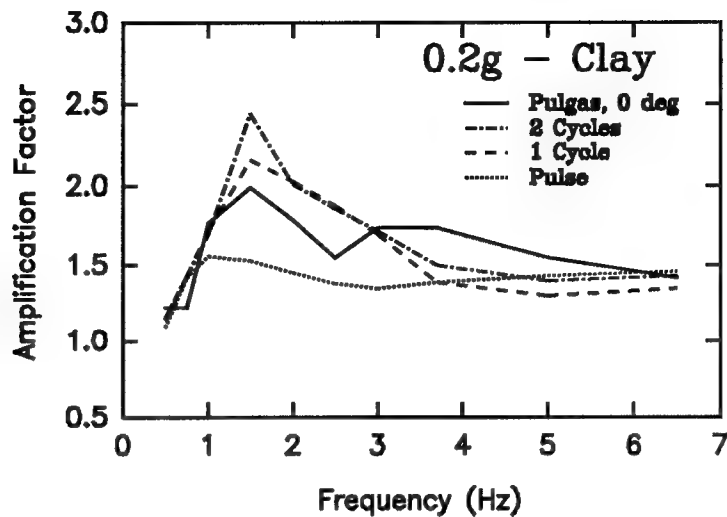


Figure 6.14: Amplification Factor vs. Input Motion Frequency, Pulgas0 and Sinusoidal Motions in Clay

sinusoidally induced amplifications. A fairly close match with the pulse develops at the 0.4g level from 5.0 to 6.5 Hz.

Figure 6.14 shows the amplification factor versus input motion frequency relationships produced in the clay profile by the Pulgas0 and sinusoidal motions having a maximum acceleration of 0.2g. The 1 cycle induced amplifications generally provide the closest conservative match to Pulgas0 from 0.5 to 3.0 Hz, and again near 5.75 to 6.5 Hz. Otherwise, the sinusoidally induced amplifications fall below those of Pulgas0.

Inspection of the Pulgas0 accelerogram in Figure 3.2 shows that the strong motion portion of the accelerogram closely resembles the shape of a 1 cycle sine wave, with one exception: It has two prominent positive peak accelerations rather than just one.

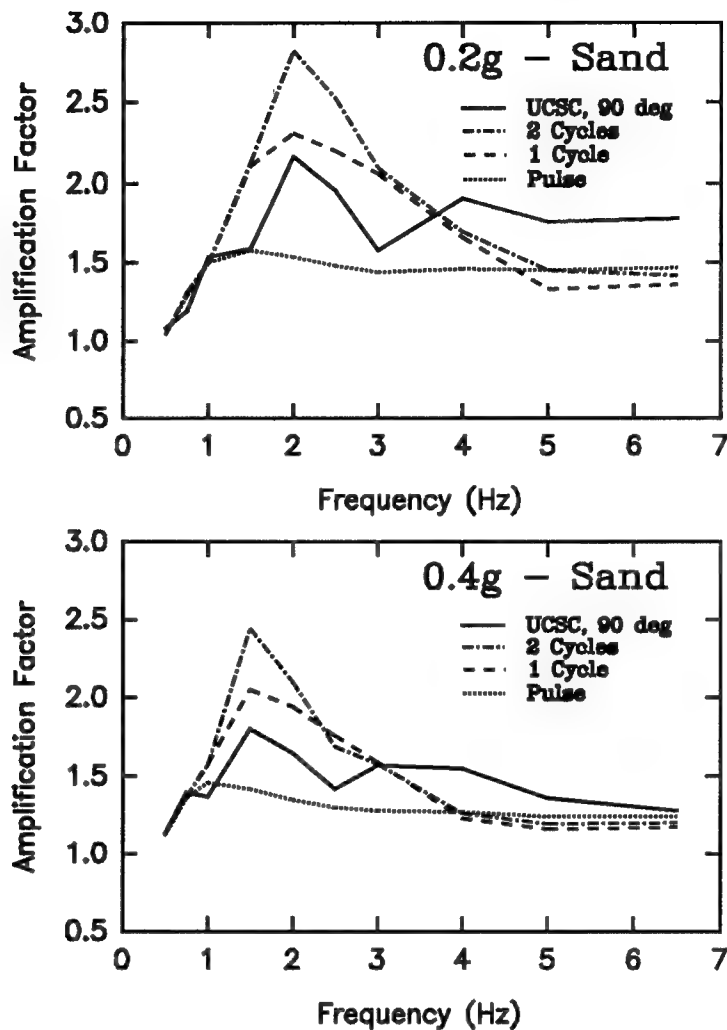


Figure 6.15: Amplification Factor vs. Input Motion Frequency, UCSC90 and Sinusoidal Motions in Sand

6.2.1.8 University of California at Santa Cruse (UCSC), 90 Degrees (E-W)

Figure 6.15 shows the amplification factor versus input motion frequency relationships produced in the sand profile by the scaled UCSC, 90 degree (UCSC90) earthquake accelerogram and the sinusoidal motions having maximum accelerations of 0.2g and 0.4g. The pulse induced amplifications are fairly

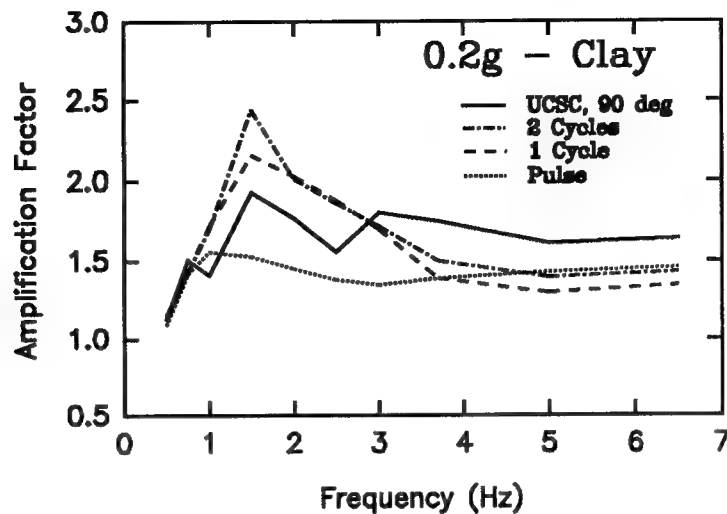


Figure 6.16: Amplification Factor vs. Input Motion Frequency, UCSC90 and Sinusoidal Motions in Clay

close to those of UCSC90 from 0.5 to 1.5 Hz at the 0.2g level, and from 0.5 to 1.0 Hz at the 0.4g level. From 1.5 to 3.75 Hz at the 0.2g level, and from 1.0 to 3.0 Hz at the 0.4g level, the 1 cycle induced amplifications provide the closest conservative match to UCSC90. The sinusoidal induced amplifications are less than those of UCSC90 at the remaining higher frequencies.

Figure 6.16 shows the amplification factor versus input motion frequency relationships produced in the clay profile by the UCSC90 and sinusoidal motions having a maximum acceleration of 0.2g. The pulse induced amplifications provide the closest match of UCSC90 from 0.5 to 1.0 Hz. From 1.0 to approximately 3.0 Hz, the closest conservative match to the UCSC90 amplifications is produced by the 1 cycle motion.

At frequencies greater than 3.0 Hz, all of the sinusoidal induced amplifications fall below those of UCSC90.

Inspection of the UCSC90 accelerogram in Figure 3.2 shows that the strong motion portion of the accelerogram consists of several, approximately equal positive and negative peak accelerations that are distributed over a wide time range. The shape of the accelerogram does not appear to resemble the shape of any of the sinusoidal motions.

6.2.1.9 University of California at Santa Cruse (UCSC), 0 Degrees (N-S)

Figure 6.17 shows the amplification factor versus input motion frequency relationships produced in the sand profile by the scaled UCSC, 0 degree (UCSC0) earthquake accelerogram and the sinusoidal motions having maximum accelerations of 0.2g and 0.4g. At the 0.2g level, the 1 and 2 cycle induced amplifications closely match those of UCSC0 from approximately 0.75 to 1.5 Hz. At the 0.4g level, all the sinusoidal induced amplifications closely match those of UCSC90 at 0.5 to 0.75 Hz. The 1 cycle induced amplifications provide the closest conservative match to UCSC90 from 1.5 to 3.0 Hz at the 0.2g level, and from 1.25 to 2.5 Hz at the 0.4g level. The sinusoidally induced amplifications fall below those of UCSC0 at the higher frequencies, except from 5.0 to 6.5 Hz at the 0.4g level, where the pulse induced amplifications provide a close match.

Figure 6.18 shows the amplification factor versus input motion frequency relationships produced in the clay profile

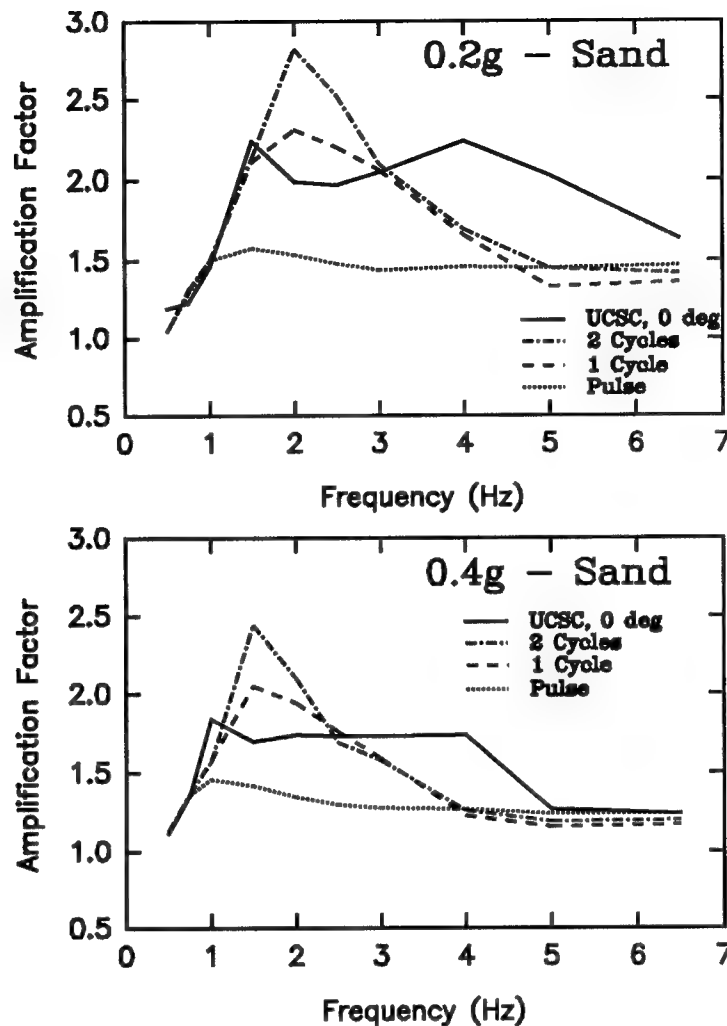


Figure 6.17: Amplification Factor vs. Input Motion Frequency, UCSC0 and Sinusoidal Motions in Sand

by the UCSC0 and sinusoidal motions having a maximum acceleration of 0.2g. All of the sinusoidally induced amplifications closely match those of UCSC0 from 0.5 to 0.75 Hz. From 0.75 to 1.25 Hz, the sinusoidal induced amplifications fall below those of UCSC0. Afterwards, the 1 and 2 cycle induced amplifications plot above UCSC0 to about 2.25 Hz, with the 1 cycle generally being the closest match.

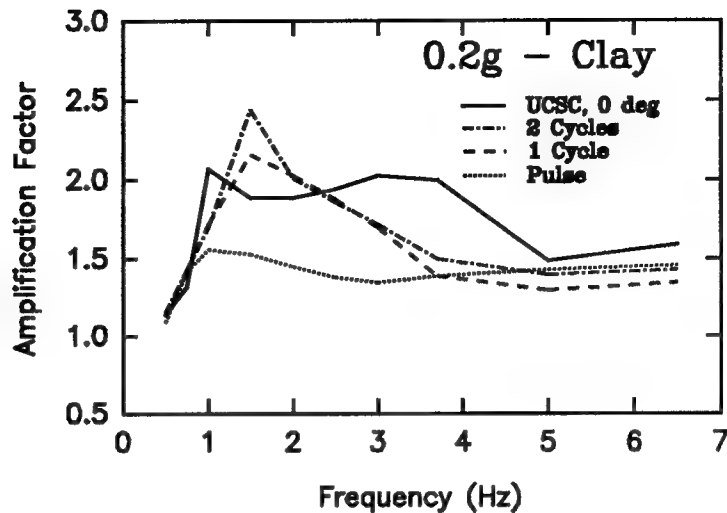


Figure 6.18: Amplification Factor vs. Input Motion Frequency, UCSC0 and Sinusoidal Motions in Clay

At frequencies higher than 2.25 Hz, the sinusoidal induced amplifications all fall below those of UCSC0.

Inspection of the UCSC0 accelerogram in Figure 3.2 shows that the strong motion portion of the accelerogram consists of several, approximately equal positive and negative peak accelerations distributed over a wide time range. The shape of the accelerogram does not appear to resemble the shape of any of the sinusoidal motions.

6.2.1.10 Pasadena 1952

Figure 6.19 shows the amplification factor versus input motion frequency relationships produced in the sand profile by the scaled Pasadena 1952 earthquake accelerogram and the sinusoidal motions having maximum accelerations of 0.2g and 0.4g. In general, the 1 cycle induced amplifications provide a fairly close match to those of Pasadena 1952 over the entire

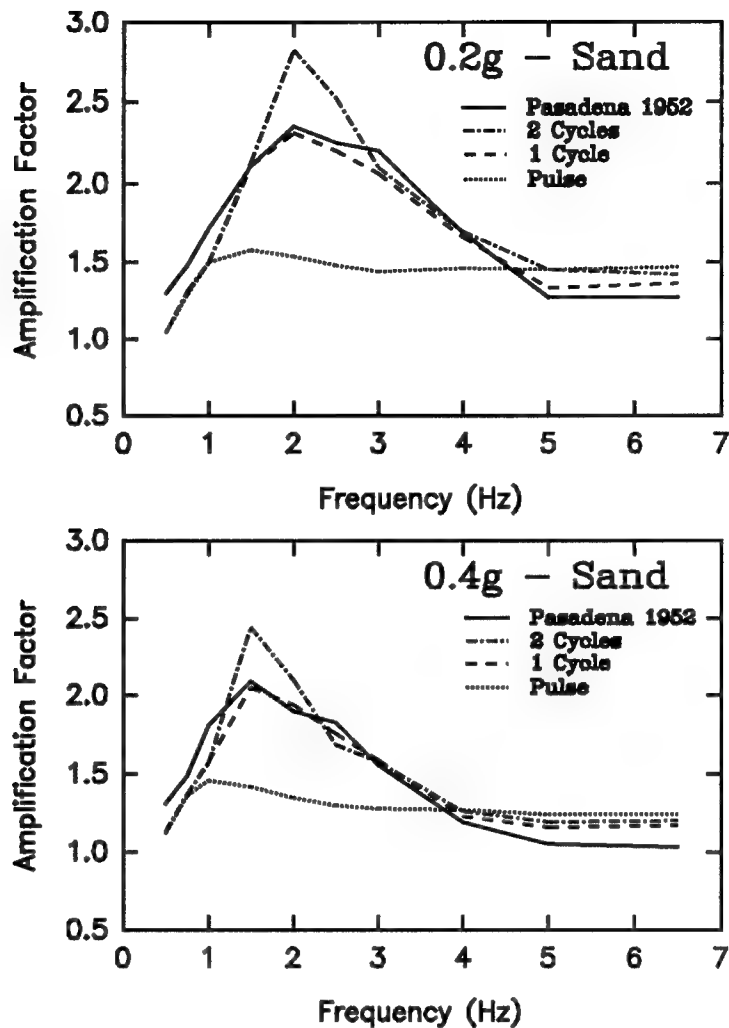


Figure 6.19: Amplification Factor vs. Input Motion Frequency, Pasadena 1952 and Sinusoidal Motions in Sand

frequency range depicted. There are a few areas, such as at the lower frequencies, where all the sinusoidal induced amplifications fall slightly below those of Pasadena 1952.

Figure 6.20 shows the amplification factor versus input motion frequency relationships produced in the clay profile by the Pasadena 1952 and sinusoidal motions having a maximum acceleration of 0.2g. As in Figure 6.19, the 1 cycle induced

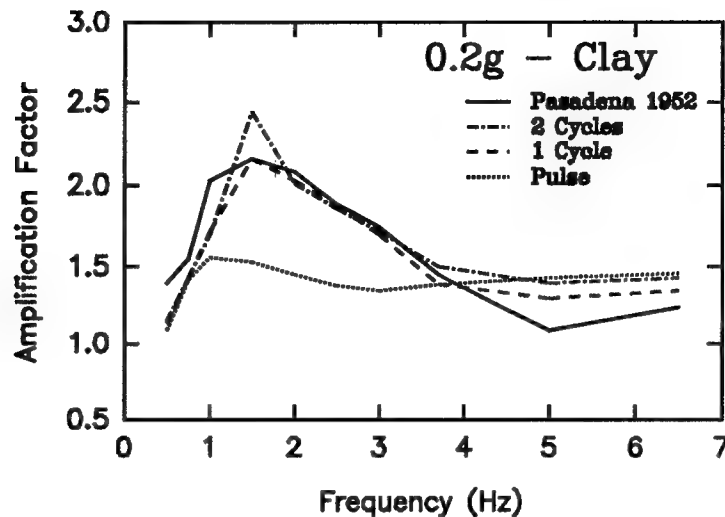


Figure 6.20: Amplification Factor vs. Input Motion Frequency, Pasadena 1952 and Sinusoidal Motions in Clay

amplifications are again a reasonably close match to those of Pasadena 1952 for most of the frequencies. None of the sinusoidal induced amplifications reach those of Pasadena 1952 from about 0.5 to 1.25 Hz. From 4.0 to 6.5 Hz, the Pasadena 1952 induced amplifications fall below those of the sinusoidal motions, with the 1 cycle induced amplifications achieving the closest match.

Examination of the Pasadena 1952 accelerogram in Figure 3.2 shows that the strong motion portion of the accelerogram appears to be uniform in changing from a positive, to a negative, peak acceleration. This produces the appearance of a multi cycle sine wave. This resemblance may also help to explain the similarity in amplifications between the 1 and 2 cycle sinusoidal motions and the Pasadena 1952 accelerogram.

It should be noted that the Pasadena 1952 accelerogram obtained for this study is an incomplete record of the actual earthquake.

6.2.2 Sinusoidal Scaled to Earthquake Parameters

This section compares the "normalized" peak surface accelerations (amplifications factors) induced in the sand and clay profiles by the ten original earthquake records and the sinusoidal motions scaled to match the maximum acceleration and predominant frequency of the original earthquake records. SHAKE-88 was used to compute the peak surface accelerations.

In preparation for the comparison, an additional tail of zeros (0's) was added to the 800 acceleration value, 0.2g, 2.5 Hz pulse, 1 cycle and 2 cycle sinusoidal motion records developed in Chapter 5. The records then consisted of 2000 acceleration values; the same as the earthquake records.

Table 6.1 displays the amplifications induced in the sand profile by each of the original earthquake records and by the sinusoidal motions scaled to match the parameters of the original earthquake records. The earthquakes are listed in order of increasing predominant frequency.

The 40 amplification factors displayed in Table 6.1 are plotted versus the predominant frequency of the original earthquake in Figure 6.21. The earthquake induced amplifications, depicted by a dark triangle, are labeled 1 through 10 as identified in Table 6.1. The scaled pulse, 1 cycle and 2 cycle induced amplifications, depicted by the

Table 6.1: Amplifications in Sand

Earthquake Record	Pred Freq (Hz)	Max Accel (g)	Amplification due to input motion			
			Earth quake	Pulse	1 Cycle	2 Cycle
1. Pasadena52	1.59	0.06	2.52	1.75	1.75	1.75
2. Presidio90	1.88	0.20	2.14	1.54	2.29	2.84
3. YBI 90	2.15	0.07	2.42	1.75	2.70	2.97
4. Presidio 0	2.16	0.10	2.52	1.68	2.63	3.34
5. Pulgas 90	2.42	0.09	2.69	1.70	2.72	3.56
6. Pulgas 0	2.48	0.16	2.18	1.54	2.36	2.87
7. Piedmont45	2.61	0.08	2.10	1.68	2.73	3.60
8. YBI 0	2.87	0.03	3.27	1.81	3.16	4.72
9. UCSC 0	4.74	0.44	1.26	1.20	1.14	1.17
10. UCSC 90	5.95	0.41	1.32	1.22	1.16	1.19

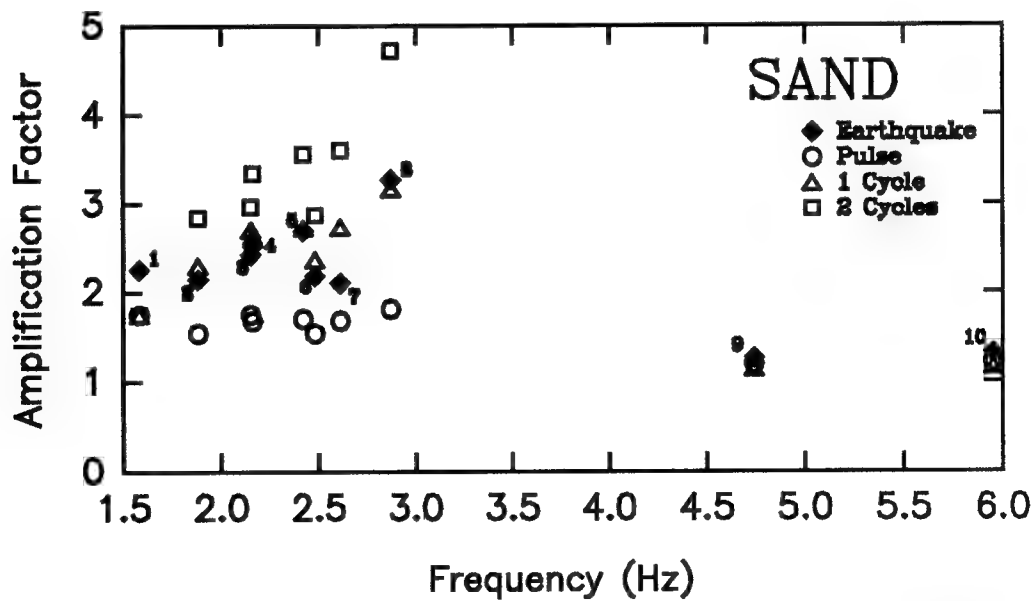


Figure 6.21: Amplification Factor vs. Predominant Frequency, Sand

symbols indicated, are plotted directly above or below the corresponding earthquakes.

Figure 6.21 shows that the 1 cycle induced amplifications closely match the amplifications of earthquake numbers 2, 3, 4, 5, 6, 8, 9 and 10. The amplifications for earthquake numbers 9 and 10 are closely matched by all of the sinusoidal induced amplifications. All sinusoidal induced amplifications fall below those of earthquake number 1. The amplification induced by earthquake number 7 falls in between the pulse and 1 cycle induced amplifications.

Table 6.2 displays the same information as Table 6.1, except that the amplification factors are those resulting in the clay profile. The 40 amplification factors displayed in Table 6.2 are plotted versus the predominant frequency of the original earthquake in Figure 6.22.

In Figure 6.22, the amplifications induced by the 1 cycle motions provide, in general, a reasonably close match to the amplifications induced by the earthquake records. Compared to Figure 6.21, the differences in amplification increased between the 1 cycle motions and earthquake numbers 2, 3, 4, 5 and 6. However, the differences in amplification also decreased between the 1 cycle motions and earthquake numbers 1 and 7. Amplifications for earthquake numbers 9 and 10 were again closely matched by all the sinusoidal induced amplifications.

Table 6.2: Amplifications in Clay

Earthquake Record	Pred Freq (Hz)	Max Accel (g)	Amplification due to input motion			
			Earth quake	Pulse	1 Cycle	2 Cycle
1. Pasadena52	1.59	0.06	2.12	1.79	1.83	1.83
2. Presidio90	1.88	0.20	1.82	1.46	2.05	2.11
3. YBI 90	2.15	0.07	2.24	1.74	2.83	3.72
4. Presidio 0	2.16	0.10	2.28	1.67	2.54	3.19
5. Pulgas 90	2.42	0.09	2.31	1.68	2.65	3.16
6. Pulgas 0	2.48	0.16	1.79	1.49	2.10	2.16
7. Piedmont45	2.61	0.08	2.13	1.66	2.62	3.10
8. YBI 0	2.87	0.03	3.06	1.80	3.22	4.88
9. UCSC 0	4.74	0.44	1.21	1.13	1.08	1.10
10. UCSC 90	5.95	0.41	1.12	1.14	1.10	1.36

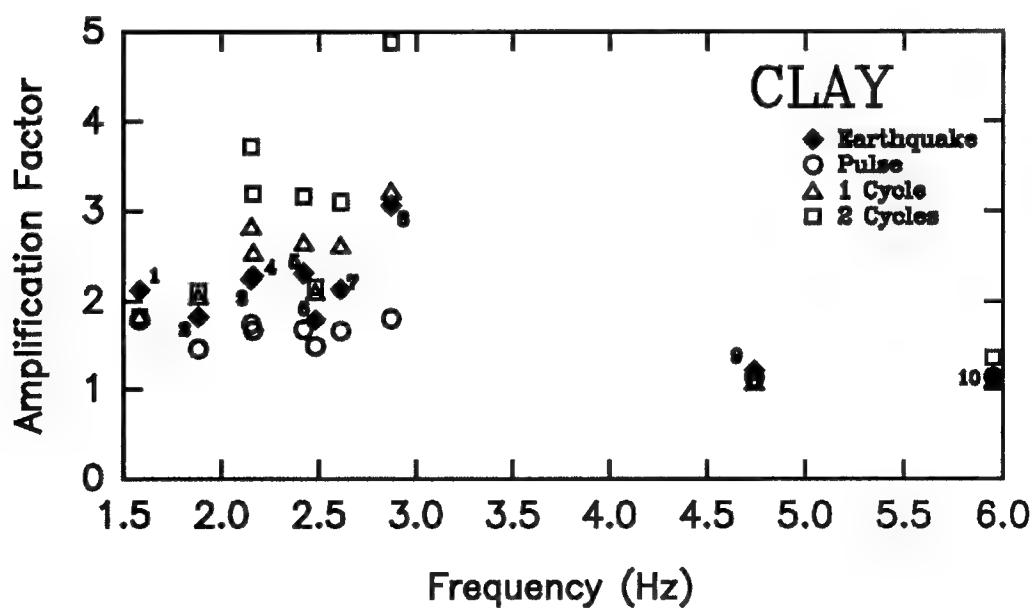


Figure 6.22: Amplification Factor vs. Predominant Frequency, Clay

The closeness of the sinusoidal and earthquake induced amplifications in Figures 6.21 and 6.22 does not appear to be influenced by whether or not the shape of the earthquake accelerogram resembles one of the sinusoidal motions. This would appear to contrast with the findings presented in Section 6.2.1.

6.3 Earthquake versus Sinusoidal Induced Amplifications in the Treasure Island Profile

6.3.1 Earthquake Scaled to Sinusoidal Parameters

To prepare data for these analyses, the original Yerba Buena Island 90 degree and 0 degree (YBI90 and YBI0) earthquake records, and the 0.2g, 2.5 Hz pulse, 1 cycle, and 2 cycle sinusoidal motions consisting of 2000 acceleration values, were scaled to maximum accelerations of 0.2g, 0.4g and 0.6g, and frequencies of 0.5, 0.75, 0.94, 1.0, 1.5, 2.0, 2.5, 3.0, 3.5, 4.0, 5.0 and 6.5 Hz. The 0.94 Hz frequency was included because this is the natural frequency of the Treasure Island UM10 site profile. SHAKE-88 was used to compute the peak surface accelerations. These accelerations were normalized to obtain the amplification factors.

6.3.1.1 YBI90 Accelerogram

Figure 6.23 shows the amplification factor versus input motion frequency relationships produced in the Treasure Island UM10 profile by the scaled YBI90 earthquake accelerogram and sinusoidal motions having maximum accelerations of 0.2g (top graph), 0.4g (middle graph), and 0.6g (bottom graph). In

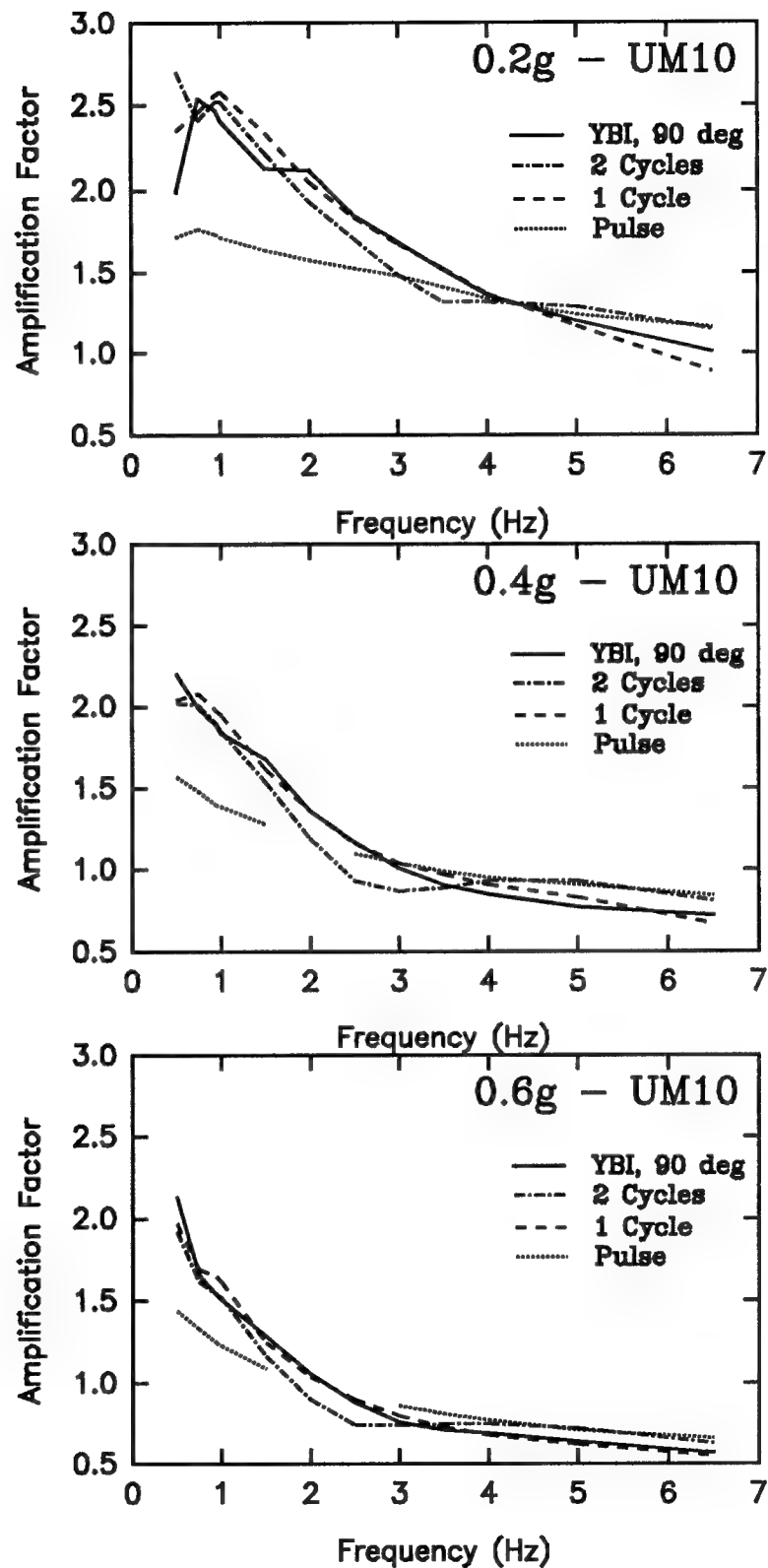


Figure 6.23: Amplification Factor vs. Input Motion Frequency, YBI90 and Sinusoidal Motions in UM10

contrast to the amplifications induced in the sand and clay profiles, the amplifications induced in the UM10 profile peak near the natural frequency of the deposit (0.94 Hz). This is the response that is expected based on the information given in Section 2.2.6.2. The three graphs of Figure 6.23 constitute 144 SHAKE-88 computer runs.

In all three graphs of Figure 6.23, the 1 cycle induced amplifications closely match those induced by YBI90, especially for the 0.4g and 0.6g levels. It was noted in section 6.2.1.1 that the strong motion portion of the YBI90 accelerogram somewhat resembles the shape of a single cycle sine wave, which again may help to explain the close similarity between the 1 cycle and YBI90 induced amplifications.

6.3.1.2 YBI0 Accelerogram

Figure 6.24 shows the amplification factor versus input motion frequency relationships produced in the UM10 profile by the scaled YBI0 earthquake accelerogram and sinusoidal motions having maximum accelerations of 0.2g (top graph), 0.4g (middle graph), and 0.6g (bottom graph). Figure 6.24 is the same as Figure 6.23, except that the YBI0 amplifications replace the YBI90 amplifications, portraying an additional 48 SHAKE-88 computer runs.

In Figure 6.24, the sinusoidal induced amplifications, while not coming as close to matching the YBI90 induced amplifications, still are fairly close to matching the YBI0

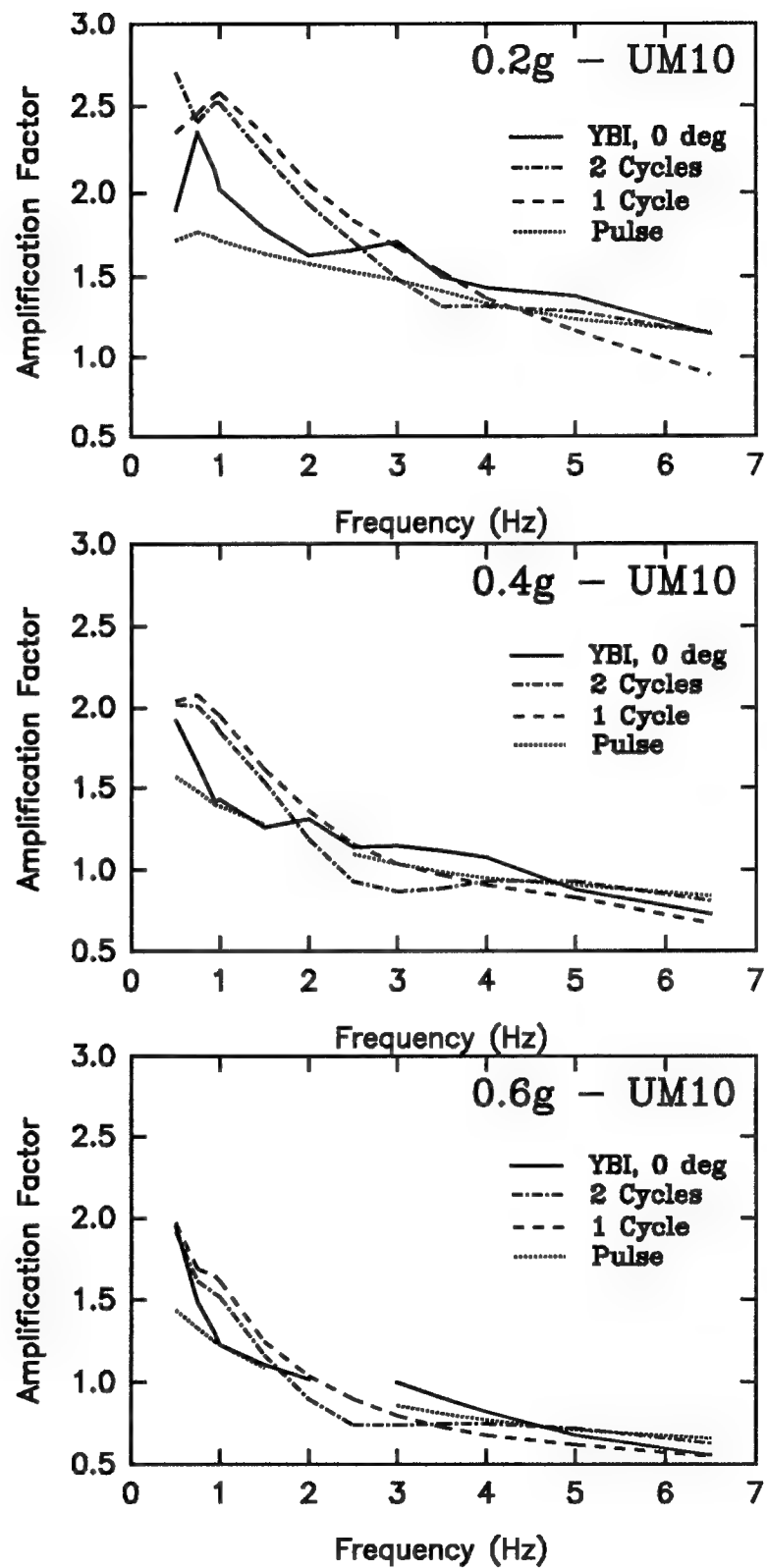


Figure 6.24: Amplification Factor vs. Input Motion Frequency, YBI0 and Sinusoidal Motions in UM10

induced amplifications at several frequencies. As pointed out in Section 6.2.1.2, the shape of the YBI0 accelerogram does not appear sinusoidal. This may account for the greater amplification differences.

As shown in Figure 6.24 (or 6.23), the amplifications induced in the UM10 profile by the 1 cycle motions are greater than those induced by the 2 cycle motions for frequencies of 0.75 to 4.25 Hz at the 0.2g level; 0.5 to 4.0 Hz at the 0.4g level; and 0.5 to 3.25 Hz at the 0.6g level. In the sand and clay profiles of Section 6.2, the 2 cycle induced amplifications were typically greater than the 1 cycle induced amplifications at all frequencies.

6.3.2 Sinusoidal Scaled to Earthquake Parameters

This section compares the "normalized" peak surface accelerations (amplification factors) induced in the Treasure Island UM10 profile by the ten original earthquake records and the sinusoidal motions scaled to match the maximum acceleration and predominant frequency of the original earthquake records. SHAKE-88 was used to compute the peak surface accelerations. As with the data given in Sections 6.2.2 and 6.3.1, the 0.2g, 2.5 Hz sinusoidal motion records consisting of 2000 acceleration values were utilized.

Table 6.3 displays the amplifications induced in the UM10 profile by the original earthquake records and the sinusoidal motions scaled to the parameters of the original earthquake records.

Table 6.3: Amplifications in UM10

Earthquake Record	Pred Freq (Hz)	Max Accel (g)	Amplification due to input motion			
			Earth quake	Pulse	1 Cycle	2 Cycle
1. Pasadena52	1.59	0.06	2.97	2.28	3.56	3.55
2. Presidio90	1.88	0.20	2.32	1.59	2.13	2.01
3. YBI 90	2.15	0.07	2.69	2.16	3.06	2.94
4. Presidio 0	2.16	0.10	2.81	1.99	2.79	2.68
5. Pulgas 90	2.42	0.09	1.97	2.02	2.71	2.58
6. Pulgas 0	2.48	0.16	1.81	1.65	2.15	2.01
7. Piedmont45	2.61	0.08	2.40	2.01	2.61	2.45
8. YBI 0	2.87	0.03	2.92	2.33	2.87	2.73
9. UCSC 0	4.74	0.44	0.76	0.85	0.77	0.89
10. UCSC 90	5.95	0.41	0.93	0.86	0.70	0.84

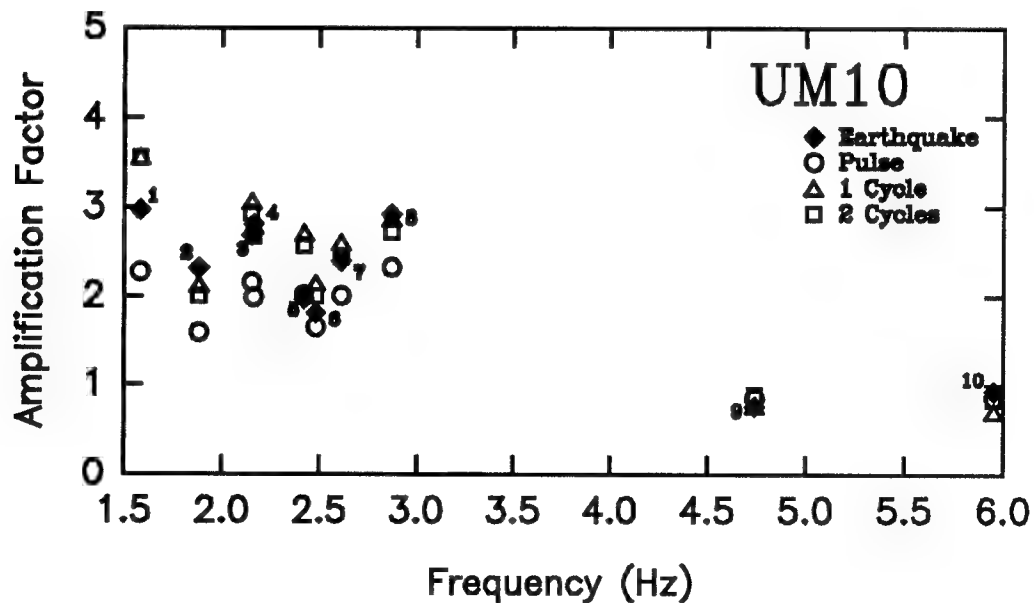


Figure 6.25: Amplification Factor vs. Predominant Frequency, UM10

The 40 amplification factors displayed in Table 6.3 are plotted versus the predominant frequency of the earthquake in Figure 6.25. As in Figures 6.21 and 6.22, the sinusoidal induced amplifications are plotted directly above or below the amplifications induced by the corresponding earthquake. The 1 cycle and 2 cycle induced amplifications fairly closely match the amplifications induced by earthquake numbers 2, 3, 4, 6, 7, 8, 9 and 10. The pulse induced amplification is a very close match to that of earthquake number 5. The amplification induced by earthquake number 1 falls between the pulse, and the 1 and 2 cycle amplifications. Figure 6.25 also shows that the 1 cycle induced amplifications in the UM10 profile are generally greater than the 2 cycle induced amplifications for frequencies less than 3.0 Hz.

As in Section 6.2.2, the closeness of the sinusoidal and earthquake induced amplifications in Figure 6.25 do not appear to be influenced by whether or not the shape of the earthquake accelerogram resembles a sinusoidal motion.

6.4 Chapter Summary

The purpose of this chapter was to determine if any of the sinusoidal motions induced peak surface accelerations that are similar to those induced by earthquake records. The normalized peak surface acceleration (amplification factor) versus input motion frequency comparisons made in this chapter (the product of 690 SHAKE-88 computer runs) indicate that peak

surface accelerations induced by pulse, 1 cycle and 2 cycle sinusoidal motions can be fair approximates to the peak surface accelerations induced by earthquake records. This can be particularly so if the shape of the earthquake accelerogram resembles the sinusoidal motion.

6.4.1 Ideal Sand and Clay Profile Results

6.4.1.1 Earthquake Scaled to Sinusoidal Parameters

In general, the amplification factor versus input motion frequency responses for the sinusoidal motions, especially the 1 cycle motion, closely matched the earthquake responses. At the lower frequencies, if the earthquake responses were not close to the sinusoidal responses, they usually lay in between the 1 cycle and pulse responses. The largest divergence where the sinusoidal response underestimated the earthquake response, was an amplification spread of 0.75 at 5.0 Hz in the sand profile.

The sinusoidal responses, particularly the 1 cycle response, matched some of the earthquake record responses better than others. The closest matches occurred where the shape of the earthquake record somewhat resembled that of the sinusoidal motion involved in the comparison. This is described in the succeeding paragraphs.

a. Sinusoidal responses, especially 1 cycle responses, closely matched the responses of the YBI90, Presidio90, and Pasadena 1952 earthquake records. The YBI90 and Presidio90 records have one prominent positive and one prominent negative

peak acceleration, which roughly resembles a single cycle sine wave. The Pasadena 1952 record roughly resembles a steady state sine wave. The 1 cycle responses are reasonably close matches to the Presidio0 and Pulgas0 responses as well. Their records also resemble a 1 cycle sine wave, with the exception that they each have two prominent positive peak accelerations rather than just one.

b. The pulse produces the closest response to that of the Piedmont45 record. The Piedmont45 record has one prominent positive peak acceleration that roughly resembles a pulse.

c. The rest of the earthquake record responses (i.e. YBI0, Pulgas90, UCSC90, UCSC0) are not matched as well by the sinusoidal motions. The strong motion portion of these accelerograms consist of several, approximately equal positive and negative peak accelerations that are distributed over a wide time range. They do not appear to resemble any of the sinusoidal motions.

6.4.1.2 Sinusoidal Scaled to Earthquake Parameters

In the sand profile, the 1 cycle response generally provided the closest match to those of the earthquake records (8 out of 10). Of the two not so close matches, the UCSC90 response was in between the 1 cycle and pulse response, and the YBI90 response was an amplification of 0.5 higher than the 1 cycle response. (This was surprising since the 1 cycle and YBI90 responses were a closer match in Section 6.4.1.1).

In the clay profile, the 1 cycle response was generally

the closest match to those of the earthquake records, but not as well as in the sand (only 4 of 10). Of the 6 not closely matching, the 1 cycle response was higher than 5 of 6 earthquake responses, and within an amplification of 0.5 of all 6 earthquake responses. The largest amplification spread (up to an amplification of 0.5) was for the YBI90, UCSC90, and both Presidio records. (This is again surprising as the 1 cycle responses were close matches to the YBI90 and Presidio90 responses in Section 6.4.1.1).

6.4.2 Treasure Island UM10 Profile Results

6.4.2.1 Earthquake Scaled to Sinusoidal Parameters

The sinusoidal responses, especially 1 cycle responses, were a very close match to the YBI90 record responses in the UM10 profile. The sinusoidal responses were also fairly close to those of the YBI0 record in the UM10 profile, but not as close as they were to the YBI90 record.

6.4.2.2 Sinusoidal Scaled to Earthquake Parameters

The 1 cycle response generally provided the closest match to those of the earthquake records (7 of 10). Of the three not so close matches, the 1 cycle response was higher than the three earthquake responses with the highest spread being an amplification of 0.7. The pulse response was closest to both Pulgas record responses.

7. SUMMARY AND CONCLUSIONS

7.1 Summary of Research

The purpose of this study was to address the effectiveness of using sinusoidal motions in seismic ground motion studies by comparing how well sinusoidally induced peak surface accelerations match those induced by an earthquake.

The study involved two objectives. The first objective was to compare the peak surface accelerations induced in two ideal soil profiles by pulse, 1 cycle, 2 cycle, 5 cycle and steady state sinusoidal motions having the same maximum amplitude and frequency, to determine if any of the lesser cycle motions induce the same peak surface accelerations as a greater cycle motion. The first objective served to establish which sinusoidal motions would be used for the second objective.

The second objective of the study was to compare the peak surface accelerations induced in two ideal soil profiles and one field site profile by both earthquake records, and the sinusoidal motions established in the first objective. For each comparison, the sinusoidal motion and earthquake record had the same maximum acceleration and predominant frequency.

The SHAKE-88 computer program was used to compute the peak surface accelerations induced by the sinusoidal and earthquake

input motions. The peak surface accelerations were normalized and plotted against the frequency of the input motion. Comparisons for both objectives were made using normalized acceleration (amplification factor) versus frequency response patterns.

7.2 Summary of Results

The following results were developed by this study:

1. Comparisons made in Chapter 5 indicate that a 2 cycle sinusoidal motion can induce the same peak surface accelerations as longer 5 cycle and steady state sinusoidal motions. The comparisons are for ideal sand and clay profiles with input motion maximum amplitudes ranging from 0.2g to 0.4g in sand and approximately 0.2g in clay, with frequencies ranging from 0.5 to 6.5 Hz.

2. Comparisons indicate that the peak surface accelerations induced by the pulse, 1 cycle and 2 cycle sinusoidal motions can be very similar to the peak surface accelerations induced by earthquake records, particularly if the shape of the earthquake record resembles the sinusoidal motion. The comparisons are for ideal sand and clay profiles with input motion maximum accelerations ranging from 0.03g to 0.44g, and frequencies ranging from 0.5 to 6.5 Hz. The comparisons are also for the Treasure Island UM10 profile with input motion

maximum accelerations ranging from 0.03g to 0.6g, with predominant frequencies ranging from 0.5 to 6.5 Hz.

7.3 Conclusions

The results of this study provided the following conclusions:

1. Pulse, 1 cycle and 2 cycle sinusoidal motions are able to induce peak accelerations that are very similar to those induced by earthquake records for a wide range of maximum accelerations and predominant frequencies. The utilization of sinusoidal motions to simulate seismic motions (e.g., earthquake) of a particular maximum acceleration and predominant frequency in soil-structure interaction (SSI) analyses, can be done with an increased level of confidence.
2. The quality (closeness) of the sinusoidal-earthquake induced peak accelerations appears to be influenced by similarities in the shapes of the motion-time histories. For example, if the shape of the earthquake record resembles a single cycle sine wave, then the peak acceleration induced by a 1 cycle sinusoidal motion is likely to come closer than other sinusoidal motions to matching the earthquake induced peak acceleration.

7.4 Recommendations

This study looked only at the peak surface accelerations induced by the sinusoidal and earthquake motions. Other studies should be conducted that compare the response spectra of the earthquake and sinusoidal motions as well. The response spectra could provide a greater level of detail for a comparative analysis. For example, a single SHAKE run can compute a response spectrum (i.e., a peak spectral acceleration vs. frequency plot) that can describe the input motion in greater detail than the single, peak surface acceleration value obtained per SHAKE run in this study.

A comparison should also be made between the sinusoidal motion records used in this study, and those in which the tail of zeros is reduced or eliminated from the sinusoidal input motion records. If it can be determined that the input motion records need only to contain a sufficient number of acceleration values to define the motion, then it will be easier and more practical to develop and utilize sinusoidal input motion records for SSI analyses.

REFERENCES

1. Aki, K. (1988) "Local Site Effects on Strong Ground Motion," in J. Lawrence Van Thun (Ed.) Earthquake Engineering and Soil Dynamics II-Recent Advances in Ground-Motion Evaluation, ASCE Geotechnical Special Publication No. 20, Park City, UT, June 27-30, 1988, pp. 103-155.
2. American Society of Civil Engineers (ASCE) (1990) "Minimum Design Loads for Buildings and Other Structures," ASCE 7-88, ASCE, New York, NY, July 1990, pp. 31-91.
3. Astaneh, A., Bertero, V.V., Bolt, B.A., Mahin, S.A., Moehle, J.P. and Seed, R.B. (1989) "Preliminary Report on the Seismological and Engineering Aspects of the October 17, 1989 Santa Cruz (Loma Prieta) Earthquake," Report No. UCB/EERC-89/14, Earthquake Engineering Research Center, University of California, Berkeley, CA, October 1989.
4. Benuska, K.L. (1990) "Some Lessons Learned From the 1989 Loma Prieta, California Earthquake," in proceedings, Fourth U.S. National Conference on Earthquake Engineering, May 20-24, 1990, Palm Springs, CA, (Volume 1), pp. 91-105.
5. Benuska, L. ed. (1990) "Loma Prieta Earthquake Reconnaissance Report," Earthquake Spectra, 6, Supplement, May 1990.
6. Borchardt, R.D. and Glassmoyer, G. (1992) "On the Characteristics of Local Geology and their Influence on Ground Motions Generated by the Loma Prieta Earthquake in the San Francisco Bay Region, California," Bulletin of the Seismological Society of America, Vol. 82, No. 2, April 1992, pp. 603-641.
7. Building Officials and Code Administrators (BOCA) (1992) "The BOCA National Building Code," BOCA International, Inc., 1992.
8. Bureau of Reclamation (BOR) (1976) "Dynamic Analysis of Embankment Dams," U.S. Department of the Interior, 1976.

9. California Strong Motion Instrumentation Program (CSMIP) (1989) "Processed Strong-Motion Data from the Loma Prieta Earthquake of 17 October 1989," California Division of Mines and Geology, Office of Strong Motion Studies, Report No. OSMS 91-06.
10. Charlie, Wayne A. (1992) Class notes from CE751-Soil Dynamics, Fall Semester 1992, Department of Civil Engineering, Colorado State University, CO, 1992.
11. Committee on Science, Space, and Technology (CSST) (1990) "The Loma Prieta Earthquake: Lessons Learned," Science, Research and Technology Subcommittee Hearing, U.S. House of Representatives, One Hundred First Congress, First Session, December 4 1989, No. 79, U.S. Government Printing Office, Washington D.C., 1990, pp. 40-84.
12. De Alba, P., Benoit, J., Youd, T.L., Shakal, A.F., Pass, D.G. and Carter, J.J. (1992) "Deep Instrumentation Array at Treasure Island Naval Station," University of New Hampshire, Durham, NH, February 1992, pp. 2-13.
13. Ferritto, J.M. (1992) "Ground Motion Amplification and Seismic Liquefaction: A Study of Treasure Island and the Loma Prieta Earthquake," Report No. TN-1844, Naval Civil Engineering Laboratory, Port Hueneme, CA, June 1992.
14. Finn, W.D. Liam (1991) "Geotechnical Engineering Aspects of Microzonation," Proceedings, 4th International Conference on Seismic Zonation, Vol. 1, EERI, August 25-29, 1991, Stanford University, Stanford, CA, pp. 199-259.
15. Hanks, T.C. and Brady, A.G. (1991) "The Loma Prieta Earthquake, Ground Motion, and Damage in Oakland, Treasure Island, and San Francisco," Bulletin of the Seismological Society of America, Vol. 81, No. 5, October 1991, pp. 2019-2047.
16. Hryciw, R.D., Rollins, K.M., Homolka, M., Shewbridge, S.E. and McHood, M. (1991) "Soil Amplification at Treasure Island during the Loma Prieta Earthquake," Proceedings, Second International Conference on Recent Advances in Geotechnical Earthquake Engineering and Soil Dynamics, March 11-15 1991, St. Louis, Missouri, pp. 1679-1685.
17. Idriss, I.M. (1978) "Characteristics of Earthquake Ground Motions," Earthquake Engineering and Soil Dynamics, Vol. 3, Proceedings of the ASCE Geotechnical Engineering Division Specialty Conference, June 19-21 1978, Pasadena, California, pp. 1151-1265.

18. Idriss, I.M., Dezfulian, H. and Seed, H.B. (1969) "Computer Programs for Evaluating the Seismic Response of Soil Deposits with Non-Linear Characteristics Using Equivalent Linear Procedures," Department of Civil Engineering, University of California, Berkeley.
19. Idriss, I.M. and Seed, H.B. (1968) "Seismic Response of Horizontal Soil Layers," Journal of the Soil Mechanics and Foundations Division, ASCE, Vol. 94, No. SM4, Proc. Paper 6043, July 1968, pp. 1003-1031.
20. Idriss, I.M. and Seed, H.B. (1970) "Seismic Response of Soil Deposits," Journal of the Soil Mechanics and Foundations Division, ASCE, Vol. 96, No. SM2, Proc. Paper 7175, March 1970, pp. 631-638.
21. International Conference of Building Officials (ICBO) (1988) "Uniform Building Code (UBC)," ICBO, Whittier, CA, May 1988, pp. 140-179.
22. Kanai, K. (1983) "Engineering Seismology," University of Tokyo Press, Japan, 1983.
23. Kausel, E. and Roesset, J.M. (1984) "Soil Amplification: Some Refinements," in Soil Dynamics and Earthquake Engineering, Vol. 3, No. 3, 1984, pp. 116-123.
24. Lysmer, J. and Seed, R.B. (1988) "Addendum to SHAKE Manual," and SHAKE-88 Computer Program, Geotechnical Engineering Department, University of California, Berkeley, March 30, 1988.
25. Lysmer, J. and Seed, R.B. (1989) Accelerograms from the 1989 Loma Prieta Earthquake and 1952 Pasadena Earthquake, Geotechnical Engineering Department, University of California, Berkeley.
26. Mitchell, J.K., Masood, T., Kayen, R.E. and Seed, R.B. (1990) "Soil Conditions and Earthquake Hazard Mitigation in the Marina District of San Francisco," Report No. UCB/EERC-90/08, Earthquake Engineering Research Center, University of California, Berkeley, May 1990.
27. National Research Council (NRC) (1985) "Liquefaction of Soils During Earthquakes," National Academy Press, Washington, D.C., 1985.
28. Ohsaki, Y. (1969) "The Effects of Local Soil Conditions Upon Earthquake Damage," Soil Dynamics-Proceedings of Specialty Session 2 Seventh International Conference on Soil Mechanics and Foundation Engineering, Mexico City, Mexico, August 1969, pp. 3-29.

29. Okamoto, S. (1984) "Introduction to Earthquake Engineering," University of Tokyo Press, Japan, 2 edition, 1984.
30. Richart, F.E., Hall, J.R. and Woods, R.D. (1970) "Vibrations of Soils and Foundations," Prentice-Hall, Inc., 1970.
31. Roesset, J.M. (1970) "Fundamentals of Soil Amplification," pp. 183-244.
32. Rogers, J.D. and Figuers, S.H. (1991) "Engineering Geologic Site Characterization of the Greater Oakland-Alameda Area, Alameda and San Francisco Counties, California," Final Report to National Science Foundation, Rogers/Pacific Inc., Pleasant Hill, CA, 30 December 1991.
33. Rosenblueth, E. and Ovando, E. (1991) "Geotechnical Lessons Learned from Mexico and Other Recent Earthquakes," Proceedings, Second International Conference on Recent Advances in Geotechnical Earthquake Engineering and Soil Dynamics, March 11-15 1991, St. Louis, MI, pp. 1799-1819.
34. Schnabel, P.B., Lysmer, J. and Seed, H.B. (1972) "SHAKE: A Computer Program for Earthquake Response Analysis of Horizontally Layered Sites," Report No. EERC 72-12, Earthquake Engineering Research Center, University of California, Berkeley, December 1972.
35. Schnabel, P., Seed, H.B. and Lysmer, J. (1971) "Modification of Seismograph Records for Effects of Local Soil conditions," Report No. EERC 71-8, Earthquake Engineering Research Center, University of California, Berkeley, December 1971.
36. Seed, H.B. (1969) "The Influence of Local Soil Conditions on Earthquake Damage," Soil Dynamics-Proceedings of Specialty Session 2, Seventh International Conference on Soil Mechanics and Foundation Engineering, Mexico City, Mexico, August 1969, pp. 33-51.
37. Seed, H.B. and Idriss, I.M. (1969) "Influence of Soil Conditions on Ground Motions During Earthquakes," Journal of the Soil Mechanics and Foundations Division, ASCE, Vol. 95, No. SM1, Proc. Paper 6347, pp. 99-137, January 1969.
38. Seed, H.B. and Idriss, I.M. (1982) "Ground Motions and Soil Liquefaction During Earthquakes," Monograph No. 5, Earthquake Engineering Research Institute, Berkeley, California, December 1982.

39. Seed, H.B., Idriss, I.M., Makdisi, F. and Banerjee, N. (1975) "Representation of Irregular Stress Time Histories by Equivalent Uniform Stress Series in Liquefaction Analysis," Report No. EERC 75-29, Earthquake Engineering Research Center, University of California, Berkeley, October 1975.
40. Seed, H.B., Lysmer, J. and Hwang, R. (1974) "Soil-Structure Interaction Analyses for Evaluating Seismic Response," Report No. EERC 74-6, Earthquake Engineering Research Center, University of California, Berkeley, April 1974.
41. Seed, R.B., Dickenson, S.E., Riemer, M.F., Bray, J.D., Sitar, N., Mitchell, J.K., Idriss, I.M., Kayen, R.E., Kropp, A., Harder, L.F. and Power, M.S. (1990) "Preliminary Report on the Principal Geotechnical Aspects of the October 17, 1989 Loma Prieta Earthquake," Report No. UCB/EERC-90/05, Earthquake Engineering Research Center, University of California, Berkeley, April 1990.
42. Shakal, A., Huang, M., Reichle, M., Ventura, C., Cao, T., Sherburne, R., Savage, M., Darragh, R. and Peterson, C. (1989) "CSMIP Strong-Motion Records from the Santa Cruz Mountains (Loma Prieta), California Earthquake of 17 October 1989," California Division of Mines & Geology, Office of Strong Motion Studies, Report No. OSMS 89-06, November 17 1989.
43. Siller, T.J. (1988) "The Dynamic Behavior of Tiedback Retaining Walls," PhD thesis, Carnegie Mellon University, Pittsburgh, PA, 1988.
44. Silver, M.L. and Seed, H.B. (1971) "Deformation Characteristics of Sands Under Cyclic Loading," Journal of the Soil Mechanics and Foundations Division, ASCE, Vol. 97, No. SM8, Proc. Paper 8334, pp. 1081-1098, August 1971.
45. Solnes, J. (1974) "Fundamentals of Dynamic Earthquake Response Analysis," Engineering Seismology and Earthquake Engineering, Noordhoff-Leiden, 1974, p. 182.
46. Su, F., Aki, K., Teng, T., Zeng, Y., Koyanagi, S. and Meyeda, K. (1992) "The Relation Between Site Amplification Factor and Surficial Geology in Central California," Bulletin of the Seismological Society of America, Vol. 82, No. 2, April 1992, pp. 580-602.

47. Whitman, R.V. ed. (1992) "Proceedings from the Site Effects Workshop (October 24-25, 1991)," Technical Report NCEER-92-0006, National Center for Earthquake Engineering Research, State University of New York at Buffalo, Buffalo, NY, February 29, 1992.
48. Ziony, J.I. (1985) "Evaluating Earthquake Hazards in the Los Angeles Region - An Earth-Science Perspective," U.S. Geological Survey Professional Paper 1360, U.S. Government Printing Office, Washington, DC, 1985.